People's Democratic Republic of Algeria
Ministry of Higher Education and Scientific Research

Ecole Nationale Polytechnique
Department of Electronics
Laboratory of Communication Devices
and Photovoltaic Conversion

# Final Year's Project thesis

To obtain the State Engineer Diploma in Electronics

# Implementation of Real–Time PWM on STM32F103 for the control of Five–Level Cascaded H–Bridge Multilevel Inverter

**Presented by:** Siradjeddine ASKAR

**Members of jury:**

| | | |
|---|---|---|
| Mourad HADDADI | Professor, ENP | President |
| Mohamed Oussaid TAGHI | MMA, ENP | Examiner |
| Mohammed. S. AIT-CHEIKH | Professor, ENP | Examiner |
| Cherif LARBES | Professor, ENP | Supervisor |
| Omar KHERIF | Dr. Of Eng | Supervisor |

**ENP - 2020**

People's Democratic Republic of Algeria
Ministry of Higher Education and Scientific Research

Ecole Nationale Polytechnique
Department of Electronics
Laboratory of Communication Devices
and Photovoltaic Conversion

# Final Year's Project thesis

To obtain the State Engineer Diploma in Electronics

# Implementation of Real–Time PWM on STM32F103 for the control of Five–Level Cascaded H–Bridge Multilevel Inverter

**Presented by:** Siradjeddine ASKAR

**Members of jury:**

| | | |
|---|---|---|
| Mourad HADDADI | Professor, ENP | President |
| Mohamed Oussaid TAGHI | MMA, ENP | Examiner |
| Mohammed. S. AIT-CHEIKH | Professor, ENP | Examiner |
| Cherif LARBES | Professor, ENP | Supervisor |
| Omar KHERIF | Dr. Of Eng | Supervisor |

**ENP - 2020**

République Algérienne Démocratique et Populaire
Ministère de l'Enseignement Supérieur et de la Recherche Scientifique

Ecole Nationale Polytechnique
Département de l'Electronique
Laboratory of Communication Devices and Photovoltaic Conversion

# Projet de Fin d'Etudes

Obtenir un diplôme d'ingénieur d'État en électronique

# Implémentation de la MLI en Temps Réel sur STM32F103 pour le Contrôle de l'Onduleur Multiniveau H-Bridge en Cascade à Cinq Niveaux

**Présenté par:** Siradjeddine ASKAR

**Soutenu devant le jury:**

| | | |
|---|---|---|
| Mourad HADDADI | Professeur, ENP | Président |
| Mohamed Oussaid TAGHI | MMA, ENP | Examinateur |
| Mohammed. S. AIT-CHEIKH | Professeur, ENP | Examinateur |
| Cherif LARBES | Professeur, ENP | Superviseur |
| Omar KHERIF | Eng. Dr. | Superviseur |

**ENP - 2020**

**الملخص — تتناول هذه الأطروحة التحكم في عاكس H-Bridge متعدد المستويات متتالي من خمسة مستويات. كما أنه يوفر تنفيذًا في الوقت الفعلي للعديد من تقنيات تضمين عرض النبضة (PWM). وتشمل هذه التعديلات تعديل المستوى (LS-PWM) وتعديل الطور (PS-PWM)، والتي يتم تنفيذها على متحكم دقيق. تم إجراء دراسة مقارنة بين هذه التقنيات المقترحة، بما في ذلك تقنية التحكم التقليدية (الموجة الكاملة). بعد ذلك، يتم تنفيذ عمليات المحاكاة في بيئة MATLAB / Simulink. بعد ذلك، يتم إجراء تحليل حدودي من أجل دراسة تأثير معلمات معينة مثل مؤشر التعديل، وتردد التبديل بالإضافة السرعة المعروضة. على المستوى العملي، يتم إجراء التجارب من أجل التحقق من صحة نتائج المحاكاة. المتحكم الدقيق المستخدم هو STM32F103 متصل بلوحة Nucleo-board، ويستخدم لتوليد إشارات التحكم في البوابة لمفاتيح العاكس.**

**الكلمات المفتاحية: العاكس متعدد المستويات، استراتيجيات التحكم في PWM، لوحة STM32F103، التحليل المعياري.**

**Résumé—Ce mémoire porte sur le contrôle d'un onduleur H-Bridge en cascade à cinq niveaux. Il propose la mise en œuvre en temps réel de différentes techniques de modulation de largeur d'impulsion (PWM). Celles-ci incluent les modulations à décalage de niveau (LS-PWM) et à décalage de phase (PS-PWM), qui sont mis en œuvre sur un microcontrôleur. Une étude comparative est effectuée entre ces techniques proposées, y compris la technique conventionnelle de commande (pleine onde). Ensuite, des simulations sont réalisées sous environnement MATLAB / Simulink. Subséquemment, une analyse paramétrique est effectuée afin d'étudier l'effet de certains paramètres tel que l'indice de modulation, la fréquence de commutation, etc. La machine asynchrone est utilisée comme charge pour la sortie de l'onduleur dont la variation des courants, le couple et la vitesse est présentée. Sur le plan pratique, des travaux expérimentaux sont effectués afin de valider les résultats de simulation. Le microcontrôleur utilisé est un STM32F103 attaché à une carte nucléo, et il est utilisé pour générer les signaux de commande de porte des commutateurs de l'onduleur.**

**Mots-clés : Onduleur multiniveau, technique MLI, carte STM32F103, analyse paramétrique.**

**Abstract—This thesis deals with the control of a five-level cascaded H-Bridge multilevel inverter. It also offers a real-time implementation of various pulse width modulation (PWM) techniques. These include level shifted (LS-PWM) and phase shifted (PS-PWM) modulations, which are implemented on a microcontroller. A comparative study is carried out between these proposed techniques, including the conventional control technique (full wave). Then, simulations are carried out in a MATLAB / Simulink environment. Subsequently, a parametric analysis is carried out in order to study the effect of certain parameters such as the modulation index, the switching frequency, etc. The asynchronous machine is used as a load for the output of the inverter whose variation of currents, torque and speed is presented. On a practical level, experiments are carried out in order to validate the simulation results. The microcontroller used is an STM32F103 attached to a nucleo board, and it is used to generate the gate control signals of the inverter switches.**

**Keywords: Multilevel inverter, PWM control strategies, STM32F103 board, parametric analysis.**

# Acknowledgment

This thesis has been conducted at the Laboratory of Communication Devicesand Photovoltaic Conversion in the Department of Electronic of Ecole Nationale Polytechnique (ENP) of Algiers.

First of all, I would like to take this opportunity to express my deepest gratitude and thanks to my project supervisors, Professor Cherif Larbes and Doctor Omar Kherif for their constant guidance, assistance and support as well as all the knowledge they shared during the course of this research.

I also wish to thank the President of jury Mr Mourad HADDADI, Professor at ENP, and the members of the jury: Mr Mohamed Oussaid Taghi, MMA at ENP, and Mr Mohamed Saleh, Professor at ENP, Ait-Cheikh for accepting to be members of the reading committee and for their constructive analysis of the present work.

Further, I sincerely thank Mr Sabri Sekhri and Mr Yasser Khelalef for their help throughout this work.

Last but not least, I would like to express my appreciation and gratitude to my parents, family members and friends, who have encouraged, motivated and supported me during my studies.

# Contents

# LIST OF TABLES

# LIST OF FIGURES

# General Introduction

Electrical energy has been obviously the cornerstone for the evolution of modern civilization. Other technologies have emerged as a result of the wide access to electrical energy such as electronics, telecommunication systems, computers and so on. The production and development of electric power has changed dramatically the daily life of humanity from domestic use to industrial activities [1], while at the same time, the modern power electronics was developed and successfully employed in power system applications [2]. Using power electronics, high levels of productivity in industry and product enhancement are achieved, which led them to become an indispensable tool in any advanced country's industrial economy.

Energy conversion can be considered as one of the most important aspects of power electronics applications such as DC and AC regulated power supply, heating and lightning control, electromechanical processes and electrical machine drive [3]. Indeed, the energy form dependency requires, through power electronic converters, the disposition of consumers of a certain level (and/or type) of voltage. These converters usually transform electrical energy by a level of voltage, current and/or frequency to another one by means of electronic-based switches semiconductors [1]. Power semiconductor switches usage involves conversion and control, and they are offering large size and cost advantages as well as a high level of performance in today's power electronics apparatus [3]. In addition, converters are widely used in several industrial applications such as railway traction, energy conversion renewables, and modern electric vehicles, etc.

Converting the power produced from renewable energy sources requires the use of converters with switches capable of driving high currents or block high voltage levels [1] [4]. This energy conversion is done either through rectifiers and/or inverters. Multilevel inverter technology has emerged recently as a very important alternative in the area of high-power medium-voltage energy control. The multilevel voltage source inverters' unique structure allows them to reach high voltages with low harmonics without the use of transformers or series-connected synchronized-switching devices [4]. The general function of the multilevel inverter is to synthesize a desired voltage from several levels of DC voltages. For this reason, multilevel inverters can easily provide the high power required of a large electric drive. As the number of levels increases, the synthesized output waveform has more steps, which produces a staircase wave that approaches a desired waveform (high quality output signal). Also, as more steps are added to the waveform, the harmonic distortion of the output wave decreases, approaching zero as the number of levels increases. As the number of levels increases, the voltage that can be spanned by summing multiple voltage levels also increases. The structure of the multilevel inverter is such that no voltage sharing problems are encountered by the active devices [5].

On the other hand, in recent years, the control of high-performance asynchronous machine drives for general industry applications and production automation has received widespread research interests. Induction machine modelling has continuously attracted the attention of researchers not only because such machines are made and used in large numbers but also due to their varied modes of operation both under steady and dynamic states. In an electric drive system, the machine is a part of the control system elements. To be able to control the dynamics of the drive system, dynamic behaviour of the motor needs to be considered. The dynamic behaviour of an induction motor can be described using a dynamic model, which considers the instantaneous effects of varying voltages/currents, frequency and torque [6].

AC motor drives are commonly used over DC motor drives because of their more advantages. Induction motor is the most commonly used AC motor drive for various industrial and domestic applications. Generally, Pulse Width Modulation (PWM) techniques are used for driving a motor drive [7]. Using multilevel inverters as drives for electric motors is a much different

application than for the utility applications for which they were originally developed. Only reactive power flows between the converter and the system in static VAR compensation, whereas the converter must handle bidirectional real power flow in the case of motor drives [6]. Furthermore, the application of microcontroller-based devices is continuing to rise with its greater processing speed and flexible control; and the electrical appliances are getting more miniaturized, less costly and low power consuming [8].

Actual technology has been evolved into stand-alone systems, which mainly take their power from powerful microcontrollers. These microcontrollers have many integrated circuits on-board so that they can achieve many different processes by themselves [9]. MCUs reduce the number of chips and the amount of wiring and circuit board space that would be needed to produce equivalent systems using separate chips or discrete elements. Moreover, each pin of a microcontroller interfaces several internal peripherals, with the pin function selected by software. This allows a wider variety of applications than single specific functions. The world of microchip and microcontroller has left the human races wondering with its incredible intelligence and control, in numerous applications such as cellular phone, automobile engine, control system, remote controls, office machines appliances, programmable interval timer, power tools and toys and analogue to digital or digital to analogue converters, etc. [8]

For instance, the STM32 family microcontrollers are designed to offer new degrees of freedom to MCU users. It offers a 32-bit product range that combines very high performance, real-time capabilities, digital signal processing, and low power, low voltage operation, while maintaining full integration and ease of development. Besides, the Technical documentation for a selected device (including datasheets, reference manuals, application notes, user manuals, programming manuals, and errata sheets) is available in one place and can be downloaded for off-line viewing. Documents are automatically updated with the latest version. Therefore, the unparalleled and large range of STM32 devices, based on an industry-standard core and accompanied by a vast choice of tools and software, makes this family of products the ideal choice, both for small projects and for entire platform decisions [10].

Entitled “Real-time PWM implementation on STM32F103 for the Control of 5-level CHB Multilevel Inverter”, this thesis deals with the control of a five-level cascaded H-Bridge multilevel inverter, realised by Bounabi et *al.* [11]. In the light of the aforementioned, and as part of the continuity of laboratory LDCCP research work and the electronics department, the thesis also offers a real-time implementation of various pulse width modulation (PWM) techniques. These include level shifted (LS-PWM) and phase shifted (PS-PWM) modulations, which are implemented on a microcontroller. A comparative study is carried out between these proposed techniques, including the conventional control technique (full wave). Then, simulations are carried out in a MATLAB / Simulink environment. Subsequently, a parametric analysis is carried out in order to study the effect of certain parameters such as the modulation index, the switching frequency, etc. The asynchronous machine is used as a load for the output of the inverter whose variation of currents, torque and speed is presented. On a practical level, experiments are carried out in order to validate the simulation results. The microcontroller used is an STM32F103 attached to a Nucleo-board, and it is used to generate the gate control signals of the inverter switches.

The first chapter gives a general overview of the different inverter technologies used in electrical power conversion, from the conventional basic inverters to multilevel structures. In addition, various control strategies are explained and detailed. These strategies are pulse modulation techniques (PWM) such as Sinusoidal- and Space Vector-PWM, which are elaborated and compared, and they are employed to adjust the inverter desired output voltage.

The second chapter outlines the different classes of electric machines. It emphasises on the mathematical and physical laws that govern the structure and operation of the asynchronous machine along with its parameters. It concludes with a presentation about the modelling of the machine that is used to control it, as well as the general equations that are derived to achieve this purpose.

In the third chapter, simulations of pulse-width modulations techniques are presented and discussed. Additionally, a comparison is made between the considered schemes and their different parameters. The simulation of the inverter output voltage and the motor control are also presented herein.

Chapter four offers guidance through the STM32 families of microcontrollers as well as their common features. It presents the implementation results of the aforementioned modulations on a STM32 board along with the resulting inverter output voltage and the measured current.

Finally, a conclusion that shows the main results are presented, summarising the essential part of this work and future investigations.

# Chapter 1

# Overview on Multilevel Inverter and Its Control Strategies

## 1.1 Introduction

Several industrial applications have begun to require higher power equipment in the recent years. Indeed, power electronic converters are becoming popular for various industrial drives applications [12]. In this light, the actual chapter provides general information on multi-level static converters and their control strategies. This chapter begins by explaining the working of the basic half and full H-bridge inverters and the constraints facing it. The transition to multilevel conversion structures is presented with their strengths and weaknesses. Then, it introduces the multilevel inverter, which is an advanced topology that outperforms the problems faced by the conventional inverter. In addition, the issue of total harmonic distortion is discussed through this chapter. Finally, space vector pulse-width modulation technique is presented and detailed for controlling the switching signals of a typical inverter.

## 1.2 Power Conversion

The main task of power converters is to process and control the flow of electric energy by supplying voltages and currents in a form that is optimally suited for the user loads [13]. According to [14], figure 1.1 shows the different types of energy conversion.

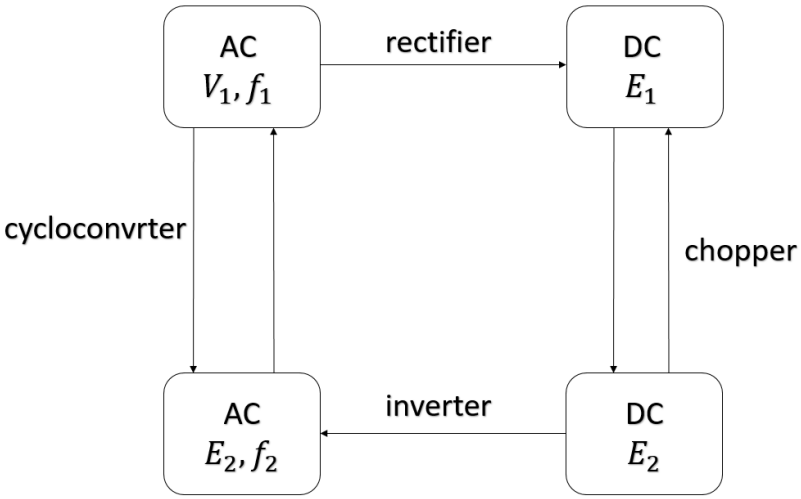


Figure 1.1 Different types of energy conversion

From this figure, one can see that power converters based on semiconductor switching devices can be categorised as follows:

- Transfer of power from an AC supply to DC form. This type of converter is usually called a rectifier.
- Transfer of power from a DC supply to AC form. This type of converter is usually called an inverter.

- Transfer of power from a direct current supply directly into a direct current load of different voltage level. This type of converter is called a chopper converter or a switch-mode converter.
- Transfer of power from an AC supply directly into an AC load of different frequency. This is called a cyclo-converter or a matrix converter.

According to [4], inverters have various structures and they are constructed using different methods and circuitry building. There are different types of inverters depending on their internal parameter (e.g., type of supply, commanding technique, operating frequency, type of semiconductor, and so on). Altogether are mainly used to achieve the desired output signal and control its parameters such as the waveform, voltage and current magnitudes as well as the signal frequency. In fact, each structure has its own advantages and disadvantages depending on the desired/required application. In addition, inverters have many applications in different domains. These mainly include [15]:

- An uninterrupted power supply supplies AC power with the help of an inverter and battery combination.
- Output of photovoltaic modules as they output a direct current, so, an inverter is used to convert the power.
- In general, as the output of the inverter is variable, thus, it can be utilized to control motors and electrical machines.
- In the compressor of an appliance like refrigerator and air-conditioner. The inverter is used to adjust the cooling temperature by controlling the speed of the compressor motor.
- In transmission networks, where it is used to convert the AC-generated power to DC with the help of rectifiers to transmit the power for long-distances.

## 1.3 Topology and Operating Principle

A power inverter, or inverter, is an electrical device or circuitry that converts DC power into AC power at desired output voltage and frequency [16]. Figure 1.2 illustrates the most basic inverter's topology, which is called the half H-bridge.

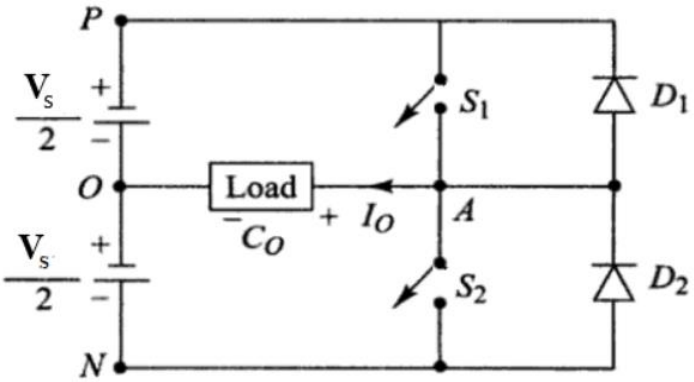


Figure 1.2 Circuit configuration of a Half-Bridge inverter

Obviously, the load is connected to 3-wire DC supply via one terminal and to switches via the other. The switches are turned-on and -off successively, each one for a half period. The load voltage, shown in figure 1.3, is an alternating voltage waveform of an amplitude equals to half of the source.

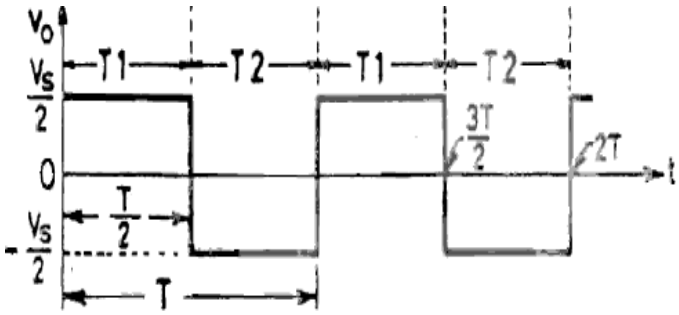


Figure 1.3 Output of single-phase half-bridge inverter [17]

It is important to note that the output frequency, f=1/T, is the same as the selected switching frequency. In addition, the load voltage is equal to the half of the positive supply voltage, and negative for the other half. A main drawback of the previous circuit is the necessity of 3-wire DC source [17]. Therefore, a better topology is presented in the coming section. The full H-bridge which is shown in figure 1.4.

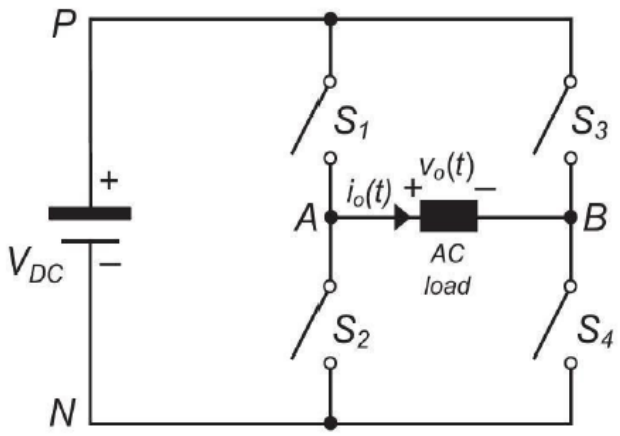


Figure 1.4 Simplified Topology of full-bridge inverter [16]

The circuit consists of DC voltage source $V_{DC}$, a load that requires AC voltage and 4 switches labelled S1 to S4. The load voltage, denoted $v_0(t)$, is taken between the points A and B as shown in figure 1.4; when the potential at point A is higher than that at B, the voltage $v_0(t)$ is assumed positive, otherwise, it is negative.
By turning the switches constantly at a switching frequency $f_0$, and depending on the switch's combination, two operating states are possible.

**State 1:** S1 and S4 are conducting, while S2 and S3 are blocking, for a certain amount of time $T/2$ ($T = 1/f_0$). The load voltage is equal to $V_{DC}$ and electrical current $i_0(t) = \frac{V_{DC}}{Z}$ flows from A to B.

**State 2:** S1 and S4 are blocking, S2 and S3 are conducting, for the same amount of time $T/2$, here the load voltage is equal to $-V_{DC}$ and current with the same intensity flows in the opposite direction (from B to A).

Turning S1 and S3 ON while S2 and S4 are turned OFF, or vice versa, will actuate a redundant state ($v_0(t) = i_0(t) = 0$). It should be also noted that S1 and S2 must not simultaneously be conducting as a short circuit of the source will occur, nor S3 and S4.

Moreover, the switching operation is performed using semiconductor switching devices. This is to say that each one of the switches is replaced with an insulated-gate bipolar transistor (IGBT) or a metal-oxide silicon field-effect transistor (MOSFET). Also, when the load is of a resistive nature, voltage and current are in phase, but they are not in phase when it is of an inductive or capacitive nature, therefore, anti-parallel diodes are placed with respect to every switching device to allow current to pass. The complete topology is illustrated in figure 1.5.

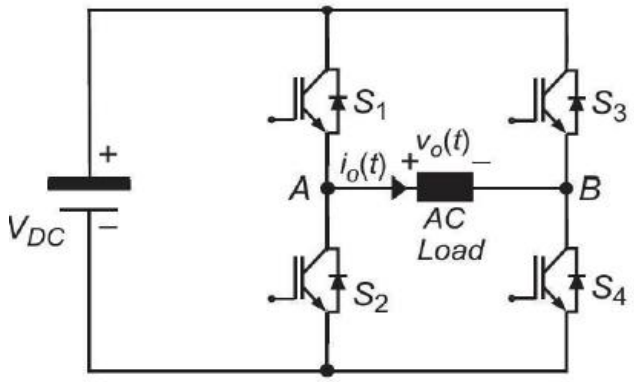


Figure 1.5 Circuit configuration of H-Bridge inverter [16]

Under the aforementioned conditions, the resulting waveform of the output voltage is a square waveform. Figure 1.6 illustrates the corresponding output results.

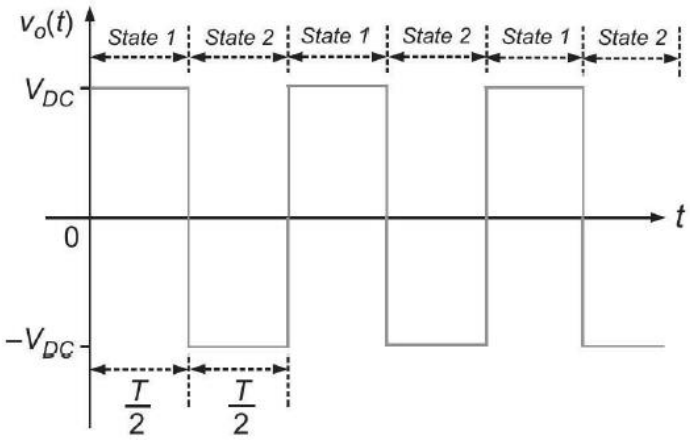


Figure 1.6 Output voltage of Full-Bridge inverter

From figure 1.6, it is clear that the desired output voltage form is an approximately sinusoidal waveform. Nevertheless, the resulting shape is far from being so. The next section discusses a solution to achieve that.

## 1.4 Fourier Analysis of Inverter Output Voltage

It is well known that the output or load voltage does not depend on the nature of the load, unlike the current waveform [17]. Considering Fourier's theorem that states that every periodic non-sinusoidal wave can be broken down into its sinusoidal components, the output voltage $v_0(t)$ (a square wave, which is a periodic non-sinusoidal function) can be written as the following:

$$v_0(t) = \sum_{n=1,3,5\ldots}^{\infty} \quad y_n(t) = \sum_{n=1}^{\infty} \quad \frac{4V_{DC}}{n\pi} sin\,(n\omega t) \qquad (1.1)$$

where, n is the order of the harmonics and $\omega = 2\pi f_0$ with $f_o$ the switching frequency.
Recall that the component whose frequency is the same as the switching frequency ($f_0$) is called the fundamental, whereas the others are called harmonics and their frequencies are integral multiples of $f_0$.
A low-pass filter might be used to eliminate the undesired harmonics and keep the fundamental, thus, obtaining the desired output voltage form. In this case, the total harmonic distortion is given by the equation:

$$THD = \frac{\sqrt{Y_3^2 + Y_5^2 + \cdots Y_n^2}}{Y_1^2} \qquad (1.2)$$

in which, $Y_1^2, Y_3^2, \ldots Y_n^2$ are the root mean square (RMS) of the output voltage components $y_1, y_3, \ldots . y_n$.

Figure 1.7 shows an example of the frequency spectrum of the voltage at the output of the above inverter.

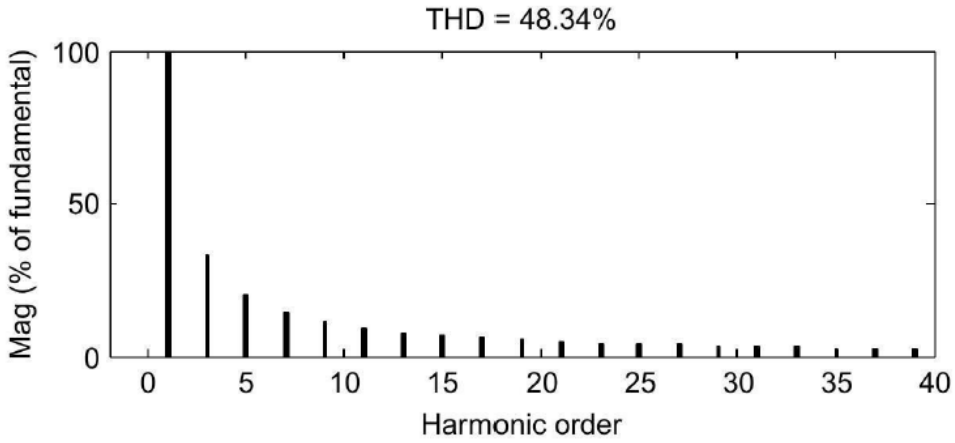


Figure 1.7 Harmonic Spectrum of the inverter output voltage

The harmonic spectrum, which represents the square wave in terms of its components where the orders of the harmonics are on x-axis and their respective magnitudes are on the y-axis.

## 1.5 Multilevel Inverter Structure

Though filtering may appear as an appealing solution, conventional inverters encounter many problems, such as the bad quality of both the output waveforms of voltage and current, the limitation in operating at high frequencies and constraints in device ratings [18]. Multilevel inverter is a promising answer to overcome the aforementioned issues, especially with the advantages that it brings over the conventional inverter, such as:

- It has many steps with fewer power electronic switches, which results in reduction of installation area and cost and has simplicity of control system [12].
- It has a low harmonic distortion, and higher efficiency compared to the simple converter [19].
- The output of the conventional inverter, which is a square waveform, would require a large filter because of the dominant presence of lower-order harmonics.
- It can operate with a lower switching-frequency [20].

Multilevel inverters (MLI) are associations of semiconductors and DC voltage sources that make it possible to obtain an output voltage above the ratings units of each switch as well as an apparent frequency greater than that of the switching of each switch [21]. The most common topologies for the MLI are neutral point clamped-diode (NPC), flying capacitor (FC) and cascade H-bridge.

### 1.5.1 Neutral Point Clamped Diode Topology

Figure 1.8 presents the electrical circuit corresponding to an inverter's arm at N levels.

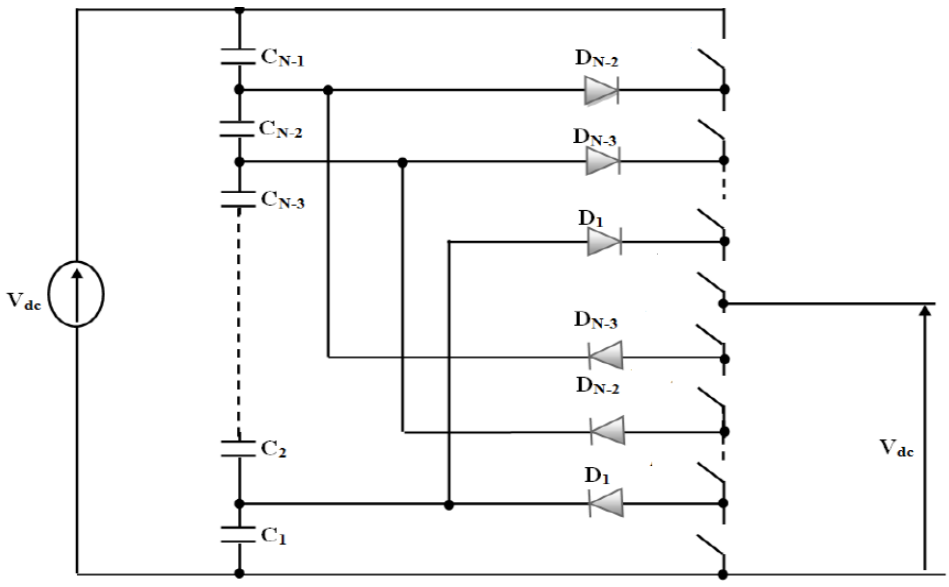


Figure 1.8 N-level floating diode inverter's arm [19].

From the circuit configuration of this inverter, a series of N-1 capacitors creates a set of N-2 midpoints with voltage potentials ranging from $2V_{DC}/(N-1), V_{DC}/(N-1)\ldots$ up to $(N-2)\ V_{DC}/(N-1)$. The distribution of the voltage $V_{DC}$ on the various switches in-series is provided by diodes (clamps) connected to a capacitive midpoint. Intermediate levels voltage on the output of the arm can therefore be created by connecting each of these points at the output, by acting on the control signals of power switches [18].

## 1.5.2 Flying Capacitor Inverter

This structure is based on the connection in-series of switching cells between which a floating voltage source is inserted. These floating voltage sources are realized by capacitors. Figure 1.9 illustrates the three-level inverter with float capacitors.

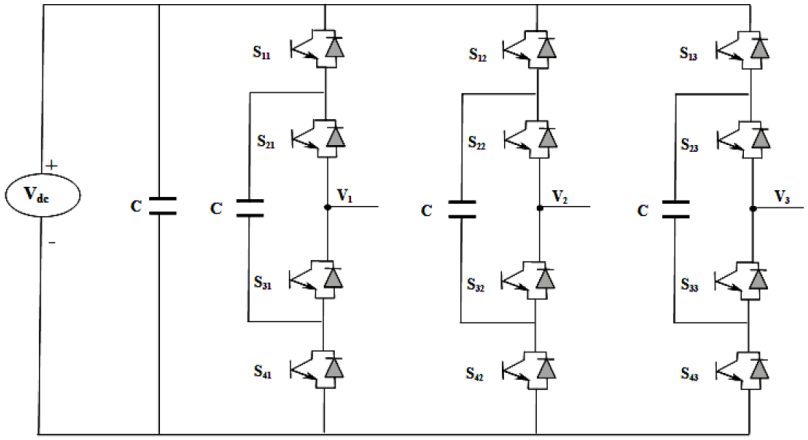


Figure 1.9 Three-level flying capacitor Inverter [19].

Each arm of these topologies can be seen as a nested cell where the voltage output is synthesized by serially connecting a set number of capacitors. The generation of intermediate voltage levels is based on the connection of several DC voltage sources, materialized by floating capacitors and by acting on the logic states of the cells of commutation.

## 1.5.3 Cascaded H-Bridge Multilevel Inverter

A cascade multilevel inverter is simply in-series connections of several inverters [16]; each one is called a cell or H-bridge, as it is depicted in figure 1.10.

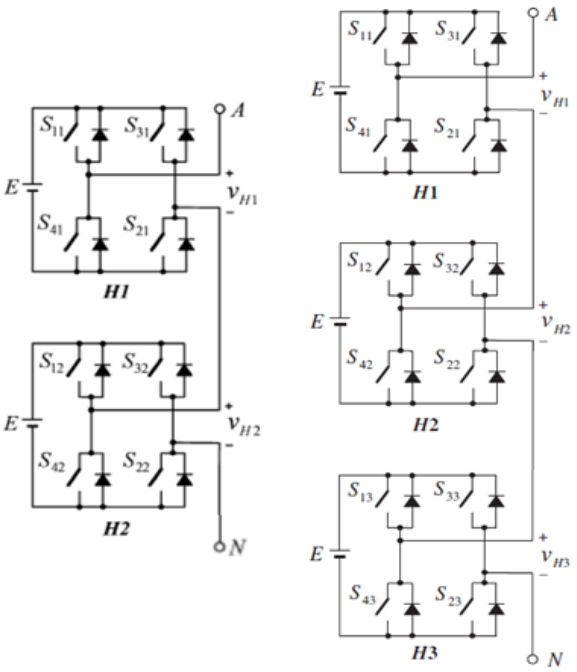


Figure 1.10 Topologies of Cascaded MLI (right 7-level, left 5level)

MLI introduced the idea of using separate and isolated DC sources to produce an AC voltage wave [19]. Each cell is connected to its own DC voltage source, and it is able to generate different levels of output voltage, thus, the overall output voltage of the MLI is the sum of the output voltage of each cell at any given state. For a given number of DC sources ($s$), the number of attainable voltage levels is $n = 2s + 1$, which are as follows:

$$(+nV_{DC}, +(n-1)V_{DC}, \dots, +V_{DC}, 0, -nV_{DC}, \dots, +(n-1)V_{DC}, -nV_{DC})$$

A single cell allows to obtain three voltage levels; $+V_{DC}$, 0 and $-V_{DC}$. As a result, a positive polarity is obtained for the case where $S_{1i}$ is enabled and $S_{3i}$ is disabled. On the other hand, a negative polarity appears for the complementary case. Zero polarity is obtained during activation or deactivation of simultaneous switches $S_{1i}$and $S_{3i}$ [22]. Table 1.1 illustrates the different output states of a five-level MLI. Only the states of the upper switches are considered, since the states of each lower switch is complementary to its corresponding upper-one in each leg.

Table 1.1 Table of switching states of 5-level Inverter

| Output Voltage | Switches combinations | Cell Voltages |
|---|---|---|
| | $S_1$ $S_4$ $S_2$ $S_3$ | $V_{H1}$ $V_{H2}$ |
| $+2E$ | 1 0 1 0 | E E |
| $+E$ | 1 0 1 1<br>1 0 0 0<br>1 1 1 0<br>0 0 1 0 | E 0<br>E 0<br>0 E<br>0 E |
| 0 | 0 0 0 0<br>0 0 1 1<br>1 1 0 0<br>1 1 1 1<br>1 0 0 1<br>0 1 1 0 | 0 0<br>0 0<br>0 0<br>0 0<br>E -E<br>-E E |
| $-E$ | 0 1 1 1<br>0 1 0 0<br>1 1 0 1<br>0 0 0 1 | -E 0<br>-E 0<br>0 -E<br>0 -E |
| $-2E$ | 0 1 0 1 | -E -E |

## 1.6 Controlling Strategies

To adjust the inverter output voltage, the switches must be turned on and off continuously for a specific duration. The most common method to achieve that is the pulse-width modulation. In this method, several pulses per half-cycle are generated with constant amplitude, while their widths are modulated to obtain the controlling signals. The pulse-width modulation techniques used to command the MLI's switches could be classified according to their switching frequency, as illustrated in figure 1.11.

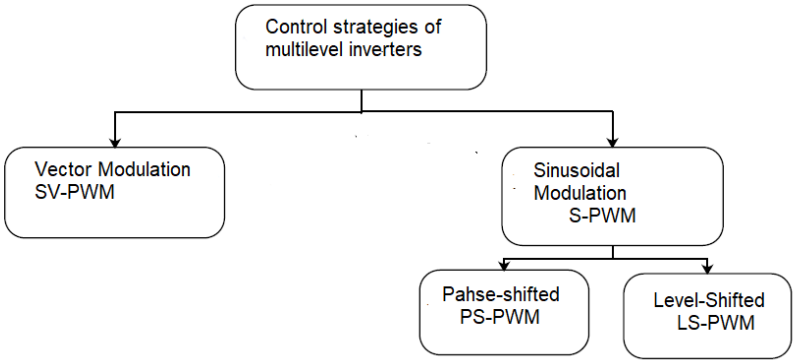


Figure 1.11 Main Control Strategies for Multilevel Inverters

Low switching frequency-based modulations perform one or two commutations of the power semiconductor (switch) during one cycle of the output voltage to obtain a staircase waveform example. In contrast, high switching frequencies-based methods perform many commutations over one period. The most popular methods are the classic multicarrier-based sinusoidal PWM and space-vector PWM. The forthcoming sections will only discuss the high switching frequency techniques [23].

## 1.6.1 Sinusoidal Pulse-Width Modulation

### 1.6.1.1 Single-phase inverter

In this technique, two signals feed the input of a comparator. A high-frequency triangular waveform called the carrier and a sinusoidal waveform called the reference. The amplitudes of both signals are constantly compared and their intersection determines the switching instants and commutation of the modulated pulses [24], as figure 1.12 indicates.

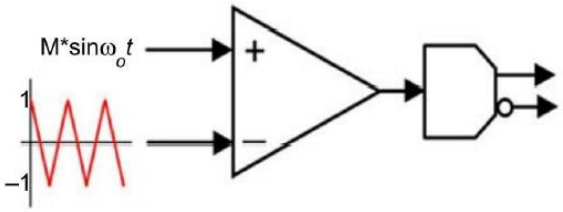


Figure 1.12 Scheme for sine-triangle pulse-width modulation (PWM)

If the amplitude of the carrier is greater than the sine's, the comparator output is high; otherwise, the output is low. The comparator output voltage controls the states of switches S1 and S4, whereas its complement controls the other ones (switches S2 and S3). The output voltage's frequency of the inverter is the same as the reference frequency. Moreover, the ratio between the magnitudes of the carrier and the reference signals is called Modulation index, which is proportional to the magnitude of the fundamental component of the output voltage, thus, by varying the modulation index, the output voltage can be controlled.
Varies amplitude modulation index greatly affects the value of Total Harmonic Distortion (THD). When the index value of fixed amplitude modulation index value is higher, THD value tends to decrease. As when the index value of fixed amplitude modulation index value is greater, the value of the same THD tends to decrease [25].

### 1.6.1.2 Cascade H-bridge Multilevel Inverter

The SPWM modulation for the CHB-MLI is based on that of the classic SPWM of two-level with a triangular carrier and a sinusoidal reference. The only difference between them is the number of used carriers. In general, for an N-level inverter, N-1 carriers are used for the command. The interaction of a particular carrier with a reference is used to generate the control signal for a particular complementary pair of switches. The carriers used in the multi-level

inverter can be shifted vertically (level shifted) or horizontally (phase shifted) [20], as shown in figure 1.13.

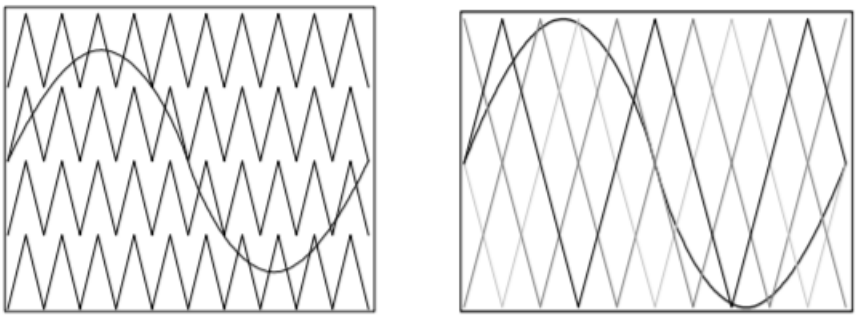

Figure 1.13 SPWM (Level-Shifted and Phase-Shifted) [20].

**A. Phase-shifted PWM**

As it has been mentioned, an N-level MLI needs N-1 carriers to generate the command signals. In shift-pashed multicarrier modulation, the triangular signals have the same frequency and peak-to-peak amplitude, but there is a phase shift between any two adjacent carrier waves, given by:

$$\varphi = 360°/(N-1). \quad (1.3)$$

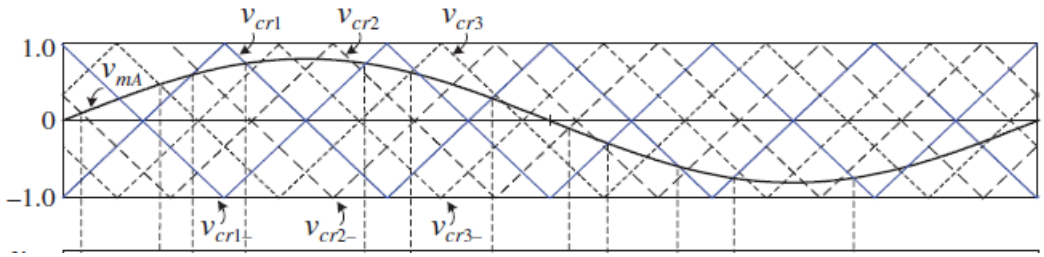


Figure 1.14 PS-PWM for a 7-level MLI [26].

The working principle of phase-shifted multicarrier modulation is illustrated in figure 1.14. For a 7-level CHB-MLI, shown earlier in figure 1.10, six carriers are needed to generate the gate signals. There is a 60° phase shift between any two adjacent carries.

The carriers $v_{cr1}, v_{cr2}$ and $v_{cr3}$ are used to generate the gating signals for the upper-left switches of each cell, so when the magnitude of the sinusoidal is greater than these carriers, switches $S_{11}$, $S_{12}$and $S_{13}$ are switched ON. Otherwise, they are turned OFF. Likewise, $v_{cr-1}, v_{cr-2}$ and $v_{cr-3}$, which are 180° out of phase with the other carriers, when compared with reference signal, control the states of the upper-right switches of each cell. Switches $S_{31}$, $S_{32}$and $S_{33}$ are switched ON when the amplitude of the sinusoidal is less than $v_{cr-1}, v_{cr-2}$ and $v_{cr-3}$ respectively, conversely, they are turned OFF. Therefore, the output voltage waveform is formed by seven voltage steps.

In this example, the output voltage waveform and its harmonic spectrum are shown in figure 1.15 for a 7-level inverter operating under the following conditions: modulation frequency $f_m = 60Hz$, modulation index $MI = 1$.

The waveforms of $V_{H1}, V_{H2}$ and $V_{H3}$, which are the output of each cell are almost identical except for one small phase shift caused by phase-shifted carriers. The waveform of $V_{AN}$, which is the phase-to-line voltage of the first cell is composed of seven voltage levels with an amplitude of 3E. As IGBTs do not switch simultaneously in the different H-bridges, the change in amplitude of the phase voltage during switching is only E.

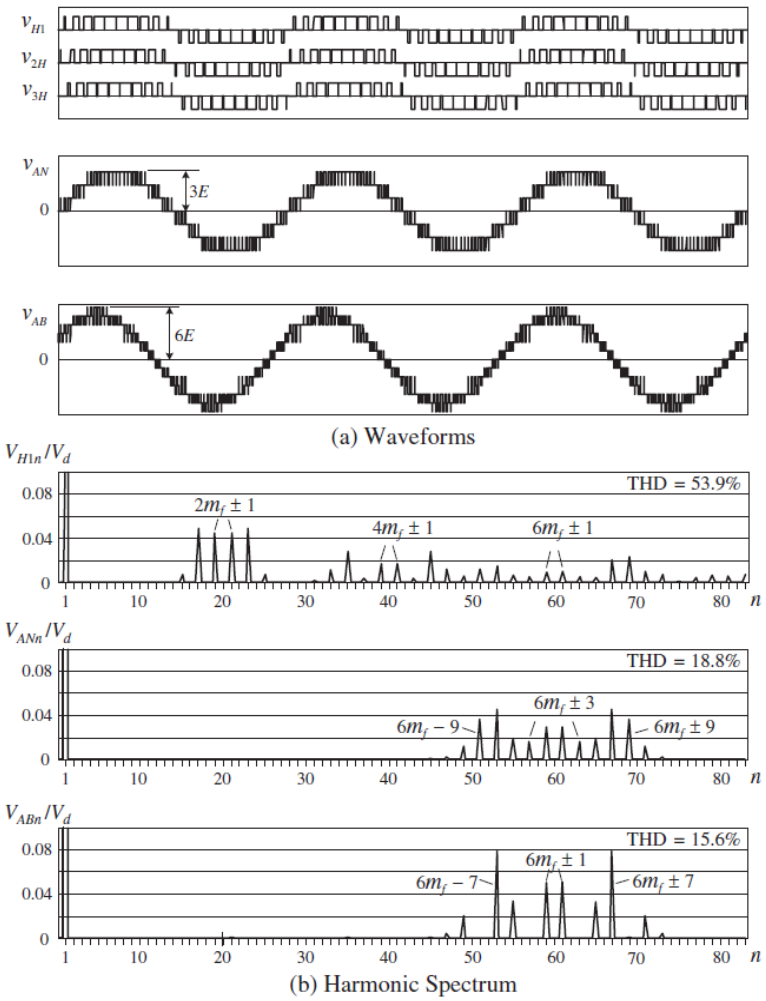


Figure 1.15 Voltage waveform and harmonic spectrum for a 7-level MLI [26].

### B. Level-shifted PWM

As with phase-shifted modulation, an N-Level CHB inverter using level-shifted multicarrier modulation system requires (N-1) triangular carriers, having all the same frequency and same amplitude. Besides, various multicarrier PWM techniques can be derived based on the placement of carrier signals. According to [18] [20] [26], the most common varieties are:

- **Phase disposition:** All carriers are in-phase but level-shifted. The zero reference is placed at the centre.
- **Phase opposition disposition:** There are two sets of carriers. Those above the zero reference are in-phase but in opposition with those below the zero reference.
- **Alternate phase opposition disposition:** The carriers are alternatively disposed in opposition to each other.

Figure 1.16 shows the phase disposition modulation principle, as well as the gating signals and the output voltage.

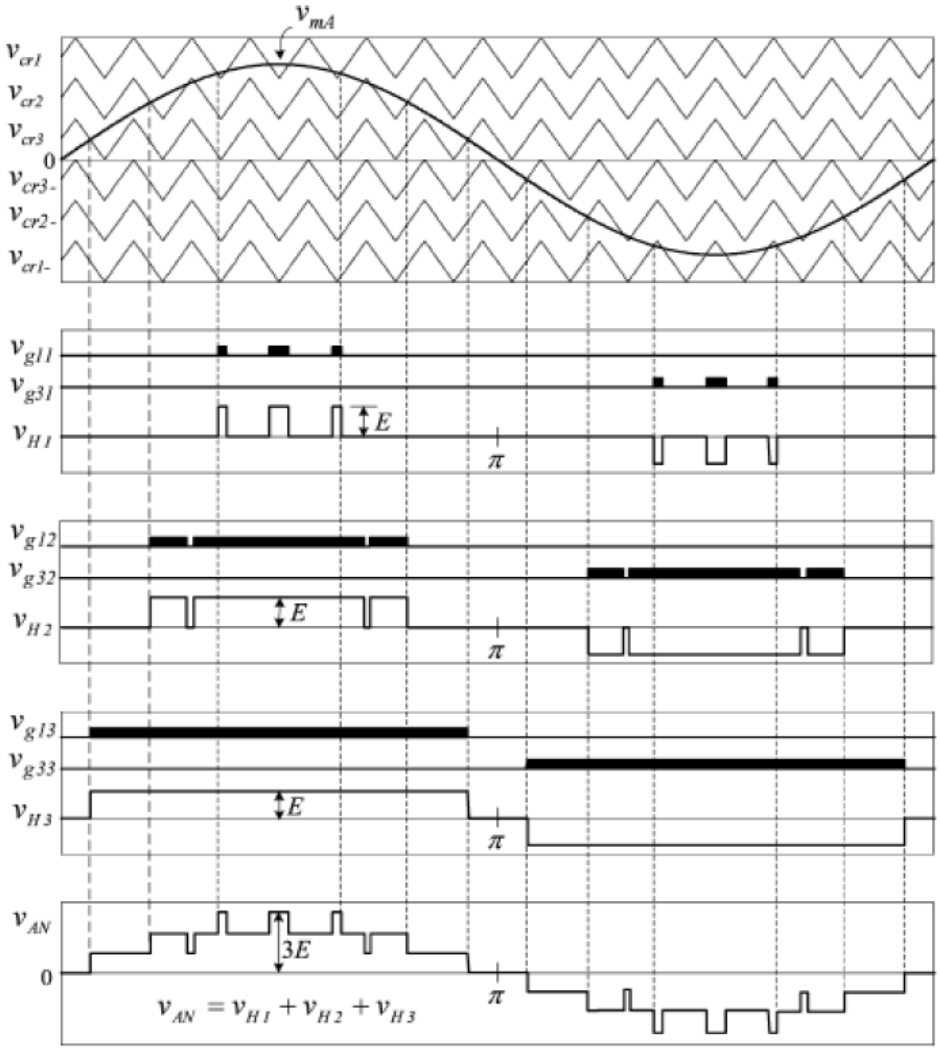


Figure 1.16 LS-PWM for a 7-level Multilevel Inverter [26]

There are six carriers, three above the zero reference labelled $v_{cr1}, v_{cr2}, v_{cr3}$ from the uppermost to the innermost, and three below the reference labelled $v_{cr-1}, v_{cr-2}, v_{cr-3}$ from the lowermost to the innermost. These carriers are continuously compared to the sinusoidal reference and the intersections between this latter and the carriers above the zero level are used to generate the gate signals for the upper-left switches, while with intersections of the modulating signal with the rest carriers is utilized to control the states of the upper-right switches. The two outermost carriers ($v_{cr1}$ and $v_{cr-1}$) are for controlling the states of the first

cell switches, while the two innermost carriers ($v_{cr3}$ and $v_{cr-3}$) are for commanding the third cell switches, that leaves $v_{cr2}$ and $v_{cr-2}$ which are for the remaining cell (second cell).

If the sinusoidal magnitude is greater than $v_{cr1}, v_{cr2}, v_{cr3}$, the switches $S_{11}$, $S_{12}$ and $S_{13}$ are switched ON; if else, they are switched OFF. In a similar manner, if the magnitude of the carriers below the zero reference $v_{cr-1}, v_{cr-2}, v_{cr-3}$ is greater than the modulating signal, the switches $S_{31}$, $S_{32}$ and $S_{33}$ are switched ON, otherwise, they are turned OFF.

In phase-shifted modulation, the switching frequency of the switch is equal to the frequency of the carrier. For instance, with the carrier frequency of 900 Hz, the frequency switching power of the switches in the first cell is only 180 Hz, which is achieved by the number of pulses per cycle multiplied by the frequency of the modulating wave (60 Hz). Also, the switching frequency is not the same for all devices. The switches in the third cell are only turned ON and OFF once per cycle, which results in a switching frequency of 50 Hz.

Although the 3.6 kHz carrier frequency seems high for high power converters, the average switching frequency of the switches is only 600 Hz. The output voltages of the H-bridge cells $V_{H1}, V_{H2}$ and $V_{H3}$ are all different, which means IGBTs operate at different switching frequencies with different conduction times. As with the waveform of the voltage produced by the phase-shifted modulation, the voltage of $V_{AN}$ phase of the inverter is composed of seven voltage levels while phase-to-phase voltage $V_{AB}$ has 13 voltage levels. Dominant harmonics in $V_{AN}$ and $V_{AB}$ appear as sidebands centred on the modulating frequency. Voltage inverter phase contains multiple harmonics such as $3f_m$ and $6f_m$, with $f_m$ dominant. Since these harmonics do not appear in the phase-to-phase voltage $V_{AB}$, the THD of $V_{AB}$ is only 10.83% compared to 18.60% for $V_{AN}$.

## 1.6.2 Space Vector Pulse-Width Modulation

Space vector pulse-width modulation (SVPWM) is an attractive technique because of its flexibility in optimizing the switching sequences and the easy implementation in a digital signal processor (DSP) alike. However, the SVPWM scheme for a multilevel inverter is complex, especially when the level number is high [27].

In the space vector system, the resulting voltage vector is formed by a space vector of defined magnitude and angle in the complex plane (x-y plane). The space vector modulation is a recently reported digital PWM generation technique that is based on the concept of Park (space) vector representation of three phase waveforms [28] [29]. In order to simplify the general principle of this technique, figure 1.17 illustrates a simplified topology of a three-phase simple inverter, which is controlled by SVPWM.

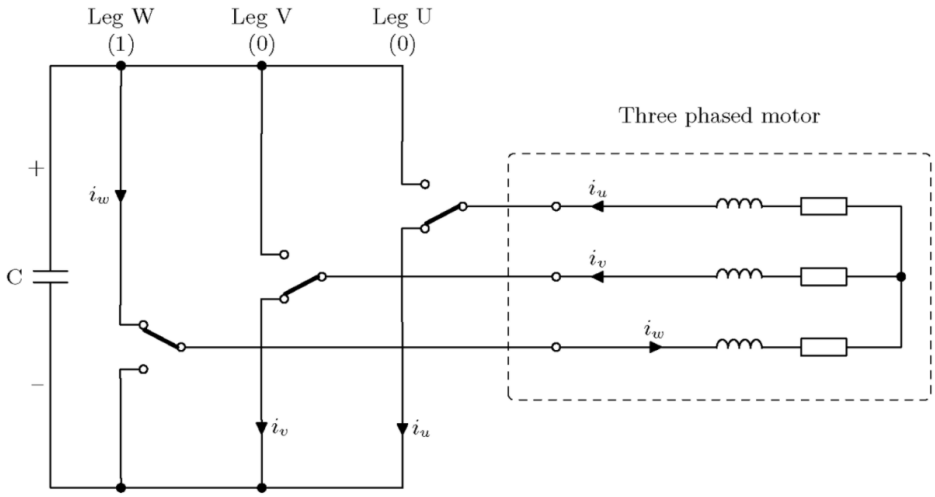


Figure 1.17 Simplified topology of three-phase two-level inverter.

In this inverter, each branch is called a leg and they are labelled U, V and W from right to left as shown in figure 1.17. In fact, switches of the same leg cannot be open or closed at the same time; therefore, there are eight possible configurations for the switches. Figure 1.18 summarizes these eight configurations and the corresponding switches states.

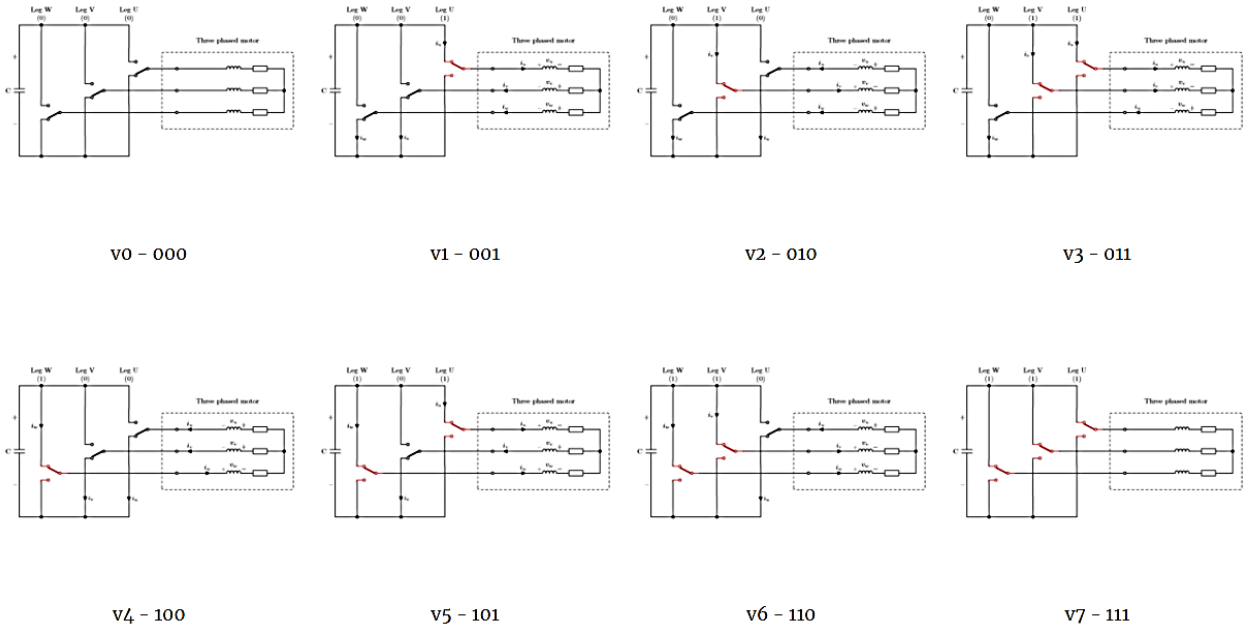


Figure 1.18 Resulting switches states according to the basic vectors.

A three-component space vector (W V U) is utilised to represent these configurations in a binary form, which is derived from the rotating field of the AC current machine that is used to modulate the output voltage of the inverter. In this modulation technique, three-phase quantities can be transformed into their equivalent quantities in two phases or in a frame rotating synchronously or in a fixed frame. Among the possible eight combinations, six of them correspond to different voltages applied to the load; the other two are called zero vectors, as they refer to two configurations where the voltage is zero. Each position on this vector reflects the state of the switches of one leg. 1 in this vector indicates that the upper switch of the

specified leg is closed and the bottom one is open, while 0 indicates the opposite, hence, the eight vectors that refer to these combinations are called the basic vectors [30]. The eight basic vectors are plotted on a hexagonal star diagram; depicted in figure 1.19.

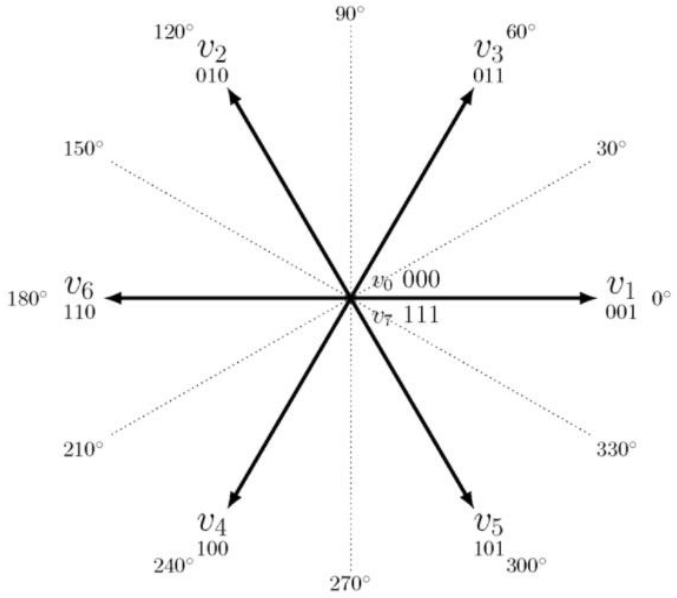


Figure 1.19 Eight basic vectors with their magnitude and direction

The vector $v_1 = (0\ 0\ 1)$, which corresponds to the positive U phase is taken as the reference with the other spanning 60° from one another, whereas the zero vectors $v_0$ and $v_7$ are plotted in the centre (origin) of the diagram. Moreover, the space between any two basic vectors is called a section and are numbered as that the Section 1 lies between the vectors $v_1$ and $v_3$, in anticlockwise direction. SVPWM consists of controlling the stator currents represented by a vector. This control is based on projections that transform a three-phase time and speed dependent system into a two-coordinate time invariant system. SVPWM consists of controlling the stator currents represented by a vector. This control is based on projections that transform a three-phase time and speed dependent system into a two-coordinate time invariant system, as following:

$$V_{ref=}V_A + V_B e^{\frac{j2\pi}{3}} + V_C e^{-\frac{j2\pi}{3}} \qquad (1.4)$$

where $V_A$, $V_B$ and $V_c$ are the three-phase voltage.

Then: $$V_{ref=}\, V_d + jV_q \qquad (1.5)$$

$$[V_d\, V_q\,] = \left[1\ -0.5\ -0.5;\ 0\ \frac{\sqrt{3}}{2}\ \frac{-\sqrt{3}}{2}\right][V_A\, V_B\, V_C\,] \qquad (1.6)$$

To synthesise a desired output voltage vector, it must geometrically be approximated by the two adjacent basic vectors, and these latter, together with the zero vectors are used to synthesise it. For instance, to synthesise the vector $V_{ref}$, depicted in figure 1.20, which is located in Sector 1. V is projected on these vectors and this projection represents the average value that must be produced by each switch.

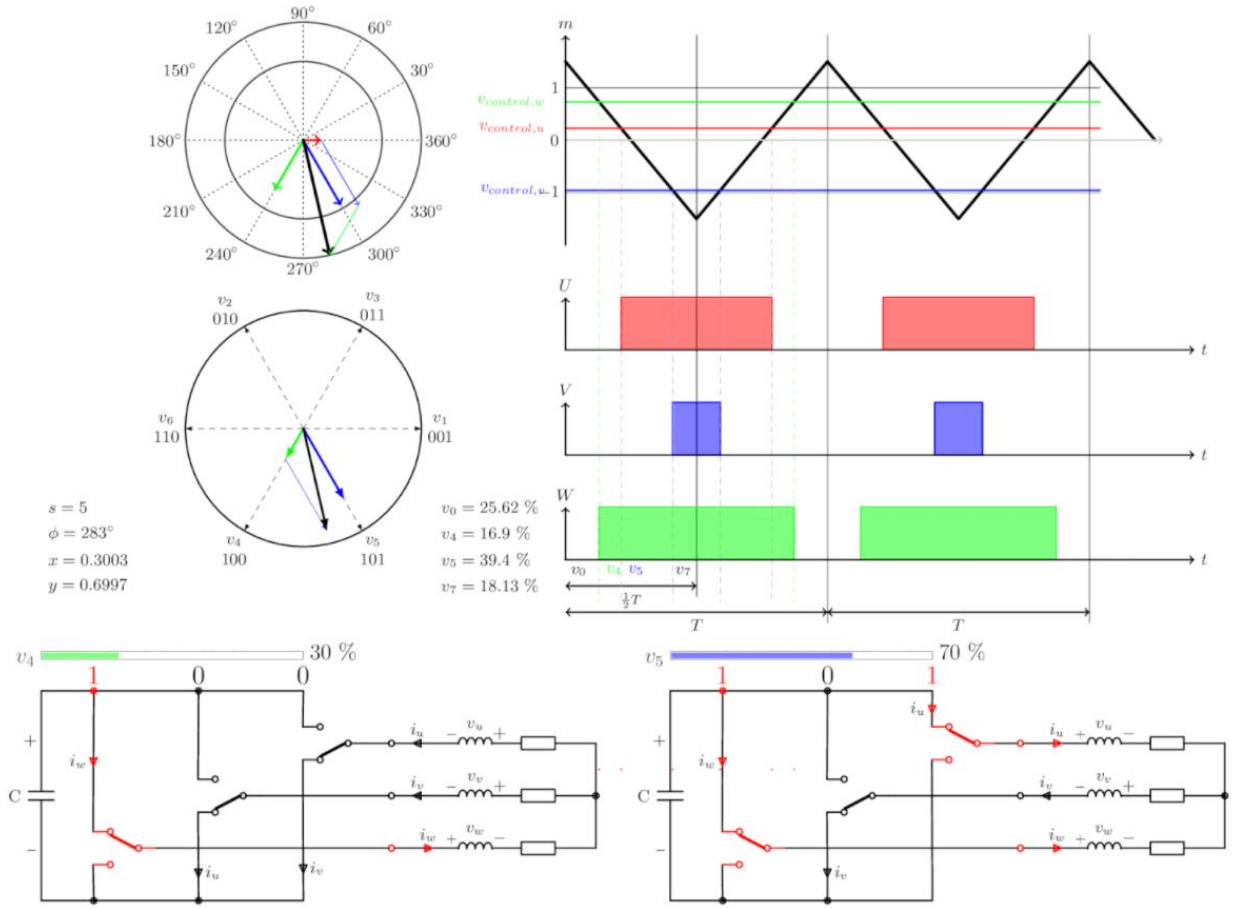


Figure 1.20 SVPWM illustration for an arbitrary vector.

The commutation time of each vector is calculated as follows:

$$T_1 = \left|\frac{V_{ref}}{V_U}\right| . T_{PWM} (1.4)$$

$$T_3 = \left|\frac{V_{ref}}{V_W}\right| . T_{PWM} (1.5)$$

$$T_0 = T_{PWM} - (T_1 + T_{3)} (1.6)$$

In this example, $v_1$and $v_3$ are applied for $T_1$and $T_3$respectively, while the null vectors are applied for the rest of the time ($T_0$).

# Conclusion

Throughout this chapter, a short summary of multilevel inverters is given, as well as their basic topologies. Different applications using different structures were also presented. This chapter has also covered the various main control strategies for multilevel inverters. I presented first sinusoidal pulse width modulation (S-PWM) then its two subclasses: phase shifted (PS-PWM) and level shifted (LS-PWM). Finally, the space vector modulation technique (SV-PWM) is presented.

# Chapter 2

# Operation and Modelling of Three-phase Asynchronous Machines

## 2.1 Introduction

This chapter deals with the operation and modelling of asynchronous machines. First, a brief discussion is given about electrical machines, their applications and classifications. Next, it presents the design characteristics of most common classes of asynchronous machines. Afterwards, the phenomena and physical laws that govern the operation of this machine are elaborated, as well as its working principle and relevant parameters. In addition, mathematical transformations, which are indispensable for controlling the machine are explained. Finally, the chapter also includes an introduction to the modelling of the asynchronous machine in transient regime and a presentation of scalar control and vector control.

## 2.2 Generalities on the Electrical Machines

Electrical machines are generating and using most of the electrical energy converted world-wide from fossil fuels or renewable sources. In fact, an optimized electrical machine means not only less input energy used but also a higher electromechanical energy available as its output. This later is usually translated into getting more with less and having an impact on the total amount of greenhouse gases released into the atmosphere, thus mitigating global warming. Benefiting from the latest developments in the electrical machine field are various industries such as electric propulsion, new electric vehicles (EVs), plug-in hybrid EVs (HEVs), renewable energy harvesting, consumer applications, and military and aerospace products [31].

In general, various devices can be used to convert electrical energy to mechanical energy or in the reverse sense [32]. The structures of these devices may be different, in terms of configuration and topology, depending on the functions they perform. For instance, some devices are used for continuous energy conversion, and these are known as electrical machines. Others are used to produce translational forces whenever necessary and are known as actuators, such as solenoids, relays, and electromagnets. The various converters may be different structurally; however, they all approximately operate on similar principles [33].

Converters that are used to continuously convert either mechanical energy to electrical energy or electrical energy to mechanical energy are called electrical machines. The process of translation is known as electromechanical energy conversion. An electrical machine is therefore a link between an electrical system and a mechanical system. In these machines, the conversion is reversible. When such a device is used to convert mechanical energy to electrical energy, it is called a generator, and when the conversion is from electrical to mechanical, the machine is called a motor [32]. Since any given electrical machine can convert power in either direction, any machine can be used as either a generator or a motor. Almost all practical motors

and generators convert energy from one form to another through the action of a magnetic field [33].

Figure 2.1 summarises the electromechanical power/energy conversion system. In the electrical system, the primary quantities involved are voltage and current, while the analogous quantities in the mechanical system are torque and speed. The coupling medium between these different systems is the magnetic field [34].

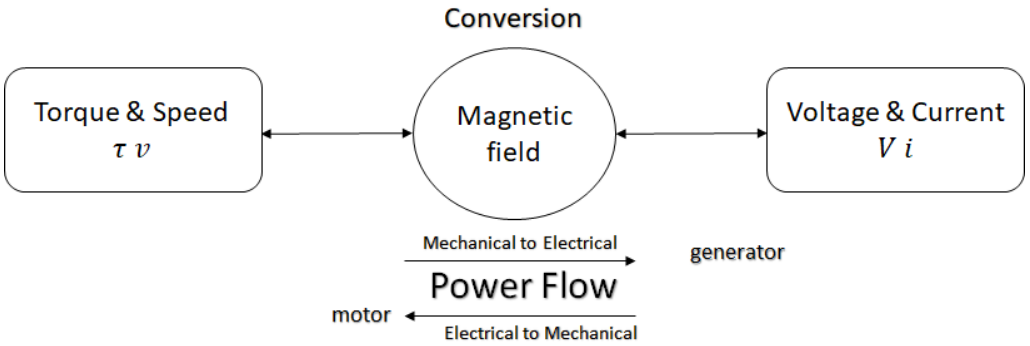


Figure 2.1 Representation of electromechanical power/energy conversion

As depicted in figure 2.2, it is clear that there are two types of electric machines: AC machines (generators or motors) where the electrical system is AC and DC machines (generators or motors) where the electrical system is DC. Note that the two systems, electrical and mechanical, are different in nature. Most DC machines are like AC machines in that they have AC voltages and currents within them. DC machines have a DC output only because a mechanism exists that converts the internal AC voltages to DC voltages at their terminals. Since this mechanism is called a commutator, DC machinery is also known as commutating machinery [35].

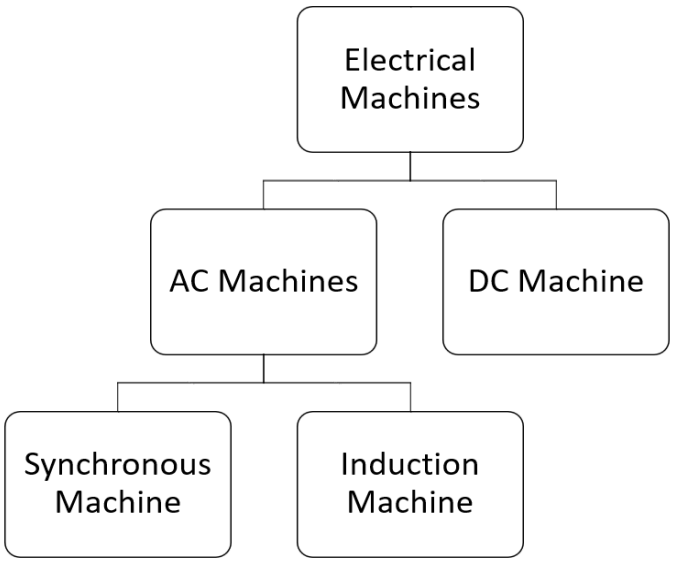


Figure 2.2 Flowchart representation of electrical machineries

AC machines are generators that convert mechanical energy to AC electrical energy and motors that convert AC electrical energy to mechanical energy. There are two major classes of AC machines: synchronous machines and induction machines. Synchronous machines are motors and generators whose magnetic field current is supplied by a separate DC power source, while AC machines are motors and generators whose field current is supplied by magnetic induction (transformer action) into their field windings [35]. Although it is possible to use an induction machine as either a motor or a generator, it has many disadvantages as a generator and so is only used as a generator in special applications. For this reason, induction machines are usually referred to as induction motors.

There are three materials that are mainly used in machine manufacture: steel to conduct magnetic flux, copper (or aluminium) to conduct electric current and insulation to insulate the voltage induced in conductors confining current to them. All machines consist of current circuits made of insulated conductors and magnetic circuits made of ferromagnetic materials [32]. Mainly, electric machinery comprises two parts: the cylindrical rotating member called the rotor and the annular stationary member called the stator with the intervening air gap that allows the former to rotate freely inside the latter. The rotor has an axial shaft that extends out at one end and it is coupled to the prime mover or the load [36], as depicted in figure 2.3.

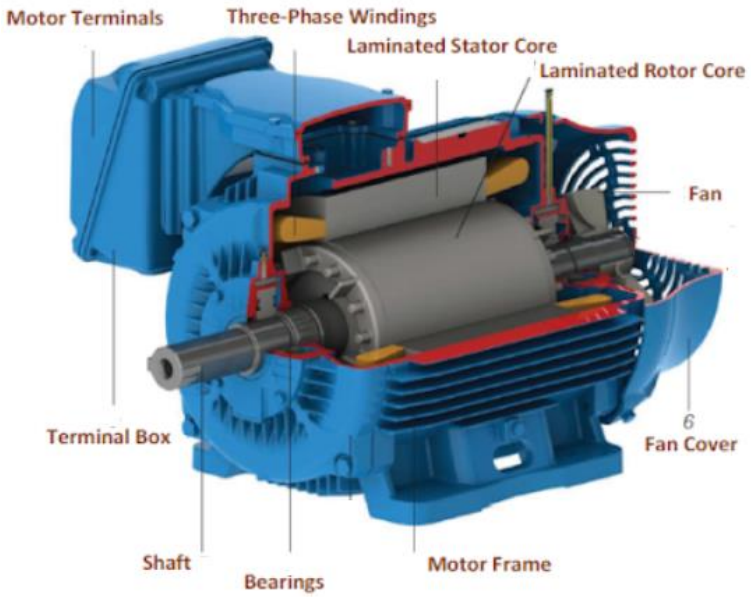


Figure 2.3 Cross-section of a three-phase induction motor [37]

In addition, the field circuits of most synchronous and induction machines are located on their rotors [35]. Also, the rotation of the machine moving part, usually the rotor, contributes to variation of the magnetic field. In turn, an electromotive force is induced in the conductors, which allows generation of electrical energy. Similarly, electrical current in the machine conductors, called windings, interacts with the magnetic field and produces the forces that excite the rotor motion. In both DC and synchronous machines, the main field is created by field poles with direct current [33] [34].

## 2.3 Constructional Features

Induction machines have a uniform air gap; they are characterized by an equal distance between their stator and rotor [33]. Figure 2.4a illustrates a pictorial view of the three-phase induction machine. In this figure, one can see that the stator is composed of laminations of high-grade sheet steel. In addition, a three-phase winding is put in slots cut on the inner surface of the stator frame as shown in figure 2.4b.

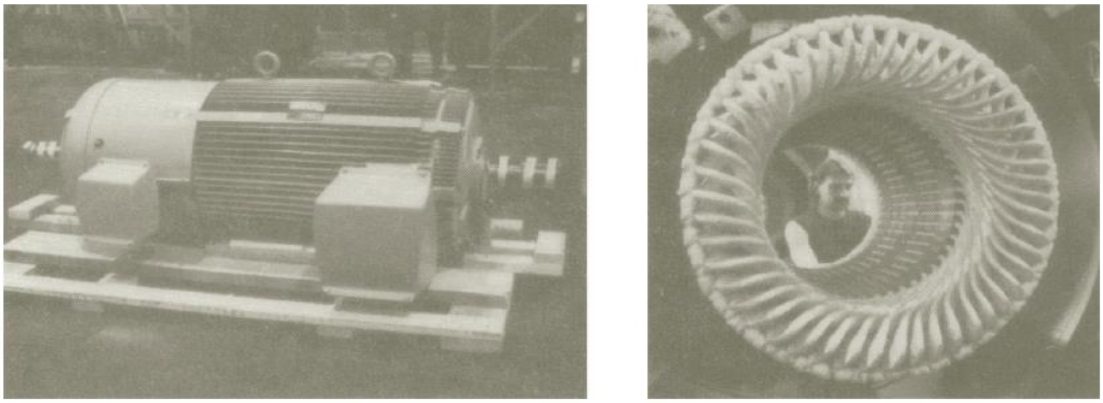

Figure 2.4 Three-phase induction machine. (a) Induction machine with enclosure. (b) Wound-Type rotor [33]

On the other hand, the rotor consists of laminated ferromagnetic material, with slots cut on the outer surface. The rotor winding may be of either two types, the squirrel-cage type or the wound-rotor type.

Usually, the squirrel-cage winding consists of aluminium or copper conducting bars embedded in the rotor slots and shorted at either sides by aluminium or copper end rings as indicated in figure 2.5a. The rotor windings are replaced by longitudinal bars placed in slots beneath the rotor's outer surface. The rotor bars are connected by circular conductors placed at the extremities. Operationally, a squirrel-cage motor is similar to a wound rotor motor with short-circuited windings [39].

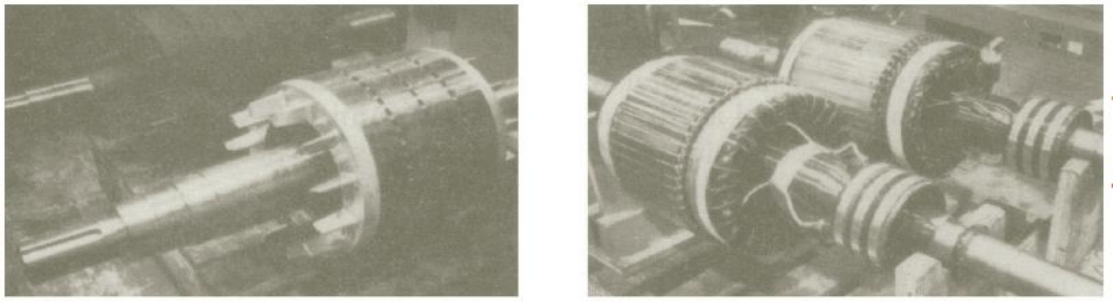

Figure 2.5 Rotor of an induction machine. (a) Squirrel-cage rotor. (b) Wound-rotor type [33]

The wound-rotor winding has a complete set of three-phase windings that are similar to the windings on the stator. The three phases of the rotor windings are usually Y-connected, and the ends of the three rotor wires are tied to slip rings on the rotor's shaft. The rotor windings are shorted through brushes riding on the slip rings, as shown in Figure 2.5b. Using the stationary brushes pressing against the slip rings, the rotor terminals can be connected to an external circuit [35].

The three-phase winding on the stator and on the rotor (in the wound-rotor type) is a distributed winding. Such windings make better use of iron and copper and also improve the magnetic motive force (MMF) waveform and smooth out the torque developed by the machine. The winding of each phase is distributed over several slots. When current flows through a distributed winding, it produces an essentially sinusoidal space distribution of the MMF [33].

## 2.4 Working Principle of Induction Motor

The induction machine has a stator and a rotor mounted on bearings and separated from the stator by an air gap. Moreover, both stator winding and rotor winding carry alternating currents. The alternating current (AC) is supplied to the stator winding directly and to the rotor winding by induction.

### 2.4.1 Working Principle

Overall, the working principle of the asynchronous motors is based on two fundamental phenomena as follows [39]:

1. The law of electromagnetic induction, called Faraday's law, which predict how an electromotive force is induced on a conductive loop when there is a time-varying magnetic field;
2. Law of interaction, i.e., the generated magnetic field by a current-carrying conductor placed in another field, will produce a force, and thus, a torque is developed.

Principally, the machine main parts (stator and rotor) are designed based on these two laws. A rotating magnetic field is generated in the stator windings which will induce an electromotive force in the rotor, which in turn will generate a current in the rotor windings. The current flowing through the rotor generates another magnetic field, thus, based on the latter law, a torque is developed which causes the rotor to turn and align itself with the main field.
Such machines are called induction machines because the rotor voltage (which produces the rotor current and the rotor magnetic field) is induced in the rotor windings rather than being physically connected by wires. The distinguishing feature of an induction motor is that no DC field current is required to run the machine like the case for the synchronous machines [40]. Furthermore, according to the law of electromagnetic induction, when a conductor or a loop

moves through a magnetic field, an EMF is generated. This can be achieved either by moving the conductor in a stationary field or by varying the magnetic field while keeping the conductor stationary.

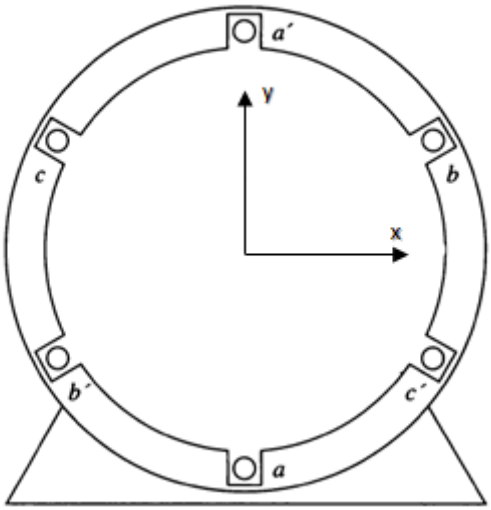


Figure 2.6 A simple three-phase stator

Figure 2.6 shows a of an induction motor which have three-phase windings represented by $a\grave{a}$, $b\grave{b}$ and $c\grave{c}$ displaced by 120° electrical degree. To producing a rotating magnetic field, a three-phase set of voltages is applied to the stator's coils, thus, a three-phase set of currents is flowing through the stator windings, which are:

$$I_A = I_M \sin(\omega t) \quad (2.1)$$

$$I_B = I_M \sin\left(\omega t - \frac{2\pi}{3}\right) \quad (2.2)$$

$$I_C = I_M \sin\left(\omega t + \frac{2\pi}{3}\right) \quad (2.3)$$

where, $I_A, I_B$ and $I_C$ are the currents of phases $a\grave{a}$, $b\grave{b}$ and $c\grave{c}$, respectively. $I_M$ is the peak of the current.

When this set of three-phase currents flow through each coil of the stator, it produces a set of magnetic fields centred on the axis of each coils, which are given by the equations:

$$H_A = H_M \sin(\omega t) \angle 0 \quad (2.4)$$

$$H_B = H_M \sin\left(\omega t - \frac{2\pi}{3}\right) \angle \frac{2\pi}{3} \quad (2.5)$$

$$H_C = H_M \sin\left(\omega t - \frac{2\pi}{3}\right) \angle \frac{2\pi}{3} \quad (2.6)$$

The resulting magnetic flux densities (magnetic induction) for each coil is given by the equation:

$$B = \mu H \quad (2.7)$$

Where $\mu$ is the permeability of the air gap, hence, they are:

$$B_A = B_M \sin(\omega t) \angle 0 \quad (2.8)$$

$$B_B = B_M \sin\left(\omega t - \frac{2\pi}{3}\right) \angle \frac{2\pi}{3} \quad (2.9)$$

$$B_C = B_M \sin\left(\omega t - \frac{2\pi}{3}\right) \angle \frac{2\pi}{3} \quad (2.10)$$

The magnitudes of the magnetic fields and their flux densities vary in time but their directions are always constant. Besides, at any time, the resulting field can be calculated by the sum of the three components.

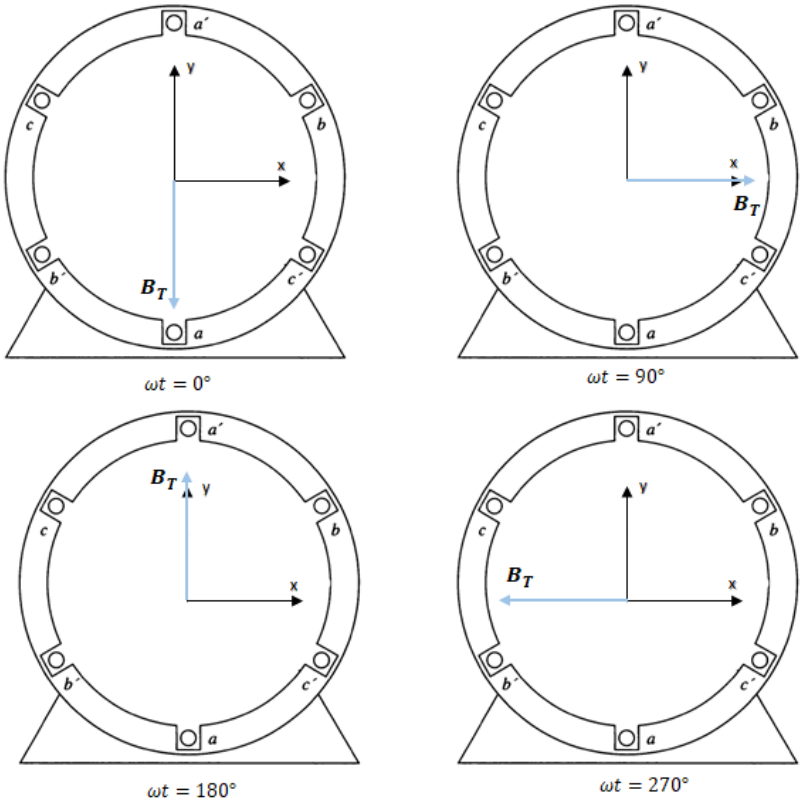


Figure 2.7 Resulting stator magnetic field for different angles

Figure 2.7 illustrates different resulting MMFs for different angles, thus, when three-phase stator windings are supplied by a three-phase set of currents, a revolving magnetic field is set-up in the stator core without physically rotating any magnet. This field rotates in anticlockwise direction with a synchronous speed $n_{syn}$ given by the equation:

$$n_{syn} = \frac{120}{P} f \quad (2.11)$$

where, f is the frequency of stator current and P is the number of poles.

The revolving stator field travels through the air gap and it is cut by the stationary rotor conductors, herein, an EMF is induced in the rotor, and since its windings are short-circuited, current flows through them. This induced electromotive force $e$ is given by the following equation:

$$e = (v \wedge B) \cdot \ell \quad (2.12)$$

where $v$ is the rotation speed and $\ell$ is the length of the conductor.

Thus, the voltage generated in the rotor is a sinusoid whose magnitude is equal to the product of the flux inside the machine and the speed of rotation of the machine. Indeed, the voltage in the machine depends on three factors:

- The flux in the machine,
- The speed of rotation,

- A constant representing the construction of the machine.

It must be noted that the relative motion of the rotor compared to the stator magnetic field that produces this induced voltage. Moreover, the current flowing through the rotor creates a new magnetic field $B_r$. Since two magnetic fields exist, a torque is produced that rotates the rotor, this torque is given by:

$$\tau = kB \wedge B_r \quad (2.13)$$

Thus, the torque induced is proportional to the strength of the stator magnetic field, the strength of the external magnetic field, the sine of the angle between them, and a constant representing the construction of the machine (e.g., geometry, etc.).

## 2.4.2 Speed, Slip and Frequency

When the torque is produced, the rotor starts rotating in the air gap. However, there is a finite upper limit to the motor's speed. For induction machines, the rotor speed is always less than the synchronous speed. The difference between the rotor speed $n$ and the synchronous speed $n_s$ is called the slip, defined as:

$$s = \frac{n_s - n}{n_s} \quad (2.14)$$

Usually, the slip is expressed as a percentage of the synchronous speed as following:

$$\% s = \frac{n_s - n}{n_s} (\times 100\%) \quad (2.15)$$

The difference between the synchronous speed and rotor speed is call *slip speed*, that is:

$$n_{slip} = n_s - n \quad (2.16)$$

If the induction motor's rotor were turning at synchronous speed, then the rotor bars would be stationary relative to the magnetic field and there would be no induced voltage. If this latter were equal to 0, then there would be no rotor current and no rotor magnetic field. With no rotor magnetic field, the induced torque would be zero, and the rotor would slow down as a result of friction losses. An induction motor can thus speed up to near-synchronous speed, but it can never exactly reach it.

It should be noted that in normal operation both the rotor and stator magnetic fields rotate together at synchronous speed, while the rotor itself turns at a slower speed [35]. Additionally, the greater the relative motion between the rotor and the stator magnetic fields, the greater the resulting rotor voltage and rotor frequency. The rotor frequency is given by:

$$f_r = \frac{n_s - n}{n_s} \cdot f = s \cdot f (2.17)$$

The frequency of rotor currents depends upon the relative speed between rotor and stator field. When the rotor is stationary, the relative speed between stator revolving field and stationary rotor conductors is ($n_s - n = n_s$), the frequency of rotor currents is the same as that of the supply frequency. Nevertheless, once the rotor starts rotating, the frequency of rotor currents decreases depending upon relative speed or slip speed [39].

## 2.5 Modelling of Induction Machines

It is well known that the asynchronous machine model is traditionally based on the assumption that the machine is operated in steady state, supplied with a three-phase system of constant effective value and rotated at a constant speed [41]. Figure 2.8 illustrates an asynchronous machine, where the stator phases are respectively identified as $S_a, S_b$ and $S_c$. On the other hand, the rotor coils are identified as $R_a, R_b$and $R_c$. Moreover, the electrical angle $\theta$(a time-varying parameter) defines the instantaneous relative position between the magnetic axes $S_a$and $R_a$.

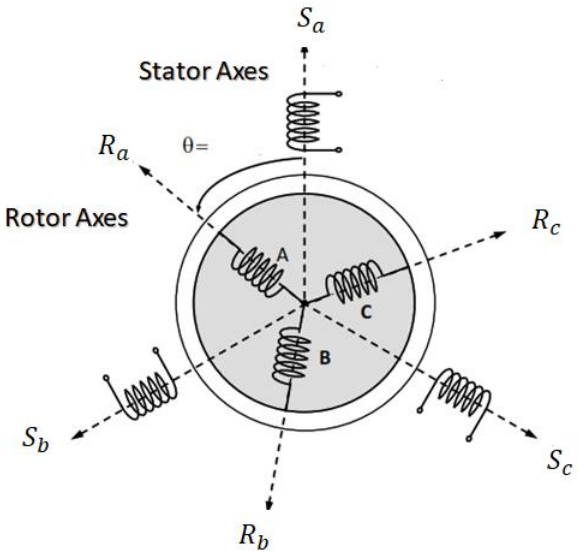


Figure 2.8 Schematic representation of a three-phase asynchronous machine

The electrical quantities are sinusoidal and the approach in complex space is valid. The simplest speed control, called a "$V$ over $f$", allows the speed of the machine to be varied over a wide range below the $n_s$. This control technique is called a scalar control technique. Nevertheless, there is also a control scheme based on the "transient" or "dynamic" model of the machine, in which the control allows obtaining a faster response and better torque control precision compared to the scalar control technique. Usually, it is more difficult to implement since it requires more real-time computing power from the controller (microcontroller, DSP Digital Signal Processor, DSC Digital Signal Controller) of the drive [42]. The transient model of the asynchronous machine makes it possible to simulate its operation in transient mode and steady state alike. In the forthcoming section, the modelling of the asynchronous machine is provided [42] [43].

## 2.5.1 General equations of Induction Machines

### 2.5.1.1 Electrical equations

The windings of the three stator phases and the three rotor phases in space can be represented as shown in Figure 2.8. The rotor phases are short-circuited on themselves. Thus, the voltage equations of the three stator phases and the three rotor phases are given by:

$$V_{sa} = R_s i_{sa} + \frac{d}{dt}\varphi_{sa} \quad (2.18)$$
$$V_{sb} = R_s i_{sb} + \frac{d}{dt}\varphi_{sb} \quad (2.19)$$
$$V_{sc} = R_s i_{sc} + \frac{d}{dt}\varphi_{sc} \quad (2.20)$$

and

$$V_{ra} = R_r i_{ra} + \frac{d}{dt}\varphi_{ra} \quad (2.21)$$
$$V_{rb} = R_r i_{rb} + \frac{d}{dt}\varphi_{rb} \quad (2.22)$$
$$V_{rc} = R_r i_{rc} + \frac{d}{dt}\varphi_{rc} \quad (2.23)$$

respectively, where:

$V_{sa,}, V_{sb}$ and $V_{sc}$ are the voltages applied to the stator phases A, B and C respectively.

$V_{ra,}, V_{rb}$ and $V_{rc}$ are rotor voltages.

$i_{sa}$, $i_{sb}$ and $i_{sc}$ are the stator currents.

$i_{ra}$, $i_{rb}$ and $i_{rc}$ are the rotor currents.

$\varphi_{sa}, \varphi_{sb}$ and $\varphi_{sc}$ are the total fluxes through the stator windings.

$\varphi_{ra}, \varphi_{rb}$ and $\varphi_{rc}$ are the rotor fluxes.

$R_s$ and $R_r$ are the stator and the rotor resistances, respectively.

### 2.5.1.2 Magnetic Equations

Each magnetic flux has an interaction with the currents of all the phases including its own. They are expressed in terms of currents as follows:

$$\varphi_{sa} = \ell_s i_{sa} + m_s i_{sb} + m_s i_{sc} + m_1 i_{ra} + m_3 i_{rb} + m_3 i_{rc} \quad (2.24)$$
$$\varphi_{sb} = m_s i_{sa} + \ell_s i_{sb} + m_s i_{sc} + m_2 i_{ra} + m_1 i_{rb} + m_3 i_{rc} \quad (2.25)$$
$$\varphi_{sc} = m_s i_{sa} + m_s i_{sb} + \ell_s i_{sc} + m_3 i_{ra} + m_2 i_{rb} + m_1 i_{rc} \quad (2.26)$$

and

$$\varphi_{ra} = m_1 i_{sa} + m_2 i_{sb} + m_3 i_{sc} + \ell_r i_{ra} + m_r i_{rb} + m_r i_{rc} \quad (2.27)$$
$$\varphi_{rb} = m_3 i_{sa} + m_1 i_{sb} + m_2 i_{sc} + m_r i_{ra} + \ell_r i_{rb} + m_r i_{rc} \quad (2.28)$$
$$\varphi_{rc} = m_2 i_{sa} + m_3 i_{sb} + m_1 i_{sc} + m_r i_{ra} + m_r i_{rb} + \ell_r i_{rc} \quad (2.29)$$

respectively, in which,

$\ell_s$ and $\ell_r$ are the stator and rotor inductances, respectively.

$m_s$ (respectively $m_r$) are the mutual inductance between two stator (respectively rotor) windings.

$m_1, m_2$ and $m_3$ are the mutual inductance between stator and rotor windings, which are given by

$$m_1 = m_{sr} sin(\theta)$$
$$m_2 = m_{sr} sin(\theta - 2\pi/3)$$
$$m_3 = m_{sr} sin(\theta + 2\pi/3)$$

where, $m_{sr}$ is the maximum mutual inductance between a stator phase and a rotor phase.

## 2.5.2 Park Transformation

The purpose of using these transformations is to switch from a three-phase system ($[k_a, k_b, k_c]$) to another equivalent one; a two-phase system ($[k_d, k_q]$). Therefore, the vector control principle on AC machines takes advantages of transforming the variables from the physical three-phase $ABC$ system to a two-dimension stationary or rotating frame $dq$ [44]. It is worth noting that the space vector $K$ may represent any motor variable (e.g., current, voltage, and flux).

A three-phase AC machine may be described using the space vector method, for this reason, the AC motor variables $k_a(t), k_b(t), k_c(t)$ for a symmetrical machine fulfil the condition:

$$k_a(t) + k_b(t) + k_c(t) = 0 \quad (2.18)$$

The space vector $K$ is given by the sum of these variables as follow:

$$K = \frac{2}{3}(K_A(t) + aK_B(t) + a^2K_C(t)) \quad (2.19)$$

where $a = e^{\frac{2\pi}{3}}$ and $a^2 = e^{\frac{4\pi}{3}}$

There are mainly two transformations: Clarke and Concordia. The Clarke transformation preserves the amplitude of the quantities but not the power nor the torque (we must multiply by a coefficient of 3/2). While that of Concordia, which is standardized, it retains the power but not the amplitudes. This section describes the basic modelling procedures of induction machines [45].

Clarke transformation (Park transformation with a null angle) is given by:

$$\begin{bmatrix} k_d \\ k_q \end{bmatrix} = \frac{2}{3}\begin{bmatrix} 1 & 0 \\ -\frac{1}{2} & \frac{\sqrt{3}}{2} \\ -\frac{1}{2} & -\frac{\sqrt{3}}{2} \end{bmatrix}\begin{bmatrix} k_A \\ k_B \\ k_C \end{bmatrix} \quad (2.20)$$

while Concordia transformation is represented as follows:

$$\begin{bmatrix} k_d \\ k_q \end{bmatrix} = \sqrt{\frac{2}{3}}\begin{bmatrix} 1 & 0 \\ -\frac{1}{2} & \frac{\sqrt{3}}{2} \\ -\frac{1}{2} & -\frac{\sqrt{3}}{2} \end{bmatrix}\begin{bmatrix} k_A \\ k_B \\ k_C \end{bmatrix} \quad (2.21)$$

It should be noted that the inverse transformation can be obtained by multiplying the measure by the transpose of the corresponding transformation matrix. Mathematically speaking, the choice of a normalized matrix (e.g., Concordia) is often used for reasons of direct and inverse transformation symmetry.

In a frame of reference linked to the rotating field (the dq coordinate system), the electrical and magnetic equations become as follows:

$$V_{sd} = R_s i_{sd} - \omega_s \varphi_{sq} + \frac{d\varphi_{sd}}{dt} \quad (2.22)$$

$$V_{sq} = R_s i_{sq} - \omega_s \varphi_{sd} + \frac{d\varphi_{sq}}{dt} \quad (2.23)$$

$$V_{rd} = R_r i_{rd} - \omega_r \varphi_{rq} + \frac{d\varphi_{rd}}{dt} \quad (2.24)$$

$$V_{sq} = R_r i_{rq} - \omega_r \varphi_{rd} + \frac{d\varphi_{rq}}{dt} \quad (2.25)$$

The magnetic flux of related the stator and rotor are given as function of the currents as follows:

$$\varphi_{sd} = L_s i_{sd} + M i_{rd} \quad (2.26)$$
$$\varphi_{sq} = L_s i_{sq} + M i_{rq} \quad (2.27)$$
$$\varphi_{rd} = M i_{sd} + L_r i_{rd} \quad (2.28)$$
$$\varphi_{rq} = M i_{sq} + L_r i_{rq} \quad (2.29)$$

in which,

$L_s = \ell_s + m_s$

$L_r = \ell_r + m_r$

$M = m_{sr}$

At the beginning, the basic differential equations describe the asynchronous machine. From these equations, there are compiled differential equations, which are useful for the description of dynamic model of asynchronous machine. The three-phase induction machine can be modelled by using different state-space variables and keeping as inputs the stator voltages and the load torque, and as outputs the electromagnetic torque and the rotor angular velocity. The state vector is selected as follows:

$$X = \begin{bmatrix} \varphi_{sd} \\ \varphi_{sq} \\ \varphi_{rd} \\ \varphi_{rq} \end{bmatrix}$$

It is worth noting that the advantage of using this reference frame is to have constant quantities in permanent mode so that it is then easier to regulate it and effectively control the asynchronous motor in speed. From the aforementioned equations, one can rewrite them as system state variables where different state vectors are possible.

According to [46], the previous procedure involves the reduction of a number of variables in dynamic equations, which greatly facilitates their solution by using analogue and hybrid computers. Even when the voltages and currents are discontinuous, the flux linkages are continuous. This gives the advantage of differentiating these variables with numerical stability. In addition, the flux linkages representation is used in motor drives to highlight the process of the decoupling of the flux and torque channels in the induction and synchronous machine.

The differential equation of the flux linkages is presented as follows:

$$[\dot{X}] = [A][X] + [V] - [R][I] \quad (2.30)$$

where,

$$[A] = \begin{bmatrix} 0 & 0 & 0 & 0 \\ 0 & 0 & 0 & 0 \\ 0 & 0 & -n_r & 0 \\ 0 & 0 & 0 & n_r \end{bmatrix}, [R] = \begin{bmatrix} r_s & 0 & 0 & 0 \\ 0 & r_s & 0 & 0 \\ 0 & 0 & r_r & 0 \\ 0 & 0 & 0 & r_r \end{bmatrix}, [I] = \begin{bmatrix} i_{sq} \\ i_{sd} \\ i_{rq} \\ i_{rd} \end{bmatrix} \; and \; [V] = \begin{bmatrix} v_{sq} \\ v_{sd} \\ v_{rq} \\ v_{rd} \end{bmatrix}$$

The electric current can be written as function of the magnetic flux. Substituting the values of the flux linkages to find the currents, it yielded:

$$[I] = \frac{1}{D}\begin{bmatrix} 0 & L_r & 0 & -M \\ L_r & 0 & -M & 0 \\ 0 & -M & 0 & L_s \\ -M & 0 & L_s & 0 \end{bmatrix}[X],\ D = L_s L_r - M^2 \quad (2.40)$$

After some algebraic calculations, the following system state variable is obtained:

$$\frac{d}{dt}\begin{bmatrix} \varphi_{sd} \\ \varphi_{sq} \\ \varphi_{rd} \\ \varphi_{rq} \end{bmatrix} = \left( \begin{bmatrix} 0 & 0 & 0 & 0 \\ 0 & 0 & 0 & 0 \\ 0 & 0 & -n_r & 0 \\ 0 & 0 & 0 & n_r \end{bmatrix} - \begin{bmatrix} r_s & 0 & 0 & 0 \\ 0 & r_s & 0 & 0 \\ 0 & 0 & r_r & 0 \\ 0 & 0 & 0 & r_r \end{bmatrix} \begin{bmatrix} 0 & \frac{L_r}{D} & 0 & -\frac{M}{D} \\ \frac{L_r}{D} & 0 & -\frac{M}{D} & 0 \\ 0 & -\frac{M}{D} & 0 & \frac{L_s}{D} \\ -\frac{M}{D} & 0 & \frac{L_s}{D} & 0 \end{bmatrix} \right) \begin{bmatrix} \varphi_{sd} \\ \varphi_{sq} \\ \varphi_{rd} \\ \varphi_{rq} \end{bmatrix} + \begin{bmatrix} v_{sq} \\ v_{sd} \\ v_{rq} \\ v_{rd} \end{bmatrix}$$

This system is completed by the motor speed (rotor speed $n_r$) expression as follows:

$$\frac{dn_r}{dt} = \frac{1}{J} p(\tau_{em} - \tau_r)$$

in which, p is the number of pairs of poles, J is the moment of inertia, $\tau_r$ is the resistive torque and $\tau_{em}$ is the electromagnetic torque that is derived from the magnetic flux as follows:

$$\tau_{em} = \frac{P}{2}(\varphi_{sd}\varphi_{rq} - \quad _{sq}\varphi_{rd})$$

## 2.6 Control of Induction Motors

In the practical part, there is a dynamic model of asynchronous machine in MATLAB or Simulink, which uses the previously described differential equations to simulate the operation of the asynchronous machine. The study of the characteristics of the asynchronous machine introduces not only electrical parameters variations (voltage, current and flux) but also mechanical parameters (torque and speed). Based on the above equations, the electromagnetic torque and rotor speed can be determined [41].

As stated previously, there are two types of control techniques; scalar commands and vector commands. Several scalar commands exist and they mainly depend on the topology of the used inverter (voltage or current inverter). Since the voltage inverter is now the most used in small and medium power, it is the $V/f$ control ($V$ over $f$) which is the most used. This control technique is based on the fact of maintaining V/f = Constant, which means to keep the flux constant. Under this condition, the torque is controlled by the action on the slip [42].

## 2.7 Conclusion

In this chapter, the different types of electrical machines are presented. Emphasis was made on the features of the asynchronous machine, its constructing and operating principles. Different motor parameters have been also discussed such as frequency and motor speed. Finally, the general equations and transformations that represent the modelling of the machine are given in details.

# Chapter 3

# Asynchronous Motor Supplied by 3-phase CHB-MLI: Simulations

## 3.1 Introduction

This chapter describes simulations of an asynchronous motor supplied by a multilevel voltage inverter. Five-level symmetrical three-phase cascaded H-bridge is considered. Indeed, this inverter is controlled by three different strategies namely; level shifted PWM, phase shifted PWM and staircase conventional technique. First, a general background of the proposed inverter with its control techniques is presented. The triggering pulses generated by the mentioned strategies are carried out together with comparison. For each strategy, the output voltage is presented and discussed. Furthermore, a parametric analysis is realised to study the effect of the modulation index and switching frequency on the quality of the output voltage. This latter is examined in terms of THD and amplitude of the fundamental signal component. Finally, arbitrary RL-load and asynchronous motor are selected. The voltage and current are visualised and the obtained results are discussed.

## 3.2 Inverter Topology and Control Strategies

In this section, the topology of the used inverter is presented. Elaboration of the modulation techniques which are used to control this inverter is carried out. Besides, the simulations of these techniques have been performed under the MATLAB environment. The results are presented and interpreted where different parameters have been varied such as frequencies and magnitudes. These parameters along with the types of this modulation are compared.

### 3.2.1 Topology of 5-level CHB-MLI

For a given phase, the circuit configuration of five-level symmetrical cascaded H-bridge inverter is depicted in Figure 3.1. It is worth noting that the said inverter is capable, under the proper working conditions, to generate five different levels of AC voltage at its output. The working principle of this converter has been well detailed in the first chapter along with a discussion about the appropriate operation of the switches that ensures the predicted results at the converter output.

The forthcoming results are obtained from simulating those techniques for a five-level inverter, and they are compared with real-time implantations of the same techniques on a microcontroller for a three-phase five-level inverter.

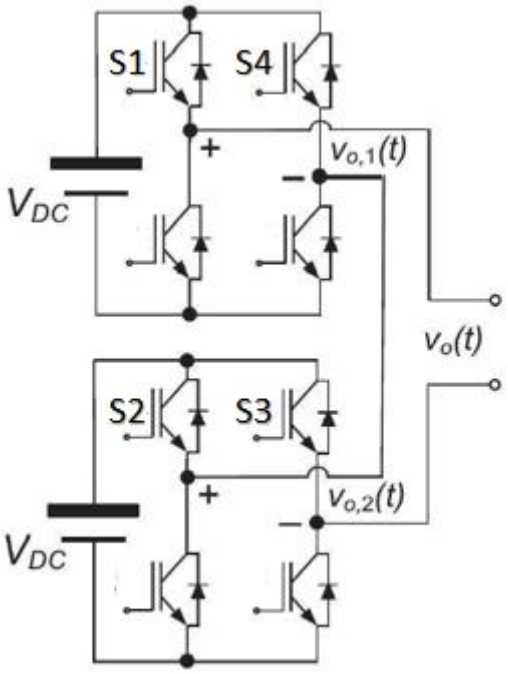


Figure 3.1 Circuit configuration of a given phase of a five-level CHB-MLI

From Figure 3.1, it is clear that the proposed CHB-MLI has two cells; each one has two branches with two switches; as a whole, eight controlling signals are needed. Despites that, only four signals that are responsible for commanding the four upper switches (S1, S2, S3 and S4) of each branch should be considered as each one of the bottom switches operates in a complementary manner to the upper one in the same branch.

## 3.2.2 PWM Techniques

Several control strategies are available for generating triggering pulses of multilevel inverters [47]. PWM techniques used here are the Sinusoidal PWMs (SPWM). It is important to note that the SPWM can be further categorised into two types based on the carriers shifting; i.e., level or phase shifting [20] [48]. Though the former has several varieties, in which a few of them have been presented in former chapters, this chapter only concentrates on the variety known as phase disposition.

For SPWM, both Level-shifted and phase-shifted modulations are simulated under the MATLAB environment. For this purpose, the modulating signal is a sinusoidal waveform of frequency $f_m = 50Hz$ and amplitude of $A_m = 4V$. Being the controlling signals of five-level MLI, both types necessitate four carriers. For the former, carriers are level shifted as shown in figure 3.2a. They share the same frequency $f_{c1} = 2kHz$ and phase, and have a peak-to-peak voltage of $2V$. Figure 3.2b shows the other said type. It is worth noting that there is a $\frac{\pi}{2}$phase-shift between any adjacent carriers and they have the same frequency $f_{c2} = 500Hz$ and amplitude$A_{c2} = 4V$.

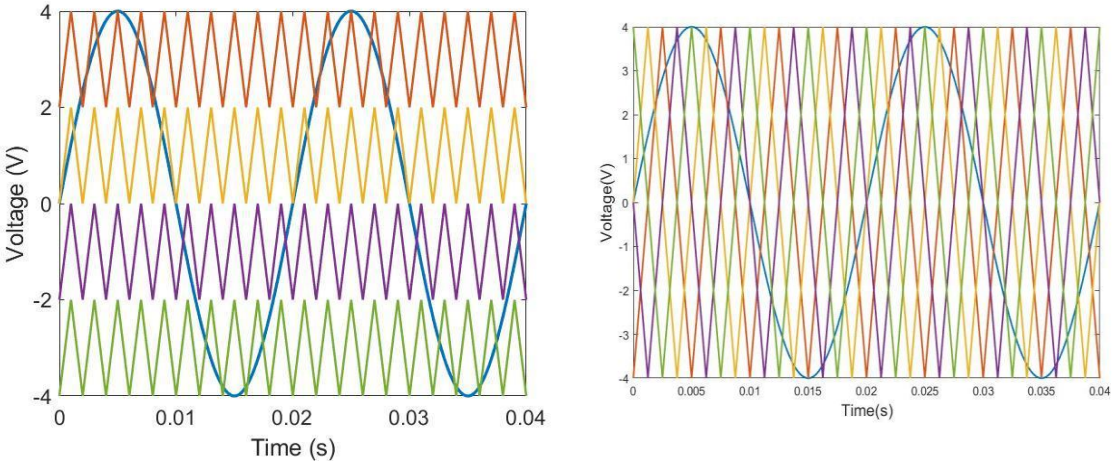


(a) LS-PWM (b) PS-PWM

Figure 3.2 Control strategies of 5-level CHB-MLI using different control techniques

For both techniques, the magnitudes of the modulating signal and the carriers are consistently compared and the modulation signals are generated according to that.

Figures 3.3a and 3.3b show the resulting pulses of LS- and PS-PWM strategies, successively. These results are obtained under the previously-mentioned parameters with a sampling frequency of $f_s = 1\ MHz$and modulation index M=1.

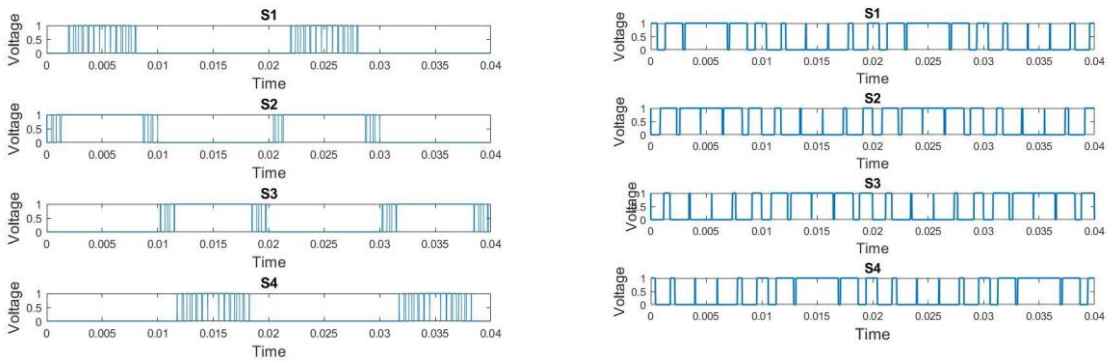


(a) LS-PWM (b) PS-PWM

Figure 3.3 Triggering pulses for 5-level CHB-MLI using different control techniques

These generated PWM signals are then used as gate signals to control the switching devices where the actual states of the corresponding switches (S1, S2, S3 and S4) are used to synthesise the inverter output voltage.

## 3.3 Simulations and Results

In this section, the resulting output voltages, as well as the total harmonic distortion of the previously-simulated techniques are presented and discussed in this section. Initially, for a conventional control strategy, which is the staircase control, the output voltage of the 5-level multilevel inverter is shown in Figure 3.4. This figure shows one phase signal obtained for a modulation index M=1 and switching frequency of about 5kHz.

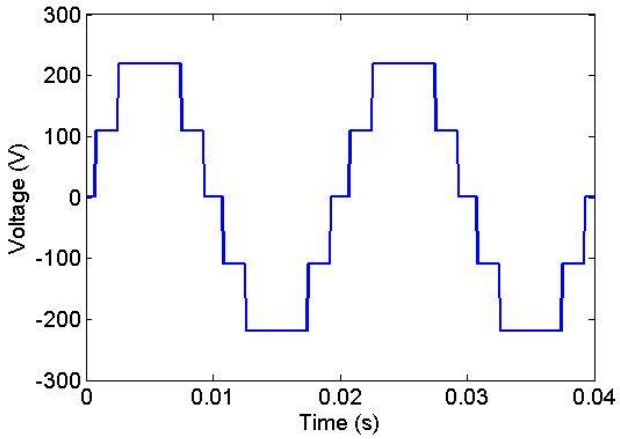


Figure 3.4 Output voltage of the staircase control technique

The harmonic spectrum of the staircase control strategy is illustrated in figure 3.

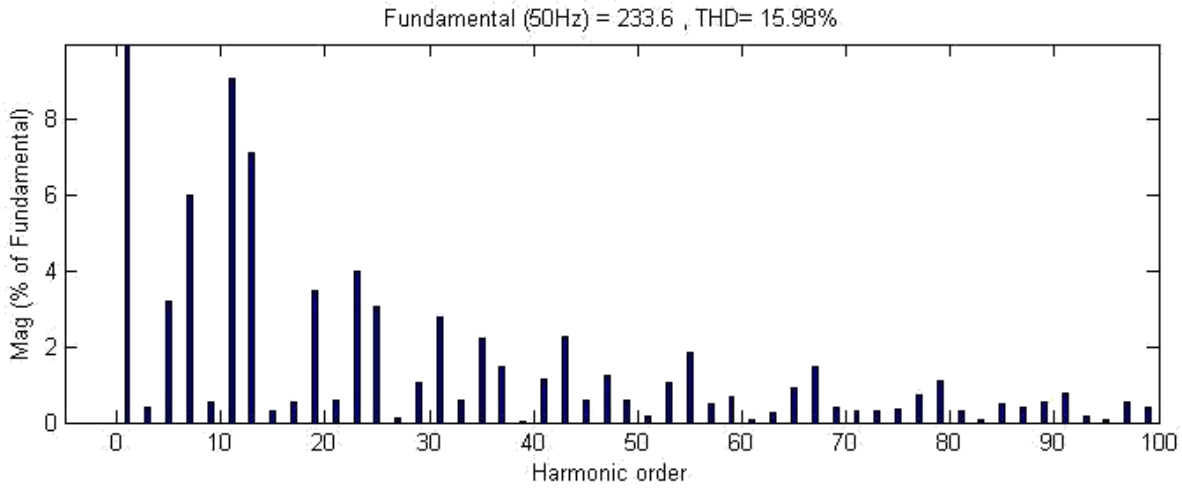


Figure 3.5 Frequency spectrum of output voltage of the 5-level inverter controlled by stair strategy

From this figure, it seems that the output voltage contains a large number of harmonics in its spectrum. Moreover, these harmonics are characterized by low frequency range, which might require an additional low-frequency filter.

Besides the necessity of an additional component (filter), the size of a low-frequency filter is large, which may result in an inconvenient and inefficient design. To overcome this problem, PWM techniques have been used to further decrease the THD as well as for the purpose of relocating the harmonics to a higher order, thus, reducing the size of the filter.

The simulated results of the desired output voltage for the LS- and PS-PWM schemes have yielded the following results, which are shown in figure 3.6a and 3.6b. The simulations are performed based on the combinations of the switch's states and the already-simulated gate signals. The supply voltage is set to 30V.

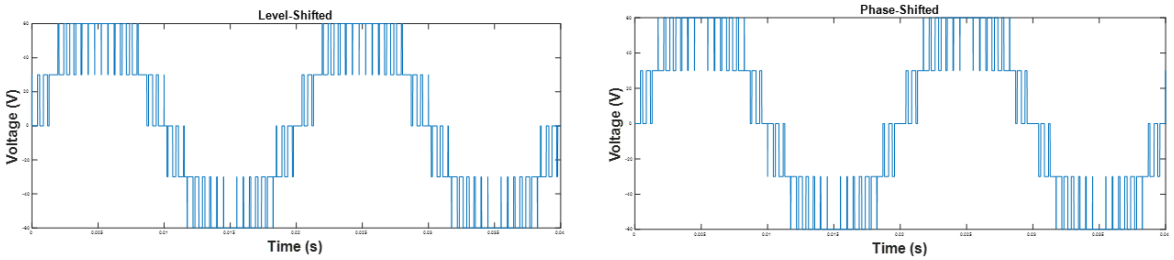


(a) LS-PWM (b) PS-PWM

Figure 3.6 Output voltage of the 5-level CHB-MLI controlled by two PWM techniques

Indeed, the obtained waveforms have a closer resemblance to a sine wave than the staircase and can be deemed a better approximation to the desired output.

Figure 3.7 illustrates the analysis of power densities of the resulting voltage. They are achieved using the FFT Analysis of SIMULINK, and they are plotted as a percentage of the fundamental component magnitude against the harmonic order.

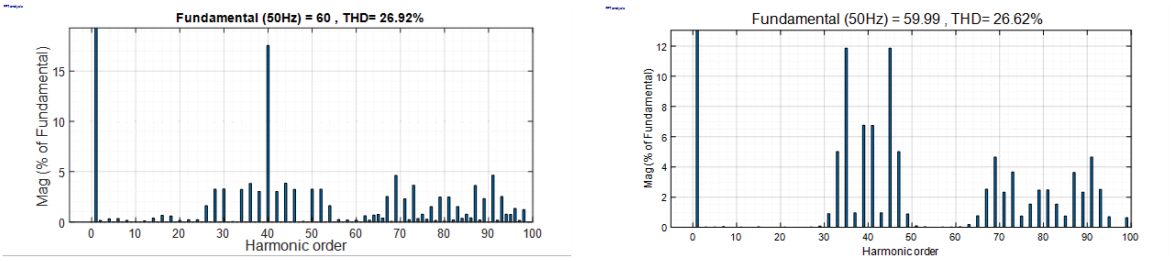


(c) LS-PWM (d) PS-PWM

Figure 3.7 Frequency spectrum of the Output voltage of the 5-level CHB-MLI controlled by two PWM techniques

Both techniques, under the previous parameters, have similar THD (26.92%) and magnitude of the fundamental component (around 60 V).

For level-shifted modulation, the low-orders components are insignificant in contrast to the high-orders harmonics, which are spread over the entire spectrum and have a tolerable increase in their magnitude that can be perceived. The uttermost magnitude (more than 15%) corresponds to the fortieth harmonic, which has a frequency of 2KHz.

On the other hand, the harmonics of phase-shifted technique are condensed within two ranges where their magnitudes can reach 12%. Also, it should be noted that there are interspaces that have no harmonics.

It can be perceived from the previous figures that both techniques have the same magnitude and distortions value, and they only differ in how harmonics are dispersed over the spectrum. Ultimately, though the conventional method has a lower total harmonics distortion and a higher fundamental amplitude among the all-discussed techniques, the existing harmonics of the shifting modulations have high orders that are easier to filter using a small-sized filter, thus, the distortions can be further reduced.

## 3.4 Parametric Analysis and Comparison

In this section, the effects of some parameters on the performance of the employed techniques are examined as well as on the harmonics. The parameters which are considered are the modulation index and the frequency of the modulating signal.

### 3.4.1 Effect of Modulation Index

The variation of the modulation index; which is the ratio of the amplitude of the carrier to that of the reference signal, is achieved by varying the amplitude of the modulating signal. Figures 3.9 and 3.10 illustrate the output voltage for several modulation indexes. These simulations are performed by guarding constant frequencies for all the signals ($f_c = 100Hz, f_m = 50Hz$) as well as constant carriers' amplitudes. The different values for the reference amplitude are: 3, 3.5, 4.5 and 5.

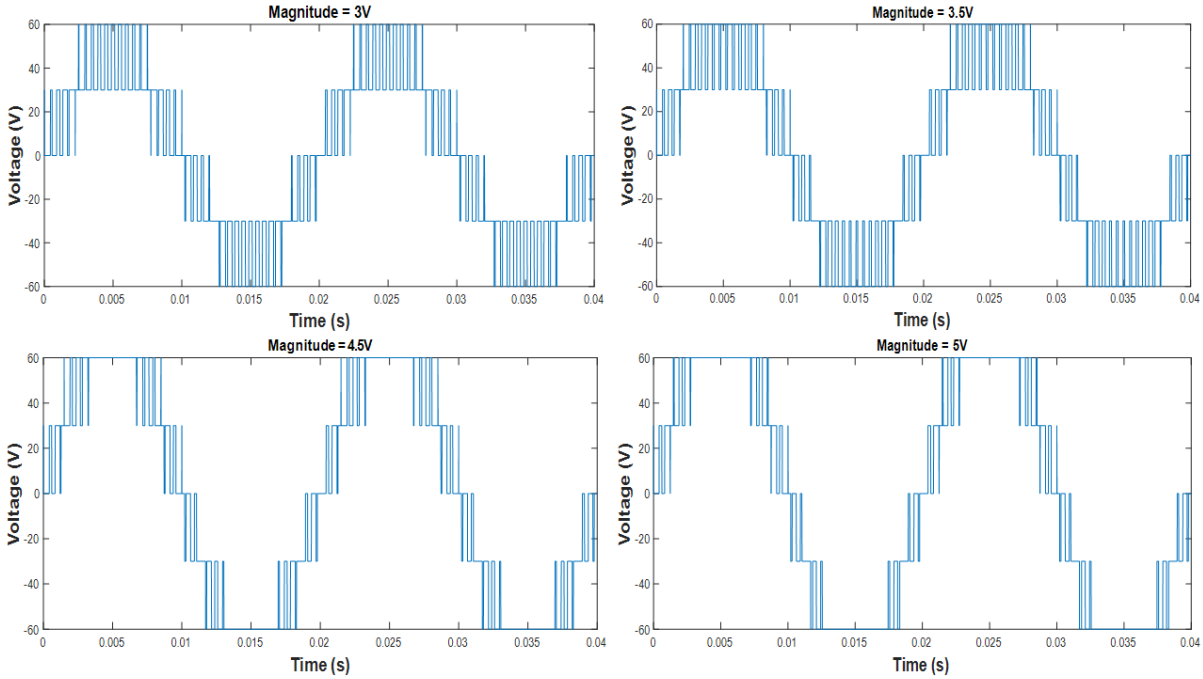


Figure 3.8 Simulation of output voltage for different amplitudes of the reference (LS-PWM)

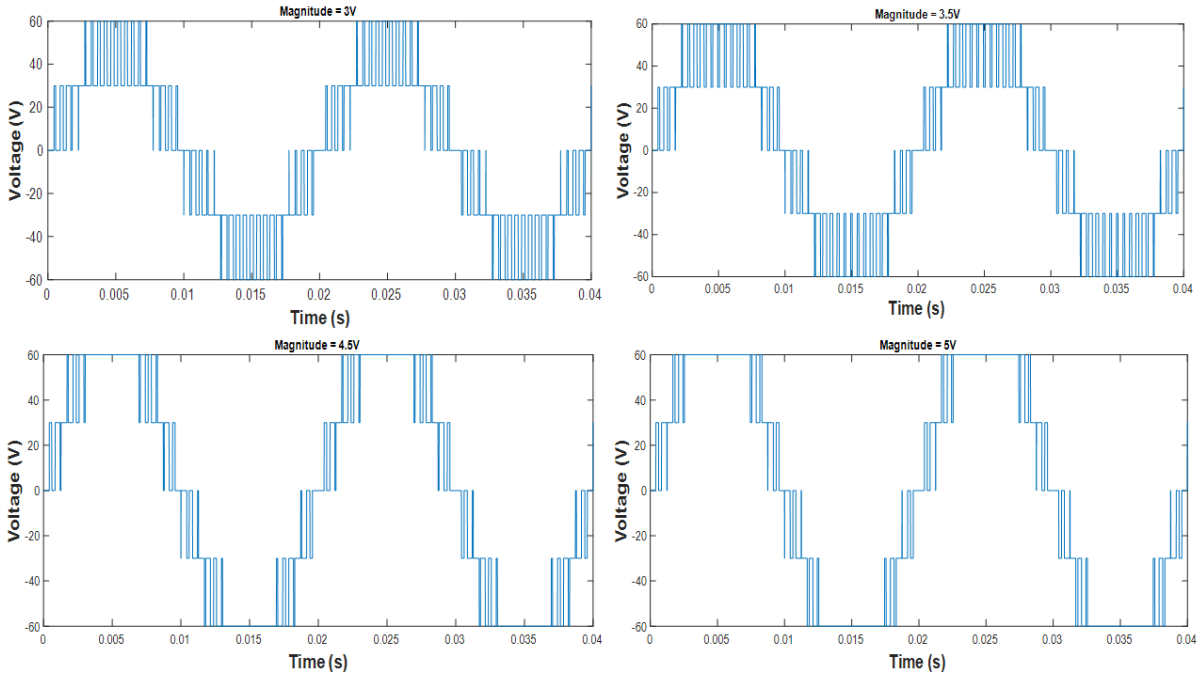


Figure 3.9 simulation of output voltage for different amplitudes of the reference (PS-PWM)

When the magnitude is less than 4V, the voltage pulses are condensed and their number is significant. However, when $A_m$is above 4V, the waveform of the output voltage is closer to a staircase. In addition, the conducting times of all voltage levels are nearly the same for all magnitude except when $A_m = 3.5V$where the conducting times of the lower levels is shortened in favour of the higher level ($\pm 2E$).

Figure 3.10 shows the variation of the THD for different amplitudes of the reference signal.

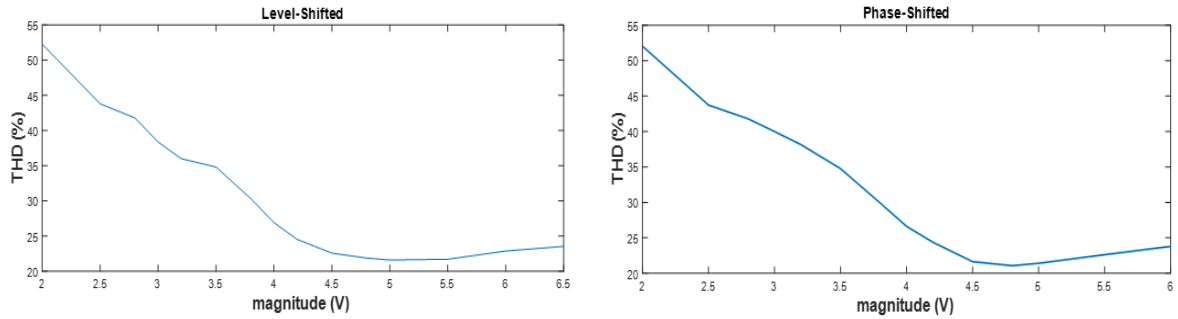


(a) LS-PWM (b) PS-PWM

Figure 3.10 Variation of the THD with respect to the carrier magnitude

For both modulations, it can be observed that increasing the sinusoidal amplitude; which corresponds to decreasing the modulation index, results in the decline of the distortions. The lowermost value attainable by the THD (around 21%) is reached when the amplitude is in the range between 5 and 5.5 Volts.

The variation of the magnitude of the fundamental components of both techniques in accordance to the modulating signal amplitude is shown in Figure 3.11. It can be concluded that for a given amplitude, the fundamental components value for both modulations are almost identical, and by increasing the sinusoidal signals amplitudes, the fundamentals components magnitudes will also increase.

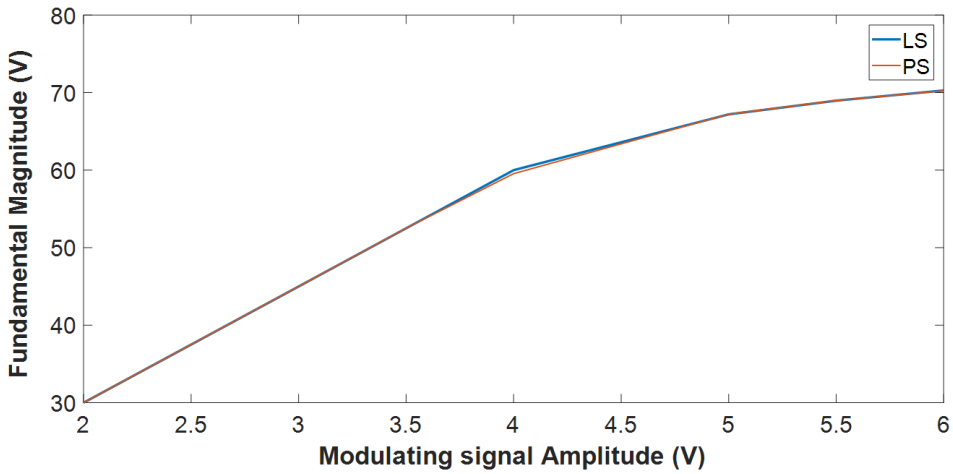


Figure 3.11 Evolution of the fundamental magnitude as function of the carrier amplitude

Eventually, it can be concluded that the value of the modulating index, which assures the best output quality with low THD and a high magnitude of the fundamental component is when the sinusoidal amplitude $A_m$ lies between 4 and 4.5 Volts.

## 3.4.2 Effect of frequency

To examine how the frequency of the reference affects the output voltage, the former has been varied while keeping the other parameters constant. Figure 3.12 shows the inverter

output simulations of four different voltage outputs for different frequencies (20, 100, 200 and 500$Hz$) for LS-PWM.

In this simulation, the triangular frequency is set to $f_{c1} = 2kHz$.

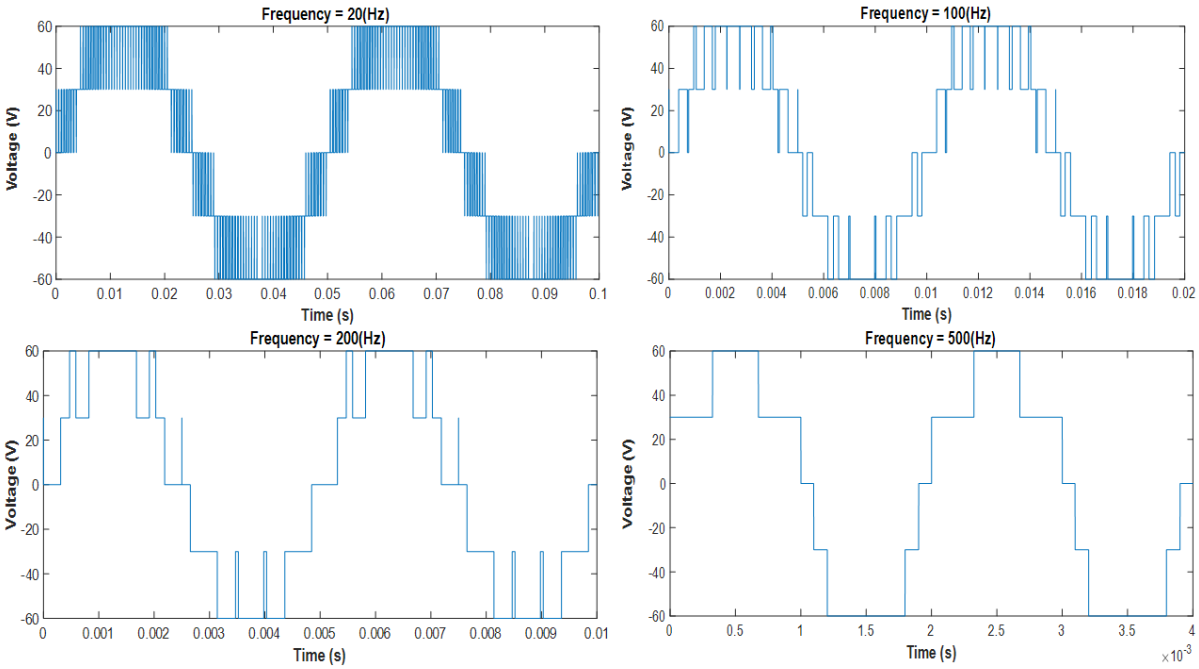


Figure 3.12 Inverter output voltage for different modulating frequency (LS-PWM)

By increasing the frequency, the quality of output signal is lost (reduced), so it can be asserted that lower working frequencies are more apropos to synthesise a pure sinusoidal wave at the inverter output.

In addition to that, the obtained THD values for different frequencies are shown in table 3.1. The frequency was varied in the range between 20Hz and 1kHz, and it can be seen that it moderately affects the distortions as the THD values slightly fluctuate between 27.12% and 22.45%, which represents a variation of 5%.

Table 3.1 THD versus reference frequency for LS-PWM

| Modulating signal frequency (Hz) | Total harmonic distortion (%) |
|---|---|
| 20 | 26.94 |
| 50 | 26.92 |
| 70 | 26.77 |
| 100 | 26.83 |
| 120 | 26.51 |
| 150 | 23.65 |
| 180 | 23.47 |
| 200 | 25.84 |
| 300 | 22.45 |
| 500 | 25.28 |
| 800 | 25.75 |
| 1000 | 27.12 |

In regard to the PS-PWM, figure 3.13 shows the effects of the frequency on the output voltage, where the triangular frequency is set to $f_{c2} = 500Hz$. The chosen values are 20, 70, 100 and $200Hz$.

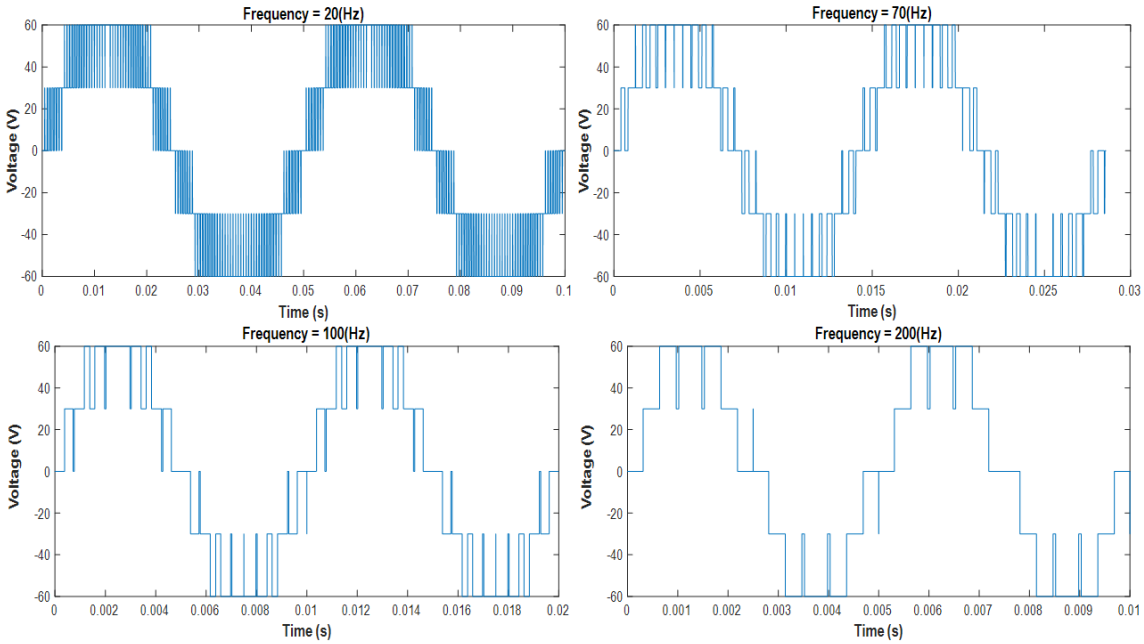


Figure 3.13 Inverter output voltages for different modulating frequency (PS-PWM)

Increasing the frequency has the same effect on this technique as on the LS technique. Moreover, the THD values for the PS technique for different modulating frequencies are shown in table 3.2. As the higher value is 27.33% and the lower is 25.52%, it can be perceived that, for this control strategy, changing the frequency of the sinusoidal signal has not much effect on the distortions, as the variation is less than 2%.

Table 3.2 THD versus reference frequency for PS-PWM

| Modulating signal frequency (Hz) | Total harmonic distortion (%) |
|---|---|
| 20 | 26.87 |
| 50 | 26.62 |
| 70 | 26.96 |
| 100 | 25.52 |
| 150 | 27.33 |
| 200 | 25.83 |
| 250 | 25.43 |

As for the magnitude of the fundamental component, Figure 3.14 depicts the effect of the frequency on both modulations.

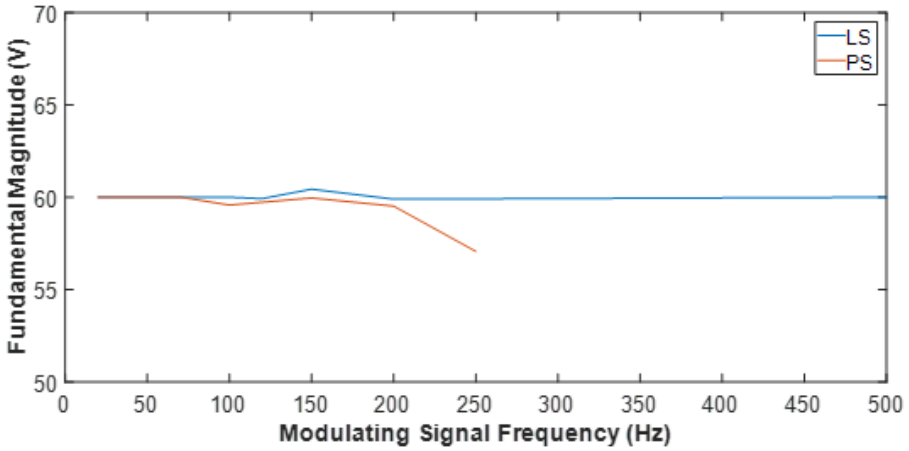


Figure 3.14 Fundamental magnitudes in respect to the frequency

When the frequency is less than 70 Hz, the fundamental components of both control strategies have the same constant magnitude, which is 60V. Although, when the frequency rises, they exhibit a different response to the changing of frequency. While the fundamental magnitude of LS strategy remains steady on the entire spectrum, with minor fluctuations, the other

modulation's magnitude undergoes a steady decrease, where it reaches its lower value around 57 V.

## 3.5 Control of Asynchronous Motor

In this section, the inverter is firstly elaborated to supply an arbitrary RL-load, providing information on the current waveform as well as on the effect of the load. Secondly, it is used to feed an asynchronous motor with low power consumption.

### 3.5.1 Arbitrary RL-load

In this part, an arbitrary three-phase RL-load has been connected at the inverter output. Figure 3.14 shows the circuit configuration of the simulation setup.

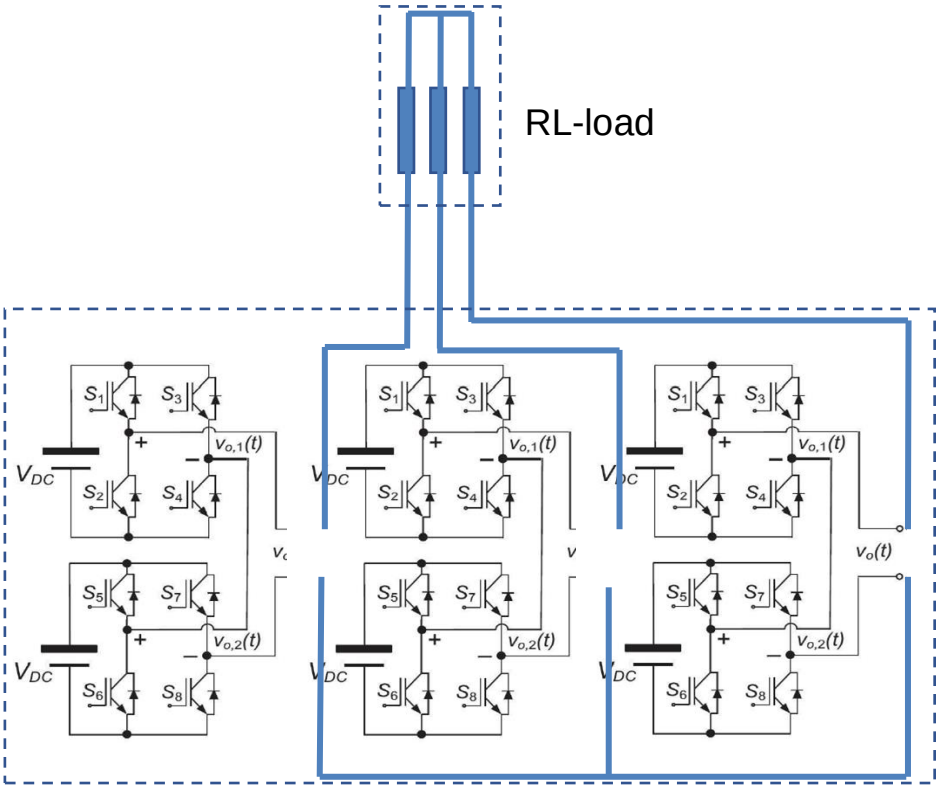


Figure 3.15 RL load supplied by a 3-phase 5-level inverter

Different values of the RL-load have been selected ranging from (R=10 Ω, L=10 mH) to (R=100 Ω, L=10 H). Figure 3.16 illustrates an example of the current waveforms obtained for a fixed resistor (R=10 Ω,) with a low and high value of inductor (L=10 mH and L= 0.5H).

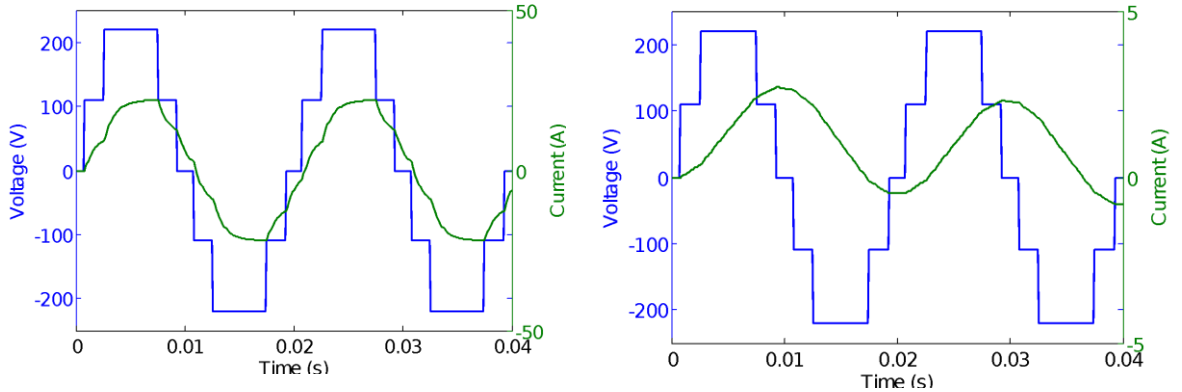


(a) R=10 and L=10mH (b) R=10 and L=0.5H

Figure 3.16 Output voltage and current for different RL-load

From this figure, it is shown that the inductor has a great impact on the quality of the current waveform. The current signal brings closer to a sine with the increase of the inductance value. It is worth noting that staircase conventional control strategy was elaborated in this result. In order to confirm such a result, LS- and PS-PWM techniques were also considered where the obtained results are illustrated, for R=10 and L=0.5H, in Figures 3.17a and 3.17b, respectively.

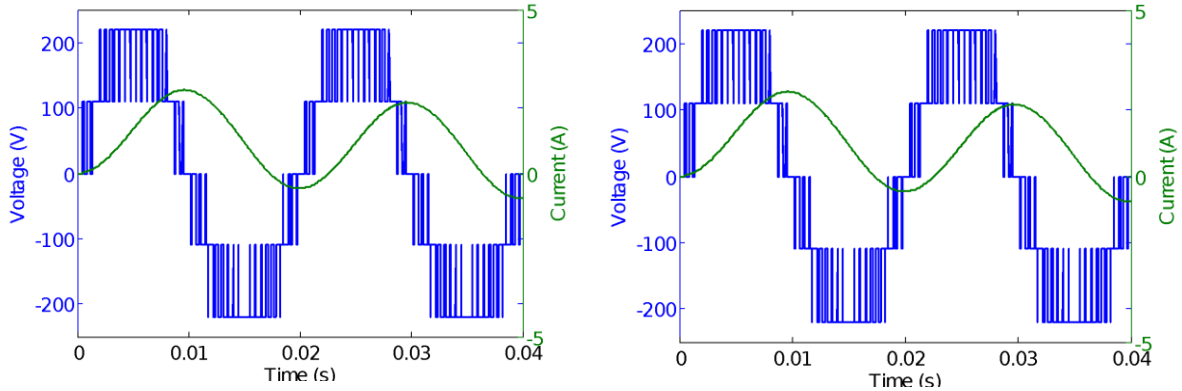


(a) LS-PWM (b) PS-PWM

Figure 3.17 Output voltage and current for R=10 and L=0.5H

Even though the little difference between the output voltages, the current waveforms are practically similar. For the same RL-load, a sinusoidal waveform is obtained for both control techniques. Such findings confirm the previous ascertainment for staircase control strategy.
Moreover, the effect of the RL-load on the THD and current signals are studied in this investigation, and are depicted in figure 3.18.

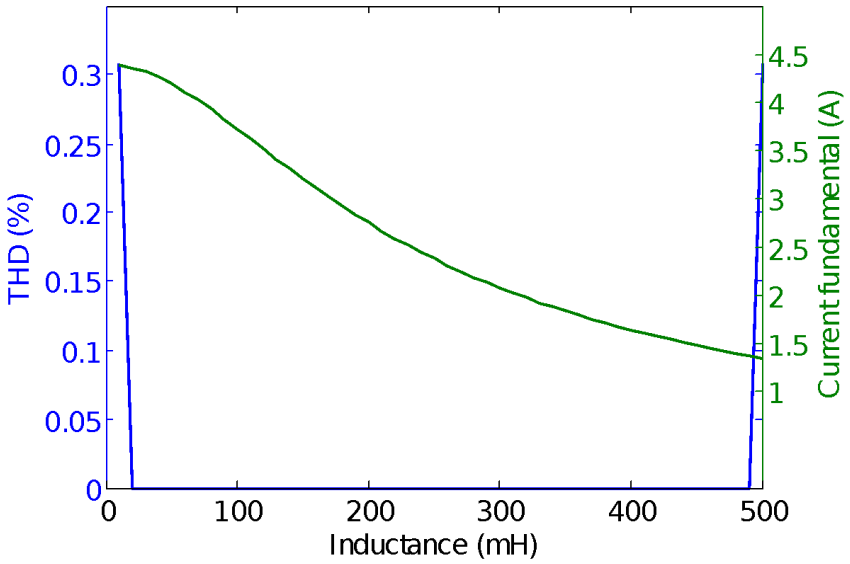


Figure 3.18 Inductance effect on the output current and its harmonic distortions

For low inductance values, the THD values outreach 0.3%. Minor changes in the inductance cause a sharp decline of the distortions until they reach zero, where they remain unchanged. Around 500 mH, the THD experiences a significant rise, where it reaches its peak value at more than 03% for an inductance of 500 mH.

## 3.5.2 Asynchronous Motor

The inverter has been used to supply a three-phase asynchronous motor.
The motor in question is characterized by the electrical and mechanical parameters given in table 3.3.

Table 3.3 The asynchronous machine parameters

| **Electrical parameters** | | **mechanical parameters** | |
|---|---|---|---|
| stator resistance | $r_s$= 0.345 Ω | moment of inertia | J = 0.075 kg.m^2 |
| rotor resistance | $r_r$= 0.816 Ω | number of poles | P = 4 |
| stator reactance | $Xl_s$= 0.754 H | resistive torque | $\tau$= 35.7 N.m |
| rotor reactance | $Xl_r$= 0.754 H | | |
| mutual reactance | XM = 26.13 H | | |

The motor has been controlled in an open loop, which means that no feedback has been considered for the purpose of the motor control. Figure 3.19 provides a representation of the

electrical circuit. In this figure, the Photovoltaic panels are the main source of electrical energy, with the presence of batteries to store the energy and provide continuous power to the load. They are all connected to a charge controller, which controls the rate at which the current is added or drawn from the batteries. In addition, the controller supplies the inverter, which in turn, is coupled with the asynchronous machine.

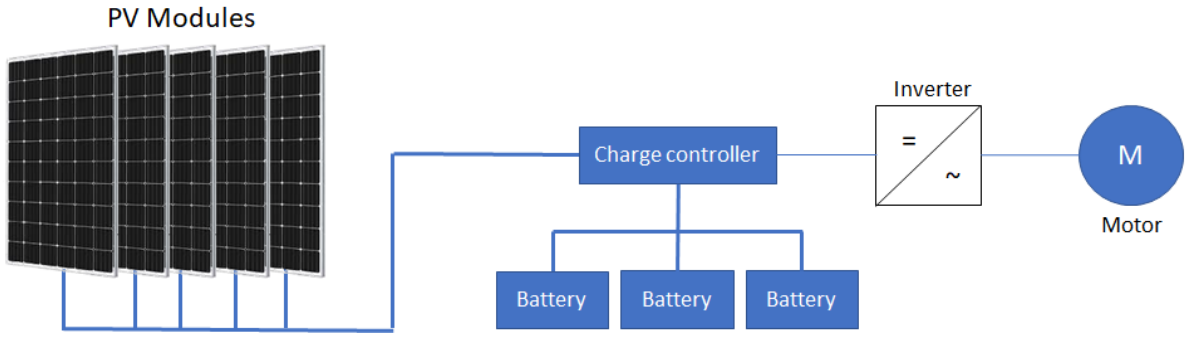


Figure 3.19 Asynchronous machine driven by an inverter in an open loop circuit

Figure 3.20 shows the simulation results of the variables (current, speed and torque) of the asynchronous motor coupled with an inverter in an open loop circuit.

First, the machine variables pass by a transitory phase, where the current oscillates between its maximal and minimal values, the motor speed rises steadily and the torque fluctuates. Then, after the transitory phase, all the variables plateau. The current and torque are null, while the speed peaks at 157 rad/s.

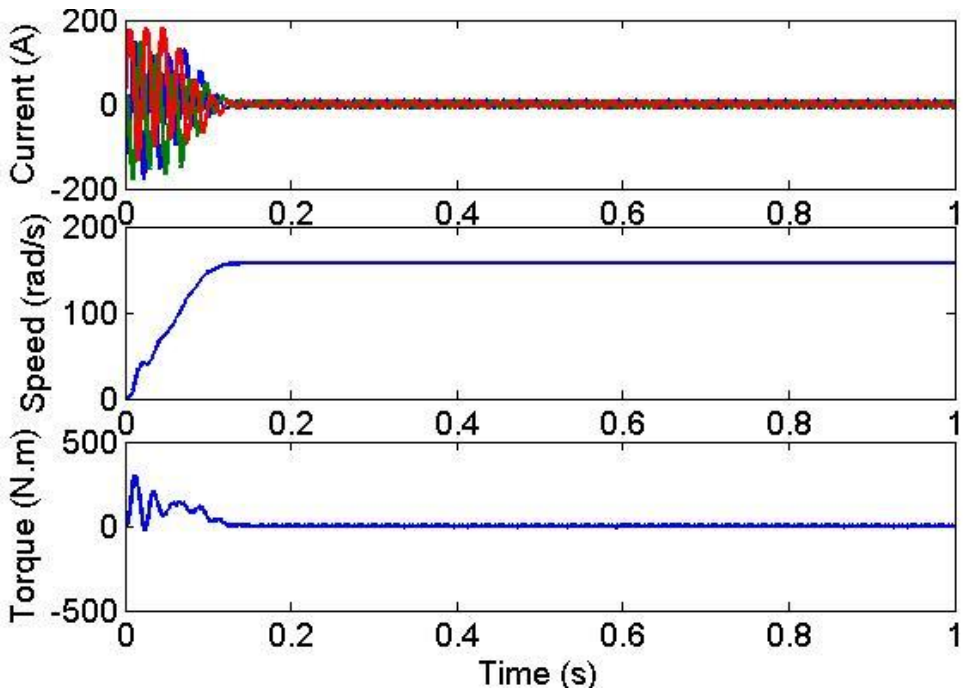


Figure 3.20 Variation of motor parameters over time

When a resistive torque is applied (a load is connected) to the motor during the period 0.5 to 0.7 seconds, the current oscillates back and forth around its steady state. Furthermore, the motor

speed drops slightly, contrary to the torque, which rises faintly. When the load is disconnected, all parameters are back at their normal states, as it is depicted in figure 3.21

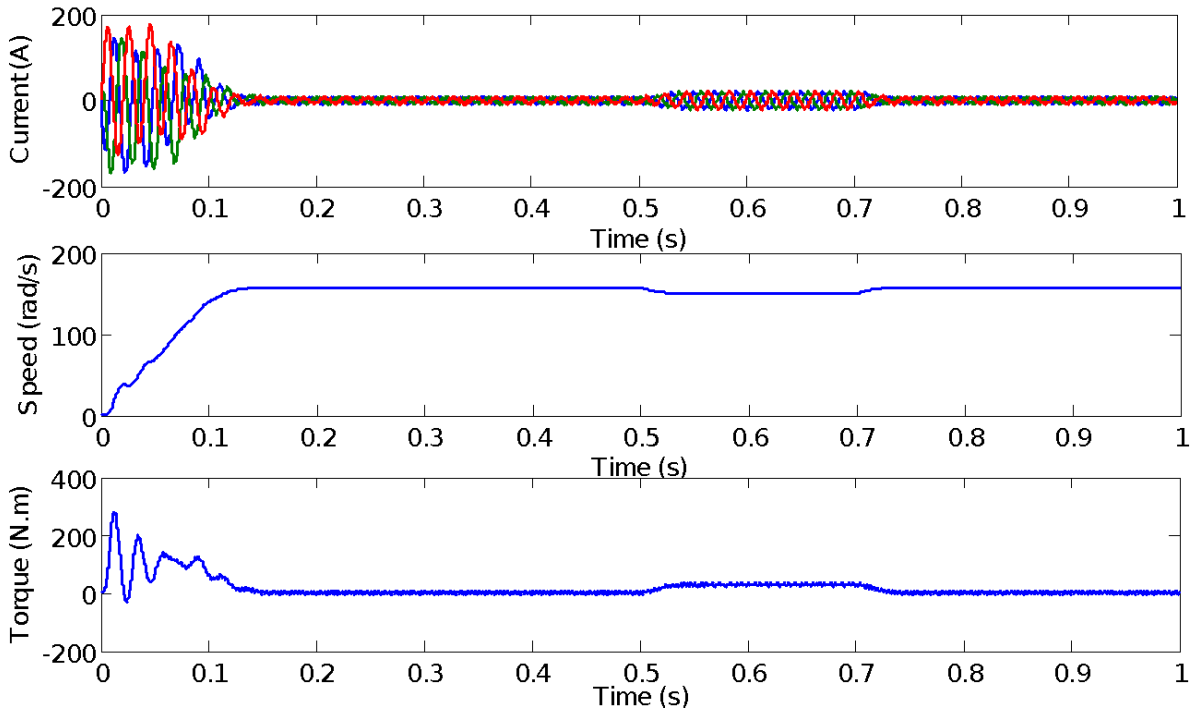


Figure 3.21 Variation of motor parameters when a torque is applied

In regard to what has been stated, some applications need to maintain a constant speed, therefore, a control system is required to adjust the inverter parameters in respect to the variations of the machine speed and torque, as depicted in figure 3.22. This control system can be centred around a microcontroller, such as STM32 family, which controls the inverter's output at real time in accordance to the desired motor speed.

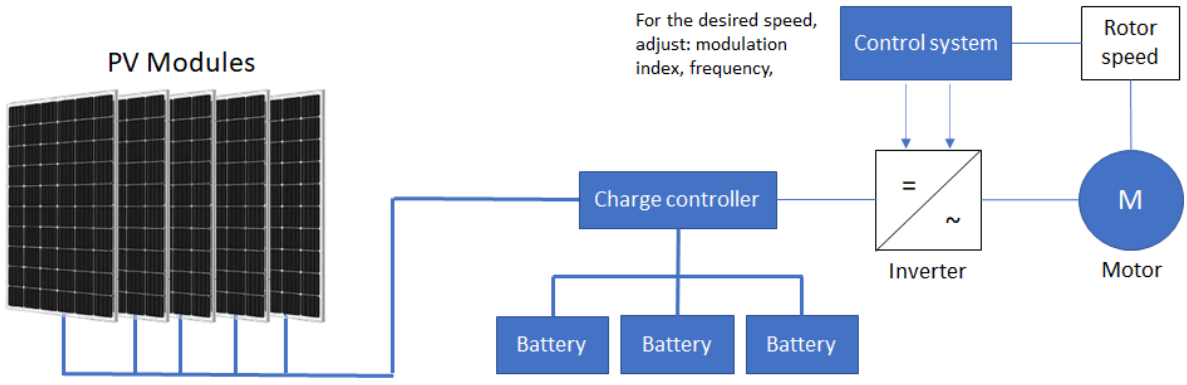


Figure 3.22 Asynchronous machine driven by an inverter in a closed loop circuit

## 3.6 Conclusion

Simulations of an asynchronous motor supplied by a multilevel voltage inverter were conducted in this chapter. Five-level symmetrical three-phase cascaded H-bridge is considered where three different strategies have been selected namely; level shifted PWM, phase shifted PWM and staircase technique. From the obtained results, it was observed that the output voltage contained a large number of harmonics in its spectrum for the three mentioned control techniques. These harmonics are characterized by low (respectively high) frequency range, which might require an additional low-frequency (respectively high-frequency) filter for the staircase (respectively LS- and PS-PWM) technique. Ultimately, though the conventional method has a lower total harmonics distortion and a higher fundamental amplitude among the all-discussed techniques, the existing harmonics of the shifting modulations have high orders that are easier to filter using a small-sized filter, thus, the distortions can be further reduced. Secondly, parametric analysis showed that the increasing of the sinusoidal amplitude; which corresponds to decreasing the modulation index, results in the decline of the distortions and the fundamental amplitude alike. Moreover, changing the switching frequency has not much effect on the distortions, as the variation is less than 2%. Finally, arbitrary RL-load and asynchronous motor are selected where the voltage and current are visualised. It was found that the inductor has a great impact on the quality of the current waveform. The current signal brings closer to a sine with the increase of the inductance value.

# Chapter 4

# Asynchronous Motor Supplied by 3-phase CHB-MLI: STM32F103 Implementation

## 4.1 Introduction

This chapter deals with the implementation of stm32F1 board to control a three-phase 5-level CHB-MLI used to supply an asynchronous motor. The methodology of the experiments are detailed where the control strategies are presented step by step so that the reader can understand the main principles of the investigation. This work also provides guidance for the control of the multilevel inverter, implementing the STM32 series F1. Experimental results are presented and discussed using different control strategies.

## 4.2 Overview on STM32 Microcontroller

The STM32 is a family of 32-bit microcontrollers developed and manufactured by STMicroelectronics [49] [10]. They are based on Cortex-M families, which represent a group of 32-bit RISC ARM processor cores licenced as an IP by ARM Holdings [50] [10]. The STM32 microcontrollers are grouped into series, each series consist of a Cortex CPU as well as numerous configurable options added by ST. Table 4.1 shows the most-common STM32 series and the ARM cores (CPU) used for each family.

Table 4.1 STM32 series and the corresponding ARM CPU core

| STM32 Series | ARM CPU core |
|---|---|
| F0 | Cortex-M0 |
| G0, L0 | Cortex-M0+ |
| F1, F2, L1 | Cortex-M3 |
| F3, F4, L4 | Cortex-M4F |
| F7, H7 | Cortex-M7F |
| L5 | Cortex-M33F |

### 4.2.1 STM32F10xxx

STM32F10xxx series are a family of microcontrollers centred on Cortex-M3 core. They share several design characteristics and features, but also, have different memory sizes, packages and peripherals [51] [10]. This family can be classified into the following types: Low-, Medium-, High and XL-density devices, plus the connectivity line devices. This classification is based primarily on the flash memory density, but there are distinct features for each sub-family. Table 4.2 gives the memory density range for each sub-family.

Table 4.2 STM32F10xxx series memory range

| **STM32F10xxx devices** | **Flash memory range in Kbytes** |
|---|---|
| Low-density | 16 - 32 |
| Medium-density | 64 - 128 |
| High-density | 256 - 512 |
| XL-density | 768 - 1000 |
| Connectivity-line devices | - |

The main system of the STM32F10xxx series consists of the Cortex-M3 processor core and its buses (ICode and DCode) which are used to fetch the instructions and data respectively, internal SRAM, internal flash memory and general-purpose Direct memory access units (DMA). The core (via the system bus) and the DMA are connected to the BusMatrix, this latter manages the access arbitration between them. Besides, more peripherals are integrated into the MC chip. The shared peripherals among the STM32F10 serie are:

- Real-Time Clock (RCC),
- Analogue-to-Digital Converters (ADC),
- Digital-to-Analogue Converters (DAC),
- Timers (TIM),
- General-Purpose Input/Output (GPIO),
- Alternate-Function Input/Output (AFIO),
- Communication interfaces such as: UART, I²C, SPI and USB.
- Control Area Network (CAN),
- Watchdog.

The peripherals are connected to two buses called the Advanced Peripheral Buses (APB1 and APB2), which are connected to the APB-AHB bridges. The main system can access this peripheral through the Advanced High-performance Bus (AHB). This later is, in turn, connected to the AHB-APB bridges. Moreover, it is worth noting that there are many peripherals that can generate a DMA request. Figure 1.1 is an illustration of the system architecture that is shared between the Low-, Medium and XL-devices of the STM32F10xx series.

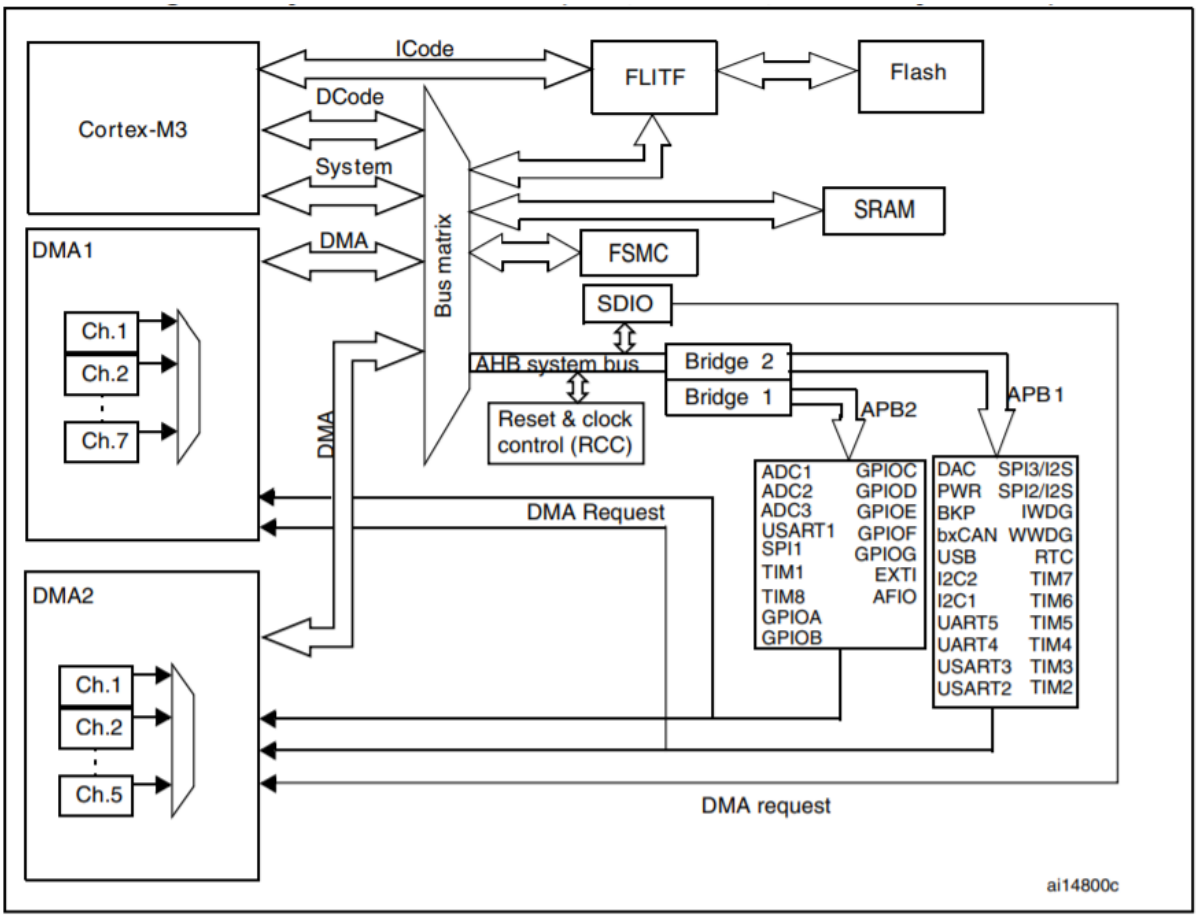


Figure 4.1 STM32F10xxx System architecture [51]

## 4.2.2 STM32F103xx

There are several varieties of this MC, which depends on the packaging (VFQFPN, UFQFPN, BGA, UFBGA or LQFP), number of pins (36, 48, 64 or 100) and the memory size (64 or 128 Kbytes). STM32F103 is driven by an internal clock with a maximum frequency of 72MHz. The peripherals are connected to either one of the APBs, and their clock and control signals supplied through one of these buses [52], as depicted in Figure 1.2. This figure illustrates the entire internal architecture of the STM32F103.

The peripheral clocks are disabled after a reset, so that they must be enabled before being used; achieved by configuring the proper bits of each peripheral in RCC_APB1ENR and RCC_APB2ENR Registers. Furthermore, the APB2 bus operates at full speed, but the APB1 is limited to 36MHz. In addition, the MC has 20 Kbytes of SRMA, and the programme memory, data memory, Registers and I/O ports are all organised within the same linear address space. In the remaining parts of this section, the peripheral units that were used to develop the application are emphasised.

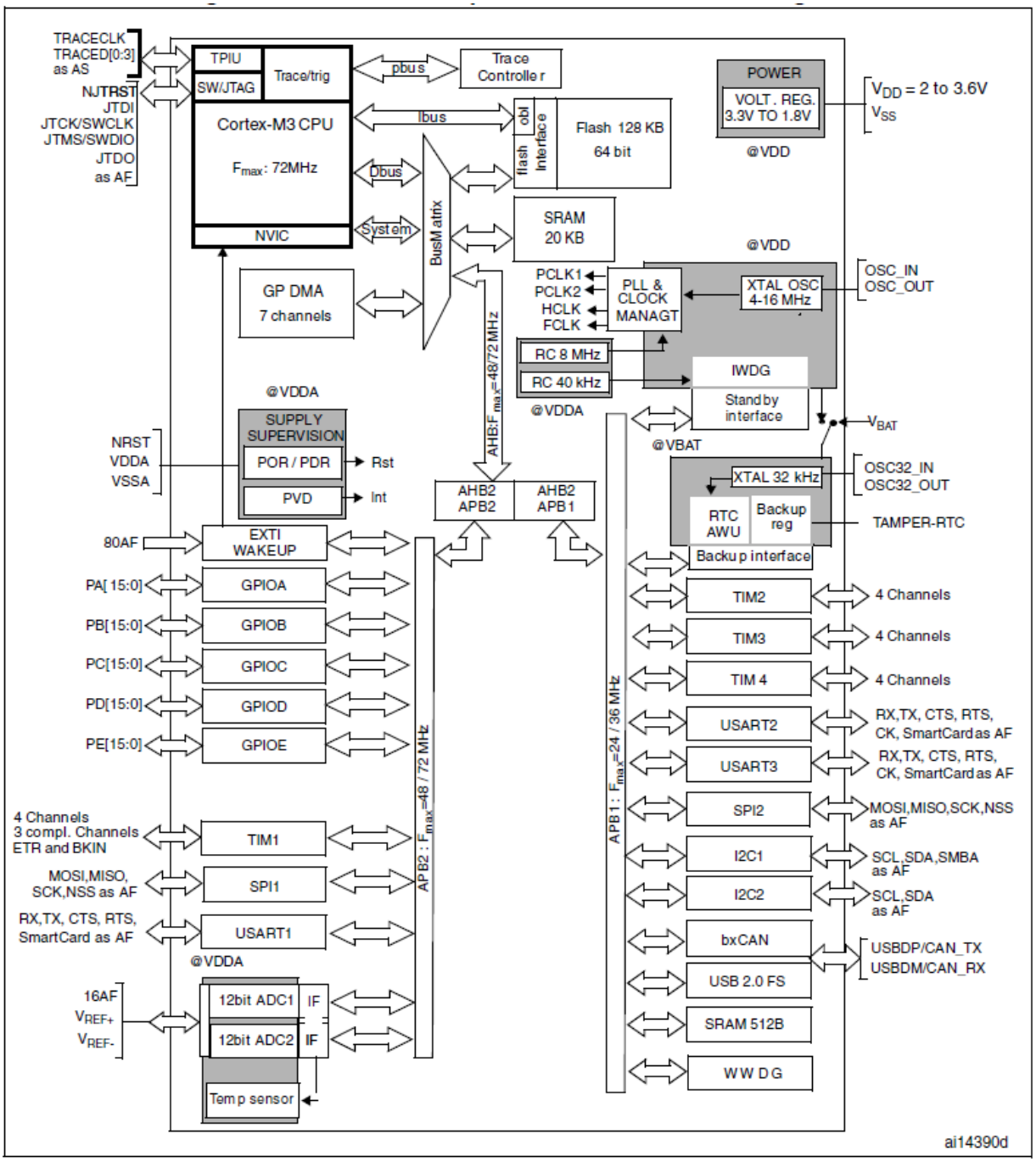


Figure 4.2 Internal architecture of STM32F103xx [52]

## 4.2.2.1 General-Purpose Input/Output

Depending on the integrated-circuit package, there are up to 80 inputs/outputs, divided into four ports labelled from A to E. Also, the I/Os are 5 volts tolerant and may be shared with other peripherals (e.g., ADC). When they are shared by the other peripheral, they are called Alternate-function Inputs/Outputs (AFIO), otherwise, they are called General-purpose Inputs/Outputs (GPIO). It is important to note that the ports must be configured either as GPIOs

or as AFIOs and they can be further configured by software into several modes, as shown in table 4.3.

Table 4.3 Configuration and modes of the Ports

| Configuration | Mode |
|---|---|
| Output | Push-Pull |
| | Open-Drain |
| Alternate Function | Push-Pull |
| | Open-Drain |
| Input | Analogue |
| | Input floating |
| | Input pull-up |
| | Input pull-down |

Among the registers that can assure the configuration and utilisation of the ports, there are two configuration registers (GPIOx_CRL and GPIOx_CRH). These configurations are used to configure the direction and the mode of each pin, two data Registers (GPIOx_IDR and GPIO_xODR) that are used to read the output data as well as to set and reset the pins, and AFIOx_MAPR that can remap the pins to the input or output channels of the peripherals.

### 4.2.2.2 Timers

Timers embedded by STM32 microcontrollers share the same backbone structure and they differ only on the level of features embedded by each one timer. They are classified into four categories [53] :

- general purpose timers,
- advanced timers,
- basic timers,
- lite configuration timers.

The STM32F103 has four timers that are labelled TIMx where x is the timer number [52]. Among these timers, there are an advanced timer and three general purpose timers. As figure 4.3 depicts, a general-purpose timer consists of a 16-bit auto reload counter driven by a Prescaler, it can count up, down or both up and down, and it is able to generate update events

(when there is an over- or underflow) as well as trigger interrupts and DMA requests depending on the configuration of the control Register (TIMx_CR1).
STM32 timers share the preload feature; which refers to the duplication of some of their registers. One instance is called the Preload Register, which the programmer can access and modify, and its content is transferred to the other instance is called the shadow Register, which is inaccessible [53]. This feature allows the synchronisation between the update events and the modification of the content of those Registers.

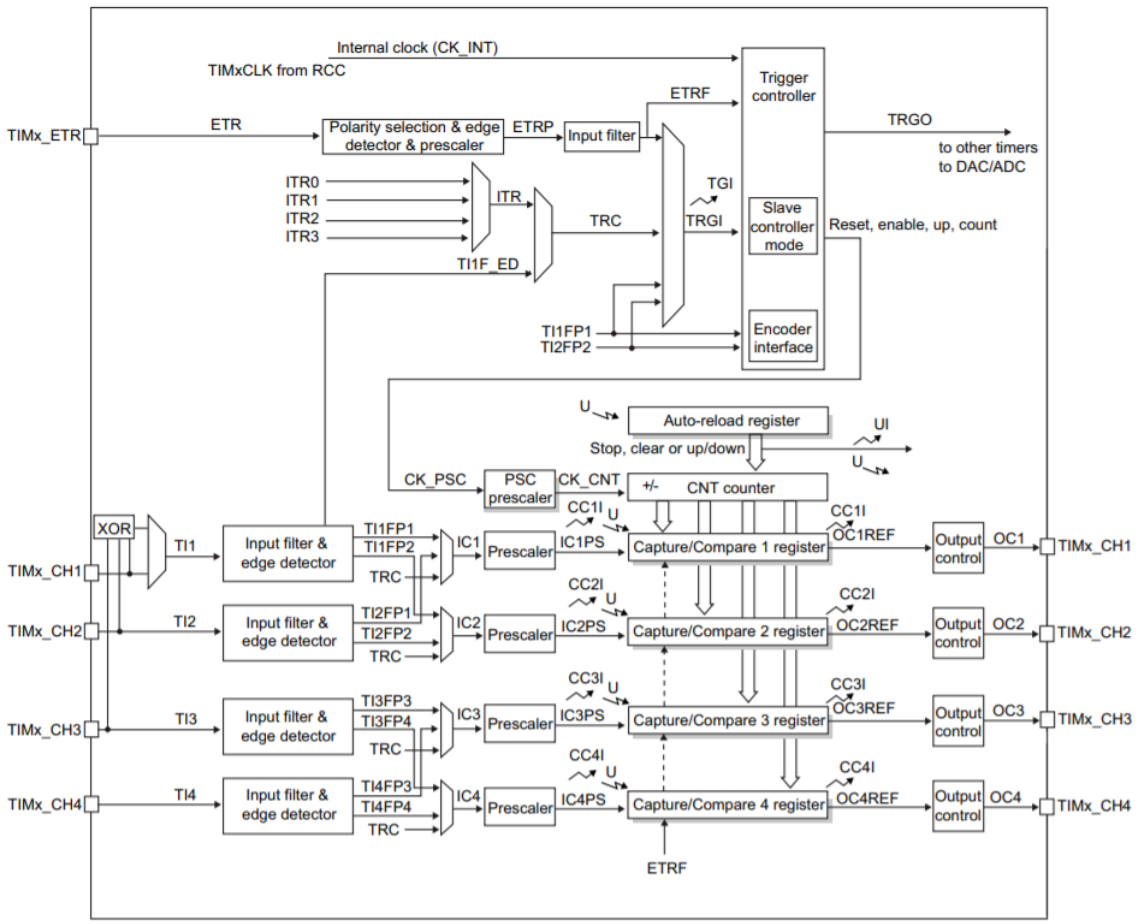


Figure 4.3 General-purpose timer block diagram [53]

Additionally, the timers do not share any resources and each one have four independent channels that can be configured and used for different purpose such as:

- Input Capture (IC),
- Output Compare (OC),
- PWM generation,
- internally or externally triggered.

## 4.2.2.3 Nested Vectored Interrupt Controller

The NVIC is an on-chip controller that is used to handle and manage all interrupts and exceptions. There are 68 interrupt lines with 16 programmable priority levels. A higher level corresponds to a lower priority, so level 0 is the highest interrupt priority [54].

The vector table, which a fragment of it is shown in Table 4.4, contains the address of the interrupt service routines (ISR or IRQ, which stands for Interrupt Request) along with each interrupt number, and it is used to prioritise the interrupt, though, the priority can be re-configured.
When an interrupt occurs, the following steps are executed:

- The execution of the current task is suspended.
- The current state of the programme is preserved.
- The NVIC initiates a call to that vector table, locates the interrupt number that has occurred, picks the address of the service routine from the vector table.
- After that, the service corresponding to the interrupt is executed.
- The state of the program is retained and normal execution of the task is resumed.

Table 4.4 Fragment of the vector table for STM32F1 [53]

| Position | Priority | Type of priority | Acronym | Description | Address |
|---|---|---|---|---|---|
| 14 | 21 | settable | DMA1_Channel4 | DMA1 Channel4 global interrupt | 0x0000_0078 |
| 15 | 22 | settable | DMA1_Channel5 | DMA1 Channel5 global interrupt | 0x0000_007C |
| 16 | 23 | settable | DMA1_Channel6 | DMA1 Channel6 global interrupt | 0x0000_0080 |
| 17 | 24 | settable | DMA1_Channel7 | DMA1 Channel7 global interrupt | 0x0000_0084 |
| 18 | 25 | settable | ADC1_2 | ADC1 and ADC2 global interrupt | 0x0000_0088 |
| 19 | 26 | settable | USB_HP_CAN_ TX | USB High Priority or CAN TX interrupts | 0x0000_008C |
| 20 | 27 | settable | USB_LP_CAN_ RX0 | USB Low Priority or CAN RX0 interrupts | 0x0000_0090 |
| 21 | 28 | settable | CAN_RX1 | CAN RX1 interrupt | 0x0000_0094 |
| 22 | 29 | settable | CAN_SCE | CAN SCE interrupt | 0x0000_0098 |
| 23 | 30 | settable | EXTI9_5 | EXTI Line[9:5] interrupts | 0x0000_009C |
| 24 | 31 | settable | TIM1_BRK | TIM1 Break interrupt | 0x0000_00A0 |
| 25 | 32 | settable | TIM1_UP | TIM1 Update interrupt | 0x0000_00A4 |

### 4.2.3 STM32F103 Nucleo-board

ST offers a wide range of boards, which are low-cost and easy-to-use development platforms used to evaluate and start a development with STM32 [55] [10]. These boards can be based on various STM32 microcontroller series, such as STM32F1, STM32F4 or STM32L4. The most-common boards are: Nucleo-, Discovery- and Evaluation-board.

It should be noted that ST has a codification for its Nucleo-boards given by STM32XXYYRT. The explanation of this codification is given in Table 4.5.

Table 4.5 STM32 Nucleo-board codification explanation [56]

| NUCLEO-XXYYRT | Description | Example: NUCLEO-L452RE |
|---|---|---|
| XX | MCU series in STM32 Arm Cortex MCUs | STM32L4 Series |
| YY | STM32 product line in the series | STM32L452 |
| R | STM32 package pin count | 64 pins |
| T | STM32 Flash memory size:<br>– 8 for 64 Kbytes<br>– B for 128 Kbytes<br>– C for 256 Kbytes<br>– E for 512 Kbytes<br>– G for 1 Mbyte<br>– Z for 192 Kbytes | 512 Kbytes |

The Nucleo-boards have a STM32 microcontroller in LQFP64 package and offers additional features, such as:

- Three LEDs,
- two Push-Buttons,
- Pin headers extension to access all the STM32 MC I/Os,
- Flexible board power supply.

Additionally, the Nucleo-board has on-board SV-LINK/V2-1 which is an in-circuit debugger and programmer used with STM32 products and allows for interactive debugging of the programme.

In this project, The F103RB-Nucleo is used for the implementation. As its name indicates, it has an STM32F103 microcontroller in LQFP64 package, 64 pins and 128 Kbytes of flash memory. It integrates the ST-LINK/V2-1 debugger and programmer and comes with the comprehensive free software libraries and examples [56]. Moreover, the board offers two types of extension connectors, illustrated in figure 4.4. The first set are female connectors (CN5, CN6, CN8 and CN9) compatible with ARDUINO standard and most of the shields designed for it, while the other set is called The ST morpho connector, which consists in male pin headers (CN7 and CN10) accessible on both sides of the board.

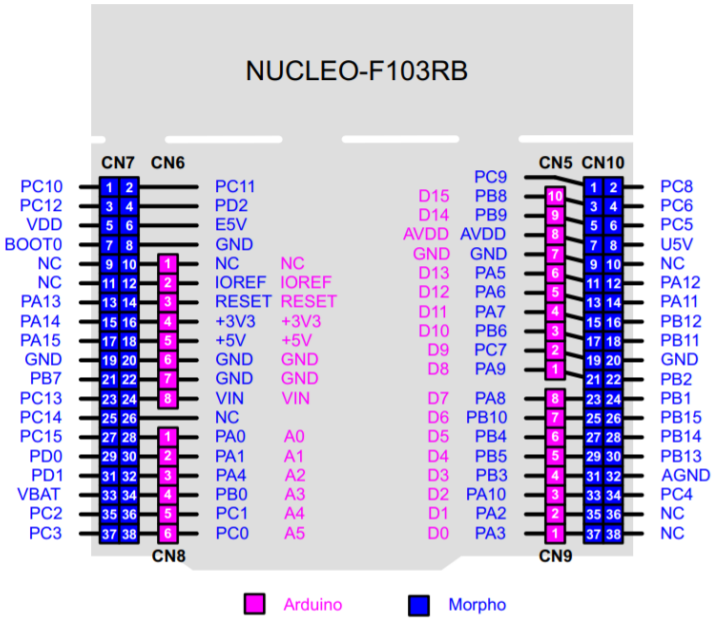


Figure 4.4 Extension connectors for F103RB-Nucleo board [56]

### 4.2.4 Software and programming

The system Workbench toolchain, called SW4STM32, used to build and debug the applications. It is a free multi-OS software development environment based on the integrated development environment Eclipse, which has been built by the service company AC6 [49] [10]. The SW4STM32 supports the full range of STM32 microcontrollers and it offers the following features, among others:

- GCC C/C++ Compiler,
- GDB-based debugger,
- ST-LINK support,
- multiple OS support.

In addition, there is comprehensive support for STM32 boards (including the Nucleo-board), as well as STM32 firmware that provides examples, applications and demonstrations [55]. Standard Peripheral Library and Hal are the firmware packages offered by ST which are intended to facilitate the programming and the debugging processes. The former is a package of libraries that encompass several pre-built and defined functions, structures and data-types which provide an abstraction layer for the developers.
Figure 4.5 shows the user interface of Eclipse IDE together with a brief description about the most important folders that contain all the necessary files to run the programme.

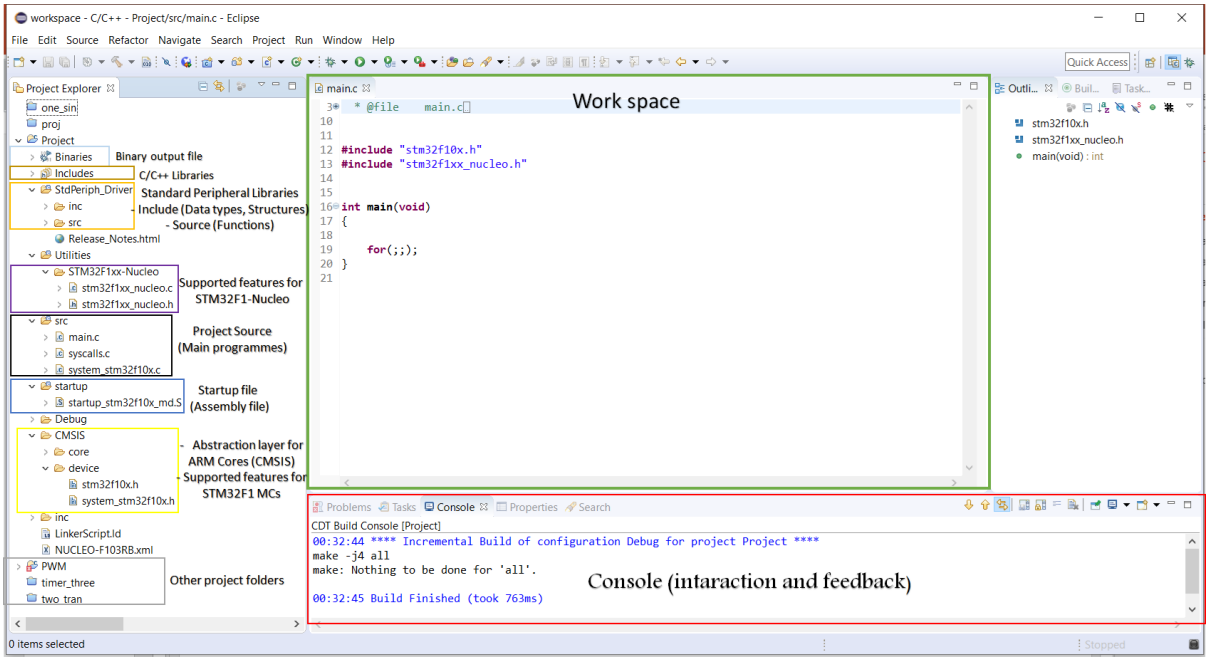


Figure 4.5 Eclipse user interface and explanations of some features

## 4.3 Experimental Setup

Figure 4.6 illustrates the experimental setup used for controlling a multilevel inverter to drive a three-phase asynchronous machine.

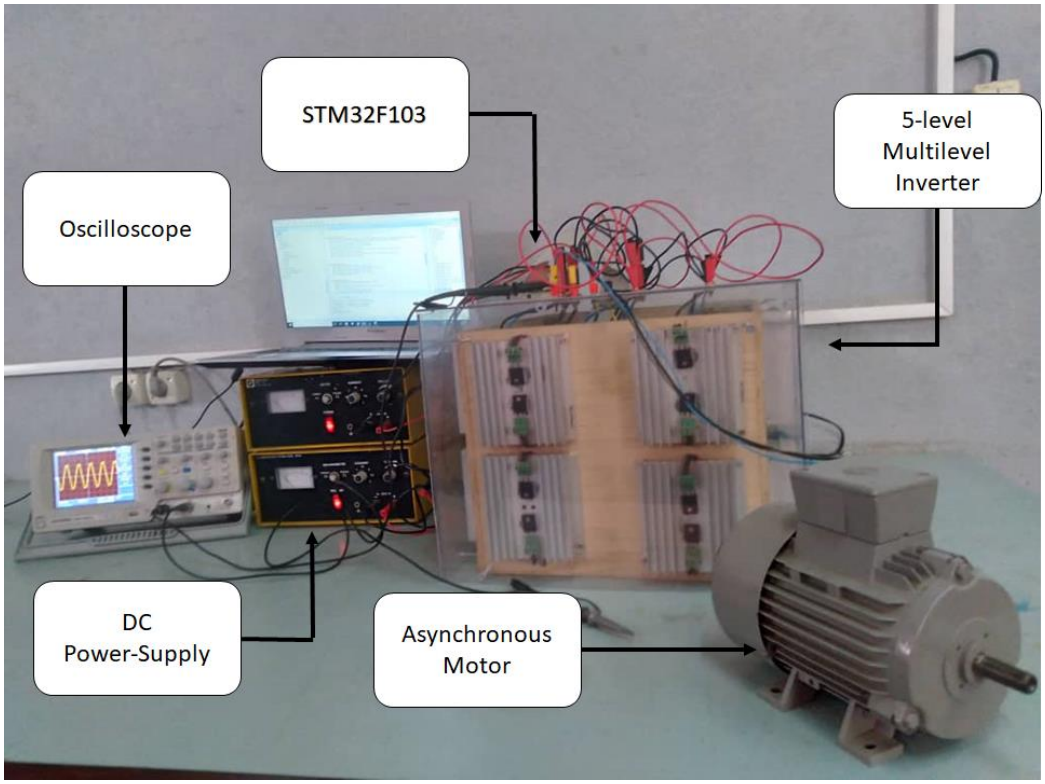


Figure 4.6 Experimental setup

The Multilevel inverter used for this experiment is a three-phase five-level inverter of Cascade H-bridge topology, which was constructed by Bounabi et *al.* [11] as part of his Ph.D. thesis. It is powered by two DC sources of 5V, each source is connected to the three phases of each inverter's cell.

STM32F103RB Nucleo-board is used to control the states of the 12 switches of the inverter. The board is powered by a laptop via an USB cable (A to mini-B). On the hand, the motor phases are connected to the inverter output voltages.

Finally, a digital storage oscilloscope is used to record and display the desired parameters such as the output voltage and inverter currents. This oscilloscope is a GwINSTEK GDS-1052-U, which has a bandwidth of $50\ MHz$with 2 input channels and a sampling frequency of $25\ GSa/s$. It allows us to detect high frequency components within the recorded signal [57].

## 4.4 Experimental Results and Discussion

The experiment involves the implementation of the phase- and level-shifted pulse width modulation techniques on the STM microcontroller. Based on the principles of these schemes, which were discussed in previous chapters, the microcontroller has been programmed to generate modulated pulses at designated output pins.

For both techniques, the frequency of the sinusoidal reference waveform is $50\ Hz$, while the sampling frequency is set to $100\ kHz$. However, different triangular frequencies were set for each technique ($500\ Hz$ for PS and $1\ kHz$for LS). The output pins are then connected to the two channels of the oscilloscope, and the resulting pulses for the Phase- and Level-shifted PWM, which were displayed on the oscilloscope, are shown in figure 4.7 and figure 4.8, respectively.

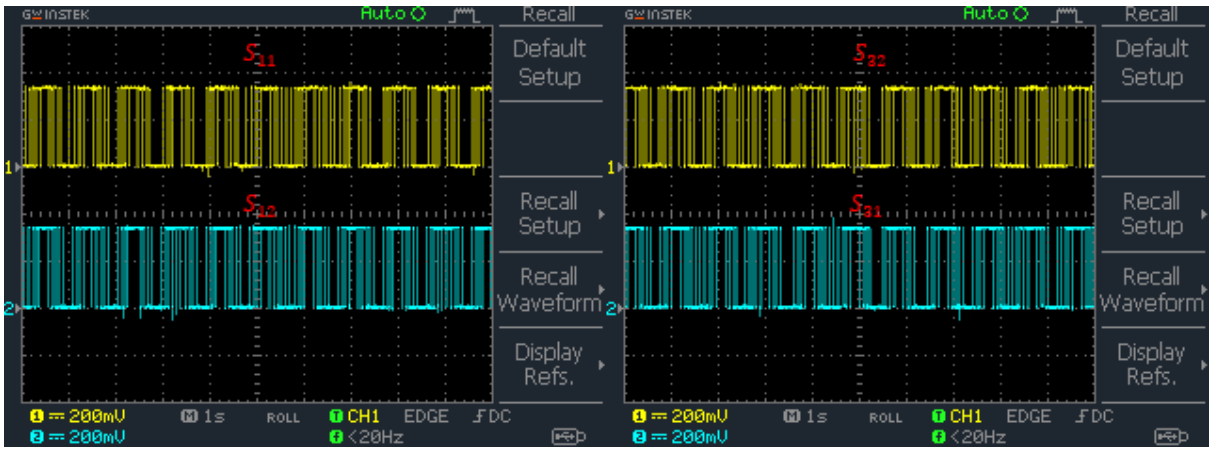


Figure 4.7 LS-PWM experimental results

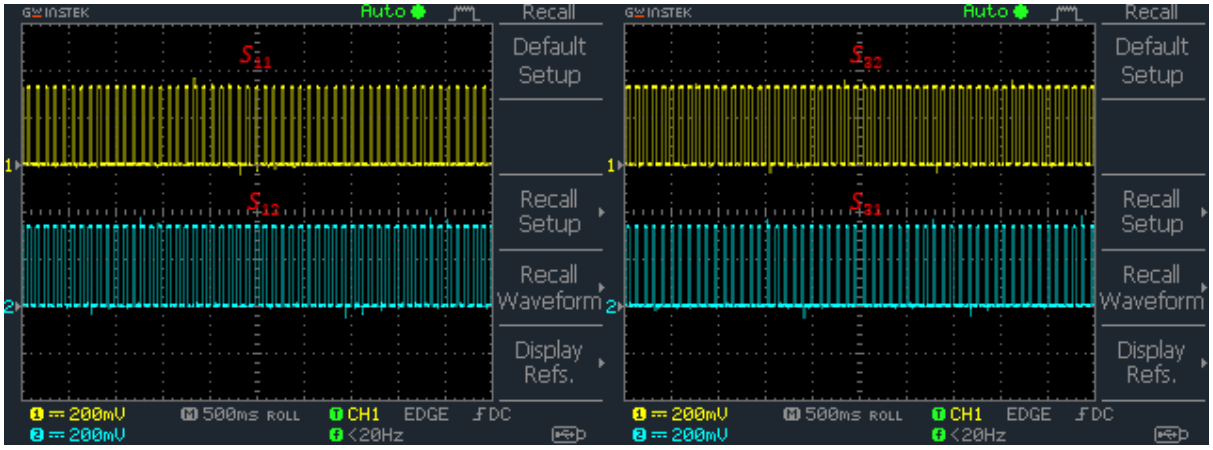


Figure 4.8 PS-PWM experimental results

In both experiments in figures 4.7 and 4.8, one can see that the conduction times of the upper cell switches ($S_{11}$ and $S_{31}$) of the inverter are shorter than that of the switches of the lower cell ($S_{12}$ and $S_{32}$). This is accountable, since the $S_{12}$ and $S_{32}$ are expected to generate the first level of the output voltage ($\pm E$), which have a longer period in contrast to the period of the higher level ($\pm 2E$), which is produced by the upper cell switches.
These resulting modulated pulses are then used as controlling signals for the invrter's gates. The board outputs are connected to the control input of MLI, and the synthesised output voltages, between a phase and the ground, are shown in figure 4.9a and 4.9b.

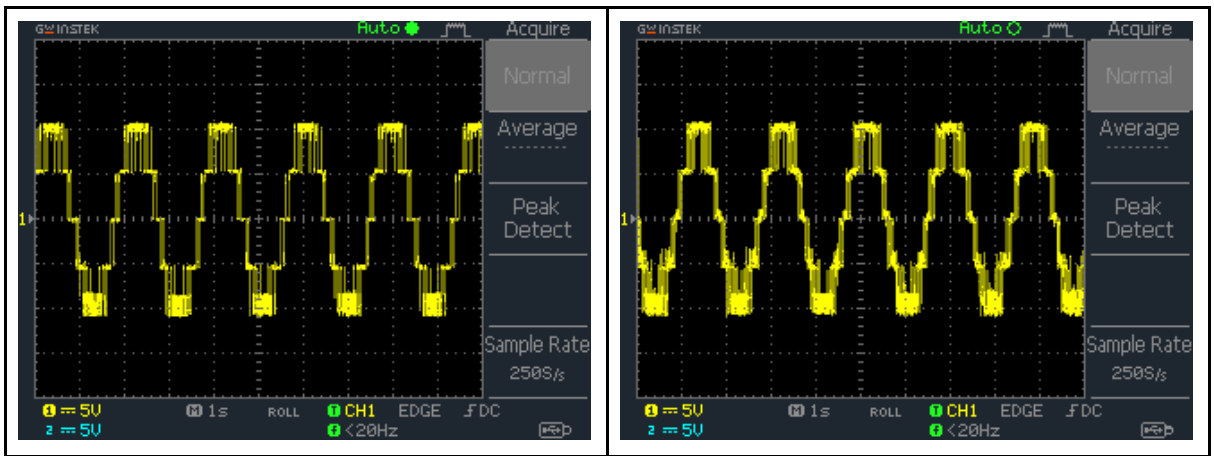


(a) LS-PWM | (b) PS-PWM

Figure 4.9 Measured phase-to-neutral output voltage of 5-level CHB-MLI controlled by PWM techniques

For both techniques, the output voltages consist of five levels with a frequency of 50Hz. The peak voltage is 10V, which is double of the DC source (set to 5V for the experiment). The voltage waveform resulted from the Level-Shifted modulation is less dense than the Phase-

Shifted one. This can be interpreted as the IGBTs switching rate of the PS modulation is greater than the LS rate, which begets significant switching losses in the IGBTs, in contrast to LS technique, which has a longer average of ON- and OFF- times.
For the same PWM parameters, Figure 4.10 illustrates the phase-to-phase output voltage of the 5-level CHB-MLI measured for 5V DC sources.

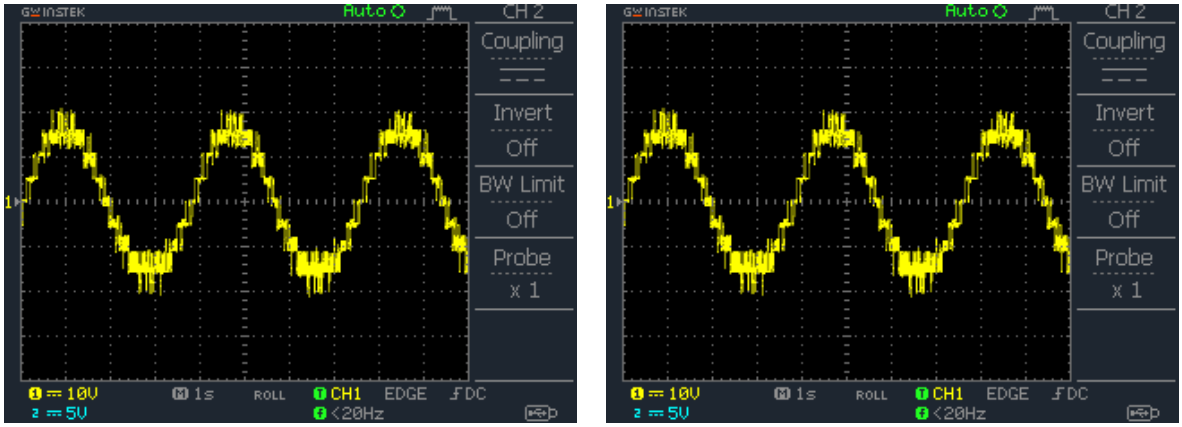


(a) LS-PWM (b) PS-PWM

Figure 4.10 Measured phase-to-phase output voltage of 5-level CHB-MLI controlled by PWM techniques

The phase-to-phase output voltage has more levels than the phase-to-ground voltage, hence, it could reach higher voltage levels, as in this example where it reaches his positive (negative, respectively) peak at 20V (-20V, respectively). Also, the resulting waveform is smoother and flatter, which results in better signals quality, and can be accurately approximated to the desired sinusoidal waveform.
The sampling frequency of the oscilloscope is 50kHz, this frequency is considered for the purpose of exploiting the measured data using MATLAB/Simulink code. The data is collected by the means of the digital oscilloscope, and represents the output voltage of the inverter. The frequency spectrum along with the total harmonics distortion of the collected data are shown in Figure 4.11.

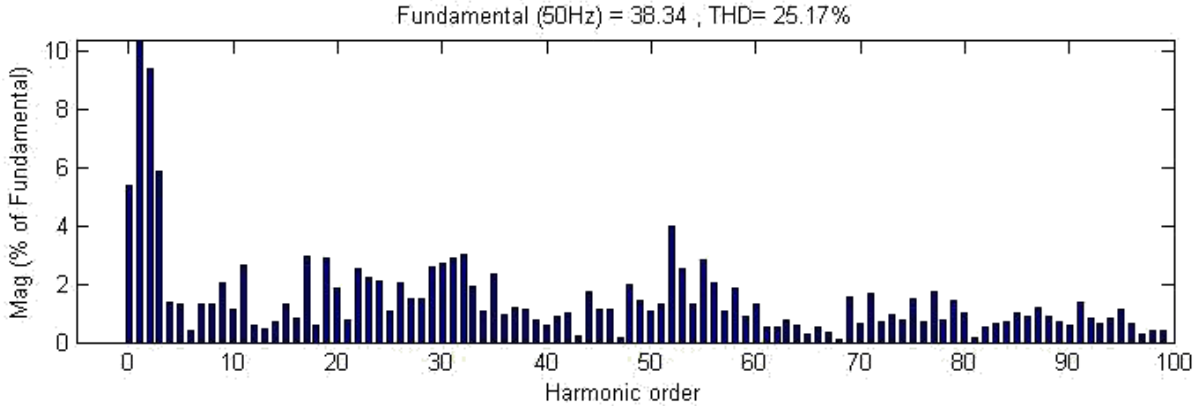


Figure 4.11 Frequency spectrum of the phase-to-phase output voltage

From this figure, it is shown that the harmonics are centred around a multiple of the fundamental frequency. These results are in good accordance with the simulation results presented in chapter 3.
Though the distortions value is seemingly high, by using an RL filter, it can practically be reduced.

## 4.5 Asynchronous motor control

The inverter output is used to supply a resistive load of 100 $\Omega$, as well as for different values of inductance (L =10:100 mH) with a fixed resistor value. The resulting currents are measured, and then illustrated in figures 3.12 and 3.13.

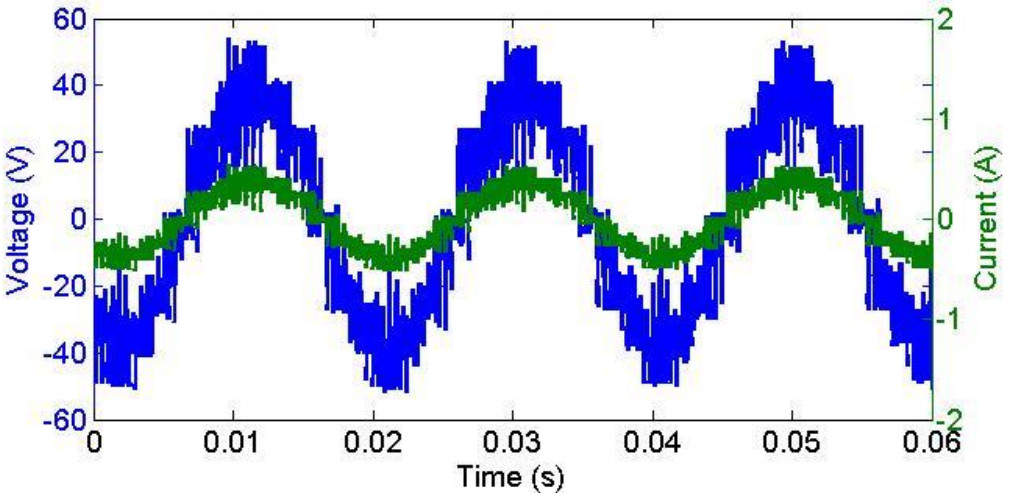

Figure 4.12 Output voltage and measured current for a resistive load

For a resistive load, current has a lot of harmonics. It can be improved by adding an induction to the load, as depicted in figure 4.13

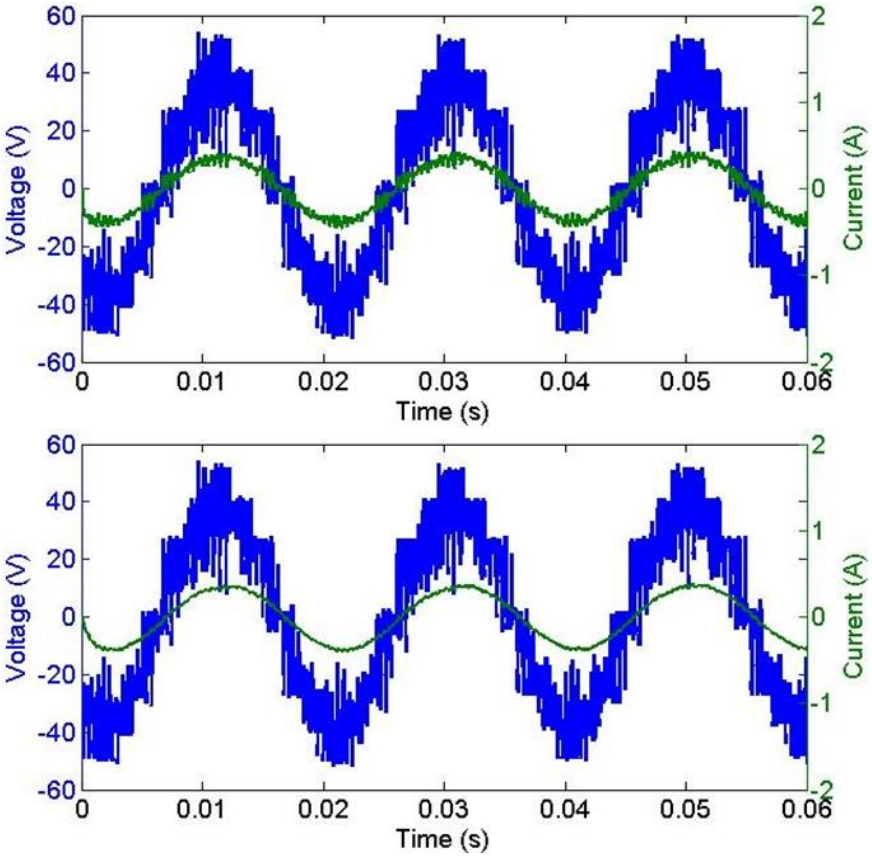

Figure 4.13 The measured currents for an RL for different induction values

By examining the previous figure, it can be seen that the inductor has improved the signal quality. Moreover, the bigger the induction value, the smoother and flatter the current becomes. It can be seen that the current is of sinusoidal nature, and it can reach up to a few hundreds of mAs.

## 4.6 Precautions and Useful Considerations

The experimental process is widely required in order to verify the simulations results. This process provides a solid base that researchers can use to build or advance in this field. However, several obstacles and difficulties have faced the effective conduct of the experiments. These mainly include, material, board coding, and so on. In this light, I have tried to summarise them so that researchers and engineers can get benefits from this experience, avoiding repetitive tasks and time wasting. Among other, they can be summarised in the following points:

- The inverter switches, as well as their corresponding DC inputs and voltage outputs in each phase, were not labelled nor indicated, so tests were performed to assign each switch to its corresponding biasing voltage, commanding-input and output phase.
- The STM32 families of MCUs and boards encompass a wide range of products and associated documentation with a special codification, which can be ambiguous especially for unfamiliar users.
- The two abstraction libraries offered by ST to help the developers with its products, though have many similarities, are non-identical and they do not differ between one and another, but also between STM32 families of MCU within the same library. Therefore,

a thorough examination and documentation are carried out for understanding and using the different syntaxes, data-types, structure and function that each library has to offer.
- The oscilloscope probe should be verified, along with its attenuation ratios.

Moreover, some of these issues have been fixed such as:
- A circuit configuration showing the inputs and output of the inverter,
- All gates have been labelled in both sides, and tickets have been sticked on the corresponding controllable device,
- A short introduction to the STM32 families and their related hardware circuits and software environment.

## 4.7 Conclusion

Within this chapter, I have tried to give a general overview of the STM32 families of Microcontrollers and boards as a guide which introduced the different STM32 products, along with their codifications, and the most important and shared features among these families. In addition, the associated hardware to power and utilise these MCUs was presented. Moreover, the software tools that facilitate the programming and debugging processes were also introduced and briefly explained.

As a second part, I implemented the pulse-width modulation techniques on an STM32F103RB Nucleo-board. Then, I used the generated pulses as gating signals to synthesise the desired inverter output voltage. Finally, the inverter was used to supply different kinds of loads and to drive an asynchronous machine. The experiment results are presented herein and discussed.

Overall, it can be concluded that the obtained results confirmed the previously-obtained simulations, and, though the two modulations manifest nearly in the same way to the parameter variation, PS-PWM has slightly better performance.

# General Conclusion

This work focused on controlling the switches of a three-phase five-level Cascade H-Bridge Multilevel Inverter using a STM32 Microcontroller for the purpose of driving an asynchronous motor. In order to formulate the problem, a general background of the inverter topologies, as well as the modulation strategies used to control the inverter are elaborated. Also, the mathematical modelling of the asynchronous machine is presented.

At first, Phase-Shifted and Level-shifted Pulse Width Modulations techniques were simulated under MATLAB environment. Throughout the entire simulation, the frequencies of the carriers are kept constant (500 Hz for the former and 2 kHz for the later), as well as their magnitudes. As for the sinusoidal reference, its frequency was primarily set to 50 Hz and its magnitude to4 V.The simulations of the inverter output voltage are also performed. Then, these parameters are varied and their effects on the voltage output is examined, as well as the total harmonic distortions. For both modulations, the effect of the modulation index is performed by varying the reference amplitude in the range between 2Vand 6Vwhile keeping the carriers' constant. Both techniques manifest in a similar manner to the variation of the sinusoidal magnitude; that is, the voltage output waveform is more approachable to a sinusoidal waveform when the amplitude is around 4V. This is in accordance with the harmonics distortions values, which decreases form nearly 55%by increasing the magnitude, and reach their minimum value (slightly above20%) at 4.7V. As for the frequency, the modulating signal frequency was varied between 20 Hz and 250 Hz for the PS scheme, and it was concluded that the frequency has insignificant effects on the distortions, as their values were between 27.33%and 25.52%, which represent less than2%.As for the other technique, the obtained THD values varied from 22.45%to 27.12% for modulating frequencies ranging from20 Hz to 1 kHz. Besides, the variations of fundamental components magnitudes in accordance to the reference magnitude is proportional and they are identical. In contrast, the frequency does not affect the fundamental magnitudes of the Phase-shifted that plateau at 60 V, while it affects the fundamental magnitude of the other technique.

Furthermore, the inverter output voltage is used to supply an arbitrary RL-load then an asynchronous machine to get information about the current waveform. For the RL-load(R= 10 Ω and L =0.5mH), the currents are of sinusoidal waveform and can outreach 100 V. Also, for increasing induction values (from 0 mH to 500 mH), the current decreases from its peak value, which is 4 A its lowest point 1.5 A. Regarding the THD, sharp decline or rise are remarked when a minor variation of the induction occurred in the two extremities, otherwise, the THD value is null. In addition to that, the motor parameters, after a transitory phase, are observed to plateau at constant values, nevertheless, a resistive torque, when applied, alters the behaviour of these parameters.

This work also provides a brief introduction to the STM32 families of Microcontrollers. It gives an example of the family hierarchy and lists the shared features between the STM32F10 family, while it concentrates on the peripheral units of the STM32F103 series, which were used within this project. Moreover, the embedded software: Standard peripherals library and Hardware Abstraction Layer are mentioned, with an emphasis put on the former with a given example that explores the most important files and folders of the library with an interface of the utilised integrated development interface (IDE).

The Standard peripheral library is exploited to programme and debug the board for the purpose of Implementing the aforementioned modulations techniques on the STM32F103RB Nucleo-board to generate modulated pulses, which were used to synthesise a five-level output voltage.

The resulting voltage were generated for a sampling frequency of 100 kHz, reference signal of 50 H zand a triangular frequency of 1kHz(respectively, 500 Hz) for LS (respectively, PS) techniques. As two 5V DC power supplies were used, the resulting voltage has a maximum value of 10 V measured between phase and ground, while the phase -to-phase voltage could reach up to 20 V. Finally, using the oscilloscope, the data are collected to measure current and distortions.

# Bibliographic References


[1] Eremia, M. (2016). Advanced solutions in power systems: HVDC, FACTS, and artificial intelligence (M. Eremia, C.-C. Liu, & A.-A. Edris, Eds.). Nashville, TN: John Wiley & Sons.
[2] V. K. Khanna, "IGBT Circuit Applications" in Insulated Gate Bipolar Transistor IGBT Theory and Design, pp. 545–608. 2003.
[3] B. K. Bose, "Recent advances in power electronics," [Proceedings] IECON '90: 16th Annual Conference of IEEE Industrial Electronics Society, Pacific Grove, CA, USA, 1990, pp. 829-838 vol.1, doi: 10.1109/IECON.1990.149248.
[4] J. Rodriguez, Jih-Sheng Lai and Fang Zheng Peng, "Multilevel inverters: a survey of topologies, controls, and applications," in IEEE Transactions on Industrial Electronics, vol. 49, no. 4, pp. 724-738, Aug. 2002, doi: 10.1109/TIE.2002.801052.
[5] L. M. Tolbert, Fang Zheng Peng and T. G. Habetler, "Multilevel converters for large electric drives," in IEEE Transactions on Industry Applications, vol. 35, no. 1, pp. 36-44, Jan.-Feb. 1999, doi: 10.1109/28.740843.
[6] A. A. Ansari, D. M. Deshpande, "Mathematical Model of Asynchronous Machine in MATLAB Simulink", International Journal of Engineering Science and Technology Vol. 2(5), 2010, 1260-1267
[7] Janiga, S., Syed, S. N., Tummala, S. K., & Pinni, S. V. (2019). Speed control of an induction motor fed by an inverter using dSPACE controller. E3S Web of Conferences, 87, 01002.
[8] T. Ahmed, Sheik Md. Kazi Nazrul Islam, I. Chowdhury and S. Binzaid, "Sustainable powered microcontroller-based intelligent security system for local and remote area applications," 2012 International Conference on Informatics, Electronics & Vision (ICIEV), Dhaka, 2012, pp. 276-280, doi: 10.1109/ICIEV.2012.6317454.
[9] Yılmaz GÜVEN, Ercan COŞGUN, Sıtkı KOCAOĞLU, Harun GEZİCİ, Eray YILMAZLAR, "Understanding the Concept of Microcontroller Based Systems To Choose The Best Hardware For Applications", Research Inventy: International Journal of Engineering And Science, Vol.6, Issue 9 (September 2017), PP -38-44.
[10] STMicroelectronics, “Products and solutions for Smart industry”, BRSI0818, 2018.
[11] Moussab BOUNABI, “Study of topologies and architectures of DC-AC photovoltaic converters connected to the grid”, Ph.D. thesis, Ecole Nationale Polytechnique, 2019.
[12] Rokan Ali Ahmed, S. Mekhilef, Hew Wooi Ping, "New multilevel inverter topology with reduced number of switches", proceedings of the 14th International Middle East Power Systems Conference (MEPCON’10), Cairo University, Egypt, December 19-21, 2010, Paper ID 236.
[13] F. Bordry, "Power converters: definitions, classification and converter topologies", CERN, Geneva, Switzerland
[14] William Shepherd, Li Zhang, "Power Converter Circuits", 2019, ISBN: 9780367394479.
[15] Vinit Kumar, "Inverter and Other Applications of Power Electronics", IJEEMF International Journal of Electrical, Electronics and Mechanical Fundamentals, Vol. 02, Issue 01, July 2012, ISSN: 2278-3989.
[16] Gupta, K. K., & Bhatnagar, P. (2017). Multilevel inverters: Conventional and emerging topologies and their control. San Diego, CA: Academic Press.
[17] Bimbhra, P. S. (2006). Power Electronics. New Delhi, India: Khanna.

[18] Ghosh, G., Sarkar, S., Mukherjee, S., Pal, T., & Sen, S. (2017b). A comparative study of different multilevel inverters. 2017 1st International Conference on Electronics, Materials Engineering and Nano-Technology (IEMENTech). IEEE.
[19] Abdelmalik BENDAIKHA, Commande par MLI Vectorielle d'un Onduleur Multi-Niveaux", Ph. D. thesis, Université Badji Mokhtar- Annaba, 2018.
[20] Sinusoidal Pulse Width Modulation (SPWM) With Variable Carrier Synchronization for Multilevel Inverter Controllers M. (n.d.). S. Aspalli.
[21] Amaia Lopez De Heredia Bermeo, "Commandes Avancées des systèmes dédiés à l'amélioration de la qualité de l'énergie : de la basse tension à la montée en tension", Ph. D. thesis, Laboratoire d'Electrotechnique de Grenoble Cidae (Mondragón, Espagne),.
[22] O. Kherif, Y. Benmahamed, D. Maadjoudj, M. Teguar, M. Bounabi, and C. Larbes, "Fault diagnosis method for cascaded h-bridge multilevel inverters under switching device failure," in 2019 19th International Symposium on Electromagnetic Fields in Mechatronics, Electrical and Electronic Engineering (ISEF), 2019.
[23] B. P. McGrath and D. G. Holmes, "Multicarrier PWM strategies for multilevel inverters," in IEEE Transactions on Industrial Electronics, vol. 49, no. 4, pp. 858-867, Aug. 2002, doi: 10.1109/TIE.2002.801073.
[24] M. S. Aspalli and A. Wamanrao, "Sinusoidal pulse width modulation (SPWM) with variable carrier synchronization for multilevel inverter controllers," 2009 International Conference on Control, Automation, Communication and Energy Conservation, Perundurai, Tamilnadu, 2009, pp. 1-6.
[25] Ismail, N., Permadi, A., Risdiyanto, A., Susanto, B., & Ramdhani, M. A. (2018). The effect of amplitude modulation index and frequency modulation index on total harmonic distortion in 1-phase inverter. IOP Conference Series. Materials Science and Engineering, 288, 012107.
[26] Wu, B., & Narimani, M. (2017). High-power converters and AC drives (2nd ed.). Nashville, TN: John Wiley & Sons.
[27] Chen, F., & Qiao, W. (2016). A general space vector PWM scheme for multilevel inverters. 2016 IEEE Energy Conversion Congress and Exposition (ECCE). IEEE.
[28] Ayman Y. Yousef, "Space Vector Pulse Width Modulation Technique", International Journal of Emerging Technology in Computer Science & Electronics (IJETCSE), ISSN: 0976-1353 Volume 15 Issue 1 –MAY 2015.
[29] J. Rodriguez, L. Moran, J. Pontt, P. Correa and C. Silva, "A high-performance vector control of an 11-level inverter," in IEEE Transactions on Industrial Electronics, vol. 50, no. 1, pp. 80-85, Feb. 2003, doi: 10.1109/TIE.2002.804975.
[30] Y. Deng, Y. Wang, K. H. Teo and R. G. Harley, "A Simplified Space Vector Modulation Scheme for Multilevel Converters," in IEEE Transactions on Power Electronics, vol. 31, no. 3, pp. 1873-1886, March 2016, doi: 10.1109/TPEL.2015.2429595.
[31] Boglietti, A., El-Refaie, A. M., Drubel, O., Omekanda, A. M., Bianchi, N., Agamloh, E. B., … Borg Bartolo, J. (2014). Electrical machine topologies: Hottest topics in the electrical machine research community. IEEE Industrial Electronics Magazine, 8(2), 18–30.
[32] Vukosavic, S. N. (2012). Electrical Machines (2012th ed.). New York, NY: Springer.
[33] Sen, P. C. (2013). Principles of electric machines and power electronics (3rd ed.). Nashville, TN: John Wiley & Sons.
[34] T. Ambros and M. Burduniuc, "The magnetic field of asynchronous machines with concentrated winding," 2016 International Conference and Exposition on Electrical and Power Engineering (EPE), Iasi, 2016, pp. 161-164, doi: 10.1109/ICEPE.2016.7781325.
[35] Chapman, S. J. (2011). Electric machinery fundamentals (5th ed.). New York, NY: McGraw-Hill Professional.
[36] D. P. Kothari, I. J. Nagrath. Electric Machines (3rd ed.). New Delhi, The Mc-Graw Hill companies, 2004.
[37] https://www.theengineeringknowledge.com/
[38] Debashis Das, Muhibul Haque Bhuyan and Rafiqul Islam, "Design and manufacturing of a low cost synchronouss motor-generator for electrical machine laboratory", Proceedings of the Conference on Engineering Research, Innovation and Education 2011, CERIE 2011, 11-13 January 2011, Sylhet, Bangladesh
[39] Sahdev, S. K. (2017). Electrical Machines. Cambridge, England: Cambridge University Press.

[40] H. Hooshyar, M. Savaghebi and A. Vahedi, "Synchronous generator: past, present and future," AFRICON 2007, Windhoek, 2007, pp. 1-7, doi: 10.1109/AFRCON.2007.4401482.
[41] H. R. Fudeh and C. M. Ong, "Modeling and Analysis of Induction Machines Containing Space Harmonics Part II: Analysis of Asynchronous and Synchronous Actions," in IEEE Transactions on Power Apparatus and Systems, vol. PAS-102, no. 8, pp. 2616-2620, Aug. 1983, doi: 10.1109/TPAS.1983.317782.
[42] S. Srilad, S. Tunyasrirut and T. Suksri, "Implementation of a Scalar Controlled Induction Motor Drives," 2006 SICE-ICASE International Joint Conference, Busan, 2006, pp. 3605-3610, doi: 10.1109/SICE.2006.314749.
[43] M. Kral and R. Gono, "Dynamic model of asynchronous machine," 2017 18th International Scientific Conference on Electric Power Engineering (EPE), Kouty nad Desnou, 2017, pp. 1-4, doi: 10.1109/EPE.2017.7967320.
[44] Abu-Rub, H. (2012). High performance control of AC drives with matlab/Simulink: Abu-rub/high performance control of AC drives with MATLAB/Simulink models (2nd ed.; D. H. Abu-Rub, D. A. Iqbal, J. Guzinski, & D. T. Phamdinh, Eds.). Hoboken, NJ: Wiley-Blackwell.
[45] Wang, Jin Jiang, et al. "Concordia Transform-Based Current Analysis for Induction Motor Diagnosis." Key Engineering Materials, vol. 569–570, Trans Tech Publications, Ltd., July 2013, pp. 481–488. Crossref, doi:10.4028/www.scientific.net/kem.569-570.481.
[46] L. K. Jisha and A. A. Powly Thomas, "A comparative study on scalar and vector control of Induction motor drives," 2013 International conference on Circuits, Controls and Communications (CCUBE), Bengaluru, 2013, pp. 1-5, doi: 10.1109/CCUBE.2013.6718554.
[47] G. J. Rushiraj and P. N. Kapil, "Analysis of different modulation techniques for multilevel inverters," 2016 International Conference on Electrical, Electronics, and Optimization Techniques (ICEEOT), Chennai, 2016, pp. 3017-3024, doi: 10.1109/ICEEOT.2016.7755254.
[48] Comparison of Phase-Shifted and Level-Shifted PWM in the Modular Multilevel Converter Rosheila Darus1,2, Georgios Konstantinou1, Josep Pou1,3, Salvador Ceballos4 and Vassilios G. (n.d.). Agelidis1.
[49] https://www.st.com/content/st_com/en.html
[50] https://www.arm.com/
[51] STMicroelectronics, Reference Manual, "STM32F101xx, STM32F102xx, STM32F103xx, STM32F105xx and STM32F107xx advanced Arm®-based 32-bit MCUs", RM0008, 2018.
[52] STMicroelectronics, Datasheet, "Medium-density performance line ARM®-based 32-bit MCU with 64 or 128 KB Flash, USB, CAN, 7 timers, 2 ADCs, 9 com. Interfaces", 2015.
[53] STMicroelectronics, Application Note, "General-purpose timer cookbook for STM32 microcontrollers", AN4776, 2019.
[54] STMicroelectronics, Programming Manual, "STM32F10xxx/20xxx/21xxx/L1xxxx Cortex®-M3 programming manual", PM0056, 2017.
[55] STMicroelectronics, User Manual, "Getting started with STM32 Nucleo board software development tools", UM1727, 2016.
[56] STMicroelectronics, User Manual, "STM32 Nucleo-64 boards (MB1136)", UM1724, 2020.
[57] https://www.gwinstek.com/en-global/products/detail/GDS-1000-U